The *Drosophila* neuromuscular junction as a model system to study the molecular mechanisms of neurodevelopment and synaptic degeneration

Dissertation

zur Erlangung des Grades eines

Doktors der Naturwissenschaften

der Mathematisch-Naturwissenschaftlichen Fakultät

und

der Medizinischen Fakultät

der Eberhard-Karls-Universität Tübingen

vorgelegt

von

Petra Füger
aus Mediasch, Rumänien

Mai - 2012

Tag der mündlichen Prüfung:	11.09.2012
Dekan der Math.-Nat. Fakultät:	Prof. Dr. W. Rosenstiel
Dekan der Medizinischen Fakultät:	Prof. Dr. I. B. Autenrieth
1. Berichterstatter:	Prof. Dr. Peter Thier
2. Berichterstatter:	Prof. Dr. Ludger Schöls
Prüfungskommission:	Prof. Dr. Peter Thier
	Prof. Dr. Ludger Schöls
	Prof. Dr. Mathias Jucker
	Prof. Dr. Philipp Kahle

Ich erkläre, dass ich die zur Promotion eingereichte Arbeit mit dem Titel:

„The *Drosophila* neuromuscular junction as a model system to study the molecular mechanisms of neurodevelopment and synaptic degeneration“

selbstständig verfasst, nur die angegebenen Quellen und Hilfsmittel benutzt und wörtlich oder inhaltlich übernommene Stellen als solche gekennzeichnet habe. Ich versichere an Eides statt, dass diese Angaben wahr sind und dass ich nichts verschwiegen habe. Mir ist bekannt, dass die falsche Abgabe einer Versicherung an Eides statt mit Freiheitsstrafe bis zu drei Jahren oder mit Geldstrafe bestraft wird.

Tübingen, den _____ _____

Datum Unterschrift

Description of personal contribution

1. The work presented in the first result section of this thesis (**A role of PP2A in synapse development in *Drosophila melanogaster***) is adapted from the published manuscript:

"PP2A and GSK-3β Act Antagonistically to Regulate Active Zone Development", N.M. Viquez, P. Füger et al., Journal of Neuroscience, 2009.

Own contribution: Experimental work, data acquisition, analysis of data and preparation of the figures presented in Chapter 4.1 of this thesis.

2. The work presented in the second result section of this thesis (***Drosophila melanogaster* in the study of the SPG10 subtype of the neurodegenerative disorder Hereditary Spastic Paraplegia**) is partially adapted from the manuscript:

"Spastic paraplegia mutation N256S in the neuronal microtubule motor KIF5A disrupts axonal transport in a Drosophila HSP model", P. Füger, V. Sreekumar et al.,

Own contribution: Experimental work, data acquisition, analysis of data and preparation of the figures (supported by V. Sreekumar and J. Kern) presented in Chapter 4.2 of this thesis. Kymographes presented in Paragraph 4.2.1.7.1 are generated by Josephine Ng.

Acknowledgements

An dieser Stelle möchte ich mich bei all denjenigen bedanken, die mich auf verschiedenste Art und Weise unterstützt haben und zum Gelingen dieser Arbeit beigetragen haben:

Mein Dank gilt Dr. Tobias Rasse für das Ermöglichen dieser Arbeit und für die Betreuung. Ferner gilt mein Dank Herrn Prof. Dr. Peter Thier und Herrn Prof. Dr. Ludger Schöls als Mitglieder meines Advisory Boards.

Herrn Prof. Dr. Mathias Jucker und Herrn Prof. Dr. Philipp Kahle danke ich für Ihr Einverständnis, in der Prüfungskommission mitzuwirken.

Meinen Kollegen, die mich über die Jahre dieser Arbeit begleitet haben, danke ich für die gute Zusammenarbeit sowie die allzeitige Hilfsbereitschaft. Mein Dank gilt:

Roman Beck, Simone Eberle, Daniel Eicke, Yvonne Eisele, Valentin Frimmer, Stefan Grathwohl, Bernadette Graus, Shabab Hannan, Götz Heilbronner, Stephan Käser, Jeannine Kern, Ellen Kilger, Michael Knopp, Fransziska Langer, Dennis Lindau, Sandra Musch, Valentina Olig, Stanislav Ott, Jelena Rößle, Vera Siegert, Natalia Veresceaghina, Libo Yu, Yao Zhang, Jun-yi Zhu.

Ein besonderer Dank geht an Raphael Zinser für die vielseitige und hervorragende Unterstützung im Labor.

Für ihre vielseitige Hilfe, guten Gespräche, Kaffeepausen, Poetry Slam Besuche, Frisbee Training und ihre Freundschaft, auch über die Zeit im Labor hinaus, möchte ich mich bei Laila Behrends, Bettina Wegenast-Braun, Katja Dreißigacker, Chris Friemel, Stella Kramer, Amrita Kuthiala, Bronwen Lasky, David Milford, Josephine Ng, Christina Nordhammer, Rebecca Radde, Vrinda Sreekumar, Doychin Stanchev, Christian Thetard und Heidrun Wölfing bedanken.

Für Ihren Anteil an der Korrektur dieser Arbeit danke ich ganz herzlich: Laila Behrends, Bettina Wegenast-Braun, Bronwen Lasky und Natalia Veresceaghina.

Meinen Eltern und Großeltern danke ich für ihre vielfältige Unterstützung, ihre Liebe und den Halt, auch in dieser Lebensphase. Meinen Brüdern und Freunden danke ich für den moralischen Beistand, ihre offenen Ohren und ihre Geduld – ich weiß nicht, was ich ohne euch gemacht hätte!

Table of contents

List of Figures

List of Tables

Abbreviations

ALS	amyotrophic lateral sclerosis
ATP	adenosine triphosphate
AZ	active zone
BMP	bone morphogenetic protein
Brp	Bruchpilot
CSP	cystein string protein
Dlg	Discs-large
EM	electron microscopy
ER	endoplasmic reticulum
Eve	Even-skipped
FTLD	frontotemporal lobar degeneration
Gbb	glass bottom boat
GFP	green fluorescente protein
GluR	glutamate receptors
GSK-3β	glycogen synthase kinase-3β
HRP	horse radish peroxidase
HSP	hereditary spastic paraplegia
Klc	kinesin light chain
Khc	kinesin heavy chain
Mad	mothers against decapentaplegic
pMad	phosphorylated Mad
MAP	microtubule associated protein
NMJ	neuromuscular junction
PP2A	protein phosphatase 2A

PSD	postsynaptic density
Sax	Saxophone
SD	standard deviation
SEM	standard error oft the mean
SPG	spastic paraplegia gene
SBMA	spinal bulbar muscular atrophy
SSR	subsynaptic reticulum
Syn	Synapsin
TGFβ	transforming growth factor β
Tkv	Thick veins
UAS	upstream activation sequence
VNC	ventral nerve cord
Wrd	Well-rounded

I. Summary

More than a century ago the fruit fly *Drosophila melanogaster* was established as a genetic model system. The *Drosophila* neuromuscular junction (NMJ) has proven as an adequate model system to study molecular mechanisms of development of glutamatergic synapses. Discoveries first made in flies had a brought impact on neuroscience research in vertebrates, as many genes and fundamental aspects of cell biology are conserved between *Drosophila* and vertebrates. In addition, *Drosophila* has established as an expedient model system in the study of human neurodegeneration during the last two decades.

The first chapter of this thesis focuses on the role of the protein phosphatase 2A (PP2A) in the development of individual synapses at the *Drosophila* NMJ. The *Drosophila* NMJ is organized in a chain of boutons, each bouton containing 10-50 individual synapses. Within each synapse the presynaptic active zone protein Bruchpilot (Brp) is directly apposed to a cluster of postsynaptic glutamate receptors (GluR). The postsynaptic clustering of GluR precedes the presynaptic localization of Brp, but within ten hours after GluR clustering Brp is localized at the apposing active zone. When PP2A was inhibited, about 30% of the GluR clusters were found to be unapposed to the presynaptic Brp. These GluR clusters were almost threefold smaller than GluR clusters apposed to Brp and were more prevalent in the distal boutons of the NMJ. *In vivo* imaging of GluR clustering further revealed that within six hours of development almost no new GluR clusters formed when PP2A was inhibited. Thus neuronal inhibition of PP2A impairs presynaptic maturation of synapses and causes additional defects in postsynaptic development.

The second and central part of this thesis focuses on the establishment of a *Drosophila* model of the degenerative motor-neuron disorder hereditary spastic paraplegia (HSP). The common pathological feature, of this group of clinically and genetically heterogeneous disorders, is a progressive retrograde axonopathy of the longest corticospinal motor-neurons. Here we establish a *Drosophila* model for the HSP subtype SPG10. The *SPG10* gene encodes the neuron specific kinesin heavy chain KIF5A of vertebrate kinesin-1. To model SPG10 in *Drosophila*, the HSP-associated mutation N256S in human KIF5A was introduced into *Drosophila* Khc at the corresponding site (N262S) and the mutated Khc^{N262S} was expressed in a *Drosophila* wild-type background.

This *Drosophila* SPG10 model recapitulates key disease features of HSP such as impairments in locomotion, axonal swellings, degeneration of synapses and a more severe affliction of longer axons. We show that Khc^{N262S} acts as a dominant-negative allele *in vivo*. Furthermore our data suggest that the pathology in the *Drosophila* SPG10 model establishes due to impaired localization of cargo necessary for maintenance of structure and/or function of the synapses or the axon. As possible mechanisms contributing to pathology in the *Drosophila* SPG10 model reduced mitochondrial density at the NMJ, a reduction in bone morphogenetic protein (BMP) signaling and alterations in axonal as well as neuromuscular cytoskeleton were identified. All of these findings have been linked to neurodegenerative disorders before.

The presented *Drosophila* SPG10 model provides a valuable tool for continuative studies of the mechanisms of initiation and progression of pathology in the HSP subtype SPG10.

II. Introduction

2.1 *Drosophila melanogaster* as a model organism

More than a century ago the fruit fly Drosophila *melanogaster* was established as a genetic model system. *Drosophila* possesses many features that have ensured its success as a model organism. The genome, contains around 14.000 genes (Adams et al., 2000) and is distributed into only four pairs of chromosomes. Most of the *Drosophila* genes are conserved in vertebrates.

There are various transgenic (e.g. P-element insertion, (Rubin and Spradling, 1982) and knockout strategies that are applicable for genome manipulations. In addition the *UAS/Gal4* system (for details see next paragraph) allows ectopically and temporally defined expression of a gene of interest (Brand and Perrimon, 1993).

Transgenic fly stocks can be easily maintained due to balancer chromosomes that preclude crossing-over. Moreover, *Drosophila* can be reared in the laboratory easily. It has a high reproduction rate and a short generation time, of about 11 days at 25℃ (Figure1).

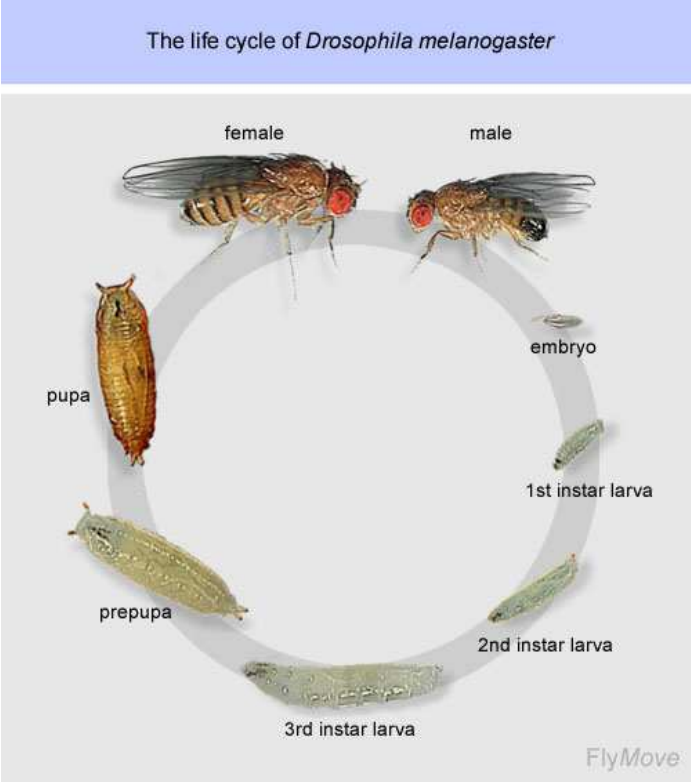

Figure 1: Life cycle of *Drosophila melanogaster*
About 24 hours after egg laying at 25℃, larva hatch to 1st instar larval stage, followed by 2nd instar latval stage and 3rd instar larval stage. Larva then reach wandering stage, followed by the pupation. After completed metamorphosis adult flies eclose.
(Picture is from http://flymove.uni-muenster.de/Genetics/Flies/LifeCycle/LifeCyclePict/life_cycle.jpg/ 01/04/2012)

2.1.1 Directed gene expression in *Drosophila*

To enable ectopically and temporally defined expression of a gene of interest in *Drosophila* the *UAS/Gal4* system was established (Brand and Perrimon, 1993). In this system the gene encoding the yeast transcriptional activator Gal4 is inserted into the *Drosophila* genome and fuses randomly to one of a diverse array of genomic enhancers (Gal4 driver lines). When a gene of interest is introduced that contains Gal4 binding sites (Upstream Activation Sequence, UAS) within its promoter, it will be activated in the cells where Gal4 is expressed (Brand and Perrimon, 1993) (Figure 2). This enables tissue-specific, temporally defined expression of the target gene dependent on the expression pattern of the Gal4 driver.

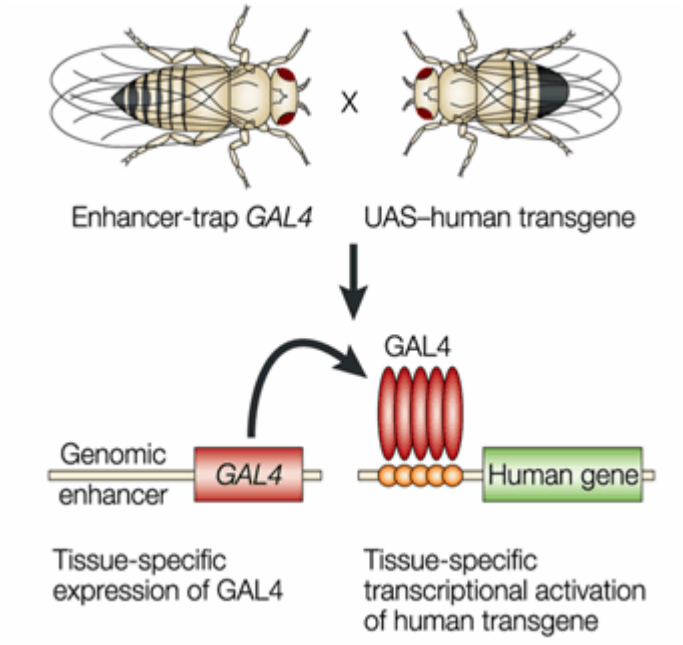

Figure 2: Directed gene expression in *Drosophila melanogaster*
Tissue specific expression of Gal4 enables tissue specific expression of transgenes, carrying a Gal4 binding site (UAS). (Figure is taken from Muqit and Feany, 2002)

One advantage using the *UAS/Gal4* system is that the target gene and its transcriptional activator are inserted into two different transgenic fly lines. Thus the target gene is expressed only after being combined with the driver line, thereby enabling the maintenance of transgenic fly lines that carry target genes that cause lethality after expression. Furthermore the *UAS/Gal4* system allows a diverse and rapid combination of different target genes and Gal4-drivers. This system has been further enhanced via the introduction of the Gal80 yeast protein, which is a negative regulator of Gal4 function that binds Gal4 and thereby hinders expression of UAS-constructs. A temperature sensitive variant of Gal80 ($Gal80^{ts}$) (Zeidler et al., 2004) only renders a functional Gal80 protein at permissive temperatures, and prevents the production of functional Gal80 at restrictive temperatures. Thus at the permissive temperature of 18℃, functional Gal80 is produced and binds to Gal4, thereby hindering the expression of UAS-constructs at this temperature. At restrictive temperatures of 29-30℃, no functional Gal80 protein is produced, and thus Gal4 can bind to the UAS sequence and induce expression of the UAS-constructs at these

temperatures. Thus using the UAS/Gal4/Gal80^{ts} system the expression of UAS-constructs in *Drosophila* can be further modified.

2.1.2 An assay to assign neurodegeneration in *Drosophila*

Parts of this thesis focus on the establishment of a *Drosophila* model of the neurodegenerative disorder HSP. Thus we use the synaptic footprint assay to assign neurodegeneration at the NMJs in *Drosophila*. The synaptic footprint assay was established in the laboratory of G. Davis (Eaton et al., 2002) to score for retraction that occurs during normal development at the *Drosophila* NMJ.

At the *Drosophila* NMJ the postsynaptic membranes are organized in a complex series of membrane folds, the subsynaptic reticulum (SSR). The gradual assembly of the SSR and proteins that localize to this structure require the presence of the presynaptic nerve terminal (Guan et al., 1996, Schuster et al., 1996). Therefore the SSR and other postsynaptic proteins are present only at sites where the presynaptic nerve resides or has recently resided. The synaptic footprint assay is based on the assumption that presynaptic retraction is more rapid than the disassembly of the SSR. Therefore, if sites of SSR are observable with no opposing presynaptic marker, the presynapse has been there but has retracted (Eaton et al., 2002). Sites where the postsynapse is present without an opposing presynapse are referred to as “postsynaptic footprints”.

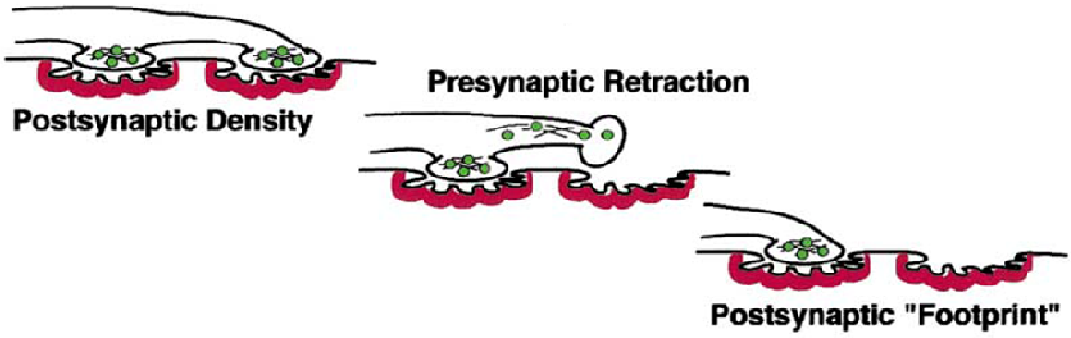

Figure 3: Synaptic footprint assay

Representation of the hypothesized series of events that lead to the formation of a postsynaptic "footprint" at the *Drosophila* NMJ. For details see main text.
(Figure is taken from Eaton et al., 2002).

To visualize the postsynaptic SSR, Discs-large (Dlg), a PSD 95-like protein that is distributed throughout the SSR has been described. Dlg has been reported to be expressed both pre- and postsynaptically (Lahey et al., 1994). However most of the Dlg is associated with the postsynaptic SSR and some Dlg was found to localize to the presynaptic membrane, while no Dlg was observed in the bouton core (Lahey et al., 1994). Thus the Dlg positive perisynaptic network observed in confocal microscopy corresponds to the SSR (Lahey et al., 1994).

To visualize the presynaptic compartment, an anti-HRP antibody was used as a marker of neuronal membranes and synaptic vesicles were identified by using a Synapsin (Syn) antibody. For analysis, the number of boutons exhibiting "postsynaptic footprints", this means the presence of the SSR marker Dlg without the presynaptic markers Syn and HRP, were quantified (Eaton et al., 2002, Pielage et al., 2008).

The synaptic footprint assay was originally established to score for retraction events that occur during synaptic development. We reasoned that this assay might also be useful to analyze degeneration occurring at the NMJ in the *Drosophila* model of HSP. Two opposing mechanisms have been described for retraction and degeneration (Saxena and Caroni, 2007). During retraction events the presynaptic material is transported back to more proximal sections of the axon and the axon retracts gradually. Degeneration entails the fractionization of presynaptic material and the axon, which is presumably followed by local uptake by phagocytes (Saxena and Caroni, 2007). Thus we concluded that if degeneration proceeds at the NMJ we should observe a change in the amount and distribution of the presynaptic components compared to the postsynaptic SSR rather than synaptic footprints, completely devoid of presynaptic markers. Therefore we changed the mode of analysis to suit to the quantification of degeneration. (For details on the performance of analysis see Material and Methods, paragraph 3.7.5).

2.2 *Drosophila melanogaster* in the study of neurodevelopment

Fundamental aspects of cell biology are quite similar in man and flies, including regulation of gene expression, membrane trafficking, the cytoskeleton, neuronal connectivity, synaptogenesis, cell signaling and cell death (Sang and Jackson, 2005). Indeed, many genes and processes first discovered in the fly have proven to be conserved in other organisms including human.

Discoveries first made in flies have had a significant impact on neuroscience research in vertebrates. For example, the functions of many proteins, such as

Synaptotagmin and Dynamin that are important for exocytosis and endocytosis in synaptic transmission have been characterized using the fly NMJ. Studies in *Drosophila* have facilitated the identification and characterization of potassium channels in mammals. Furthermore, a role of cAMP in learning and memory was first unraveled in flies. Moreover, players of a variety of pathways that are important in vertebrate neurogenesis, neuronal migration, growth cone guidance and differentiation of neural stem cells, were first identified in flies (For review see Bellen et al., 2010).

2.2.1 The *Drosophila* neuromuscular synapse as a model system to study synaptic function and development

The *Drosophila* NMJ is a popular model system to study development, function and plasticity of vertebrate glutamatergic central synapses that are the most important and prevalent excitatory synapses in the central nervous system of vertebrates and the key elements of information processing.

2.2.1.1 Structure of the *Drosophila* neuromuscular junction

The neuromuscular system in *Drosophila* is organized in a stereotypical way, in which 30 identified postsynaptic muscle cells are innervated by 32 identified motor-neurons (Landgraf et al., 1997). Therefore each NMJ is identifiable and thereby enables reliable comparison of the same NMJ between different individual flies of the same genotype or individual flies of varying genotypes. In addition, the NMJ is easily accessible in *Drosophila* embryos and larvae by a variety of physiological, histological and microscopic techniques.

The NMJ is organized in a chain of boutons, each bouton containing 10-50 individual synapses (Figure 4A). I will refer to the entire connection formed between motor-neuron and muscle as NMJ, and use the term synapse or neuromuscular synapse for individual synapses at the NMJ.

The most important feature of *Drosophila* neuromuscular synapses, making them a valuable model system in the study of vertebrate glutamatergic central synapses, is that they are glutamatergic. In addition the majority of synaptic proteins, the features of synaptic function and most probably the mechanisms of development of *Drosophila* neuromuscular synapses are conserved with vertebrate glutamatergic synapses (Collins and DiAntonio, 2007).

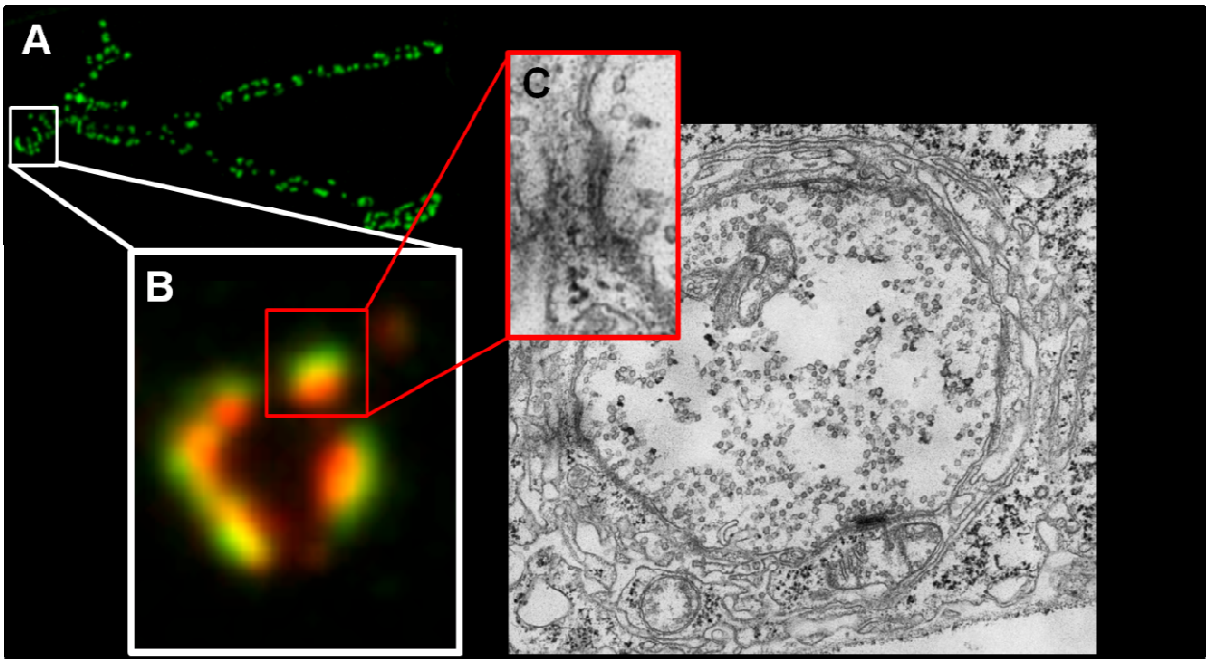

Figure 4: Organization of the *Drosophila* neuromuscular junction.
The NMJ is organized in a chain of boutons (A), each bouton containing 10-50 individual synapses (B). Individual synapses as visualized presynaptically by Bruchpilot (red) and postsynaptically by the glutamate receptor subunit DGluRIIC (green) (B). In electron microscopy (EM) synapses are characterized by close apposition and a high electron density of presynaptic and postsynaptic membrane (C). The EM picture was kindly provided by J. Kern.

To enable efficient signal transmission, the glutamatergic synapse consists of highly specialized presynaptic and postsynaptic structures that are highly similar between *Drosophila* and vertebrates.

2.2.1.2 The presynaptic compartment of glutamatergic synapses

The site of neurotransmitter release from the presynaptic nerve terminal is termed the active zone (AZ). It is a specialized region of the presynaptic cell membrane that is precisely aligned to the postsynaptic membrane and the location of GluR clusters. This close apposition of presynaptic and postsynaptic membrane displays a high electron density in electron microscopy (Figure 4C).

Various proteins localize to the AZ and play an essential role in the organization of the AZ and in the regulation of neurotransmitter release. In *Drosophila* homologs of several vertebrate AZ proteins have been identified. A homolog of vertebrate Liprin-α was found in *Drosophila,* that localizes to the AZ and is important for AZ formation (Kaufmann et al., 2002). The presynaptic protein Bruchpilot (Brp) that was identified in *Drosophila*, possesses an N-terminal domain that exhibits significant sequence homology to vertebrate ELKS/CAST/ERC and a large C-terminal domain that is rich in coiled-coil structures similar to several cytoskeletal proteins (Wagh et al., 2006). Brp was recently shown to be a component of the T-bar (Kittel et al., 2006), an electron dense structure at the AZ of *Drosophila* (Atwood et al., 1993, Zhai and Bellen, 2004). Similar dense body projections have also been described at vertebrate CNS synapses (Bloom and Aghajanian, 1968, Phillips et al., 2001). These dense

body projections are important for the tethering of synaptic vesicles at the AZs and thus for efficient signal transmission.

2.2.1.3 The postsynaptic compartment of glutamatergic synapses

The postsynaptic density (PSD) is a specialized subcellular organization of the postsynaptic cell. It is characterized by an electron dense thickening of the cell membrane, that lies exactly opposite of the presynaptic AZ.

The *Drosophila* PSD contains cytoskeleton proteins (e.g. actin), cell-adhesion molecules (e.g. neuroligin, fasciclin) and signaling proteins like kinases and phosphatases (e.g PAK p21-activated kinase) (Albin and Davis, 2004, Prokop and Meinertzhagen, 2006) and clusters glutamate receptors. The GluRs expressed at the *Drosophila* NMJ are structurally and functionally similar to vertebrate AMPA-/Kainate-type receptors (Heckmann and Dudel, 1997). *Drosophila* GluRs are tetramers comprised of the subunits GluRIIC, GluRIID, GluRIIE and either the subunit GluRIIA or GluRIIB (Marrus et al., 2004). Receptors containing GluRIIA or GluRIIB differ in their channel properties, synaptic responses and localization (Marrus et al., 2004). Beneath the PSD the SSR folds in a typical manner. It contains various scaffolding and adhesion proteins such as the PSD-95 homolog Dlg (Budnik et al., 1996), that is important for structural organization and efficient function of the NMJ.

To ensure accurate assembly and thereby proper function, formation and maturation of the NMJ and the synapses need to be precisely regulated. Two classical morphogenes have been identified as essential regulators of synaptic growth (Marques, 2005). While Wingless, a member of the Wnt family, acts as an anterograde regulator of synaptic growth, the transforming growth factor β (TGF-β)

Glass bottom boat (Gbb) signals retrogradely to affect synaptic growth during larval development (Marques, 2005).

Recently the protein phosphatase 2A (PP2A) was shown to play a role in the development of the *Drosophila* NMJ (Viquez et al., 2006).

2.2.2 A role of the protein phosphatase 2A in the developing nervous system

Reversible protein phosphorylation is a key regulatory mechanism in many cell biological processes. The phosphorylation of proteins is achieved by protein kinases, while dephosphorylation is performed by protein phosphatases.

The protein phosphatase 2A is a ubiquitous serine-threonine phosphatase, that plays a role in the regulation of cell cycle, cell morphology and development (Janssens and Goris, 2001). PP2A is highly enriched in central synapses and neuronal microtubules of the nervous system of vertebrates (Barnes et al., 1995, Sontag et al., 1995, Price et al., 1999), and its expression in the brain has been linked to the regulation of long-term potentiation (Woo and Nguyen, 2002, Jouvenceau et al., 2003, Belmeguenai and Hansel, 2005). Furthermore, reduced abundance and activity of PP2A was linked to the pathogenesis of Alzheimer´s disease (Vogelsberg-Ragaglia et al., 2001, Sontag et al., 2004a, Sontag et al., 2004b), due to increased levels of hyperphosphorylated Tau.

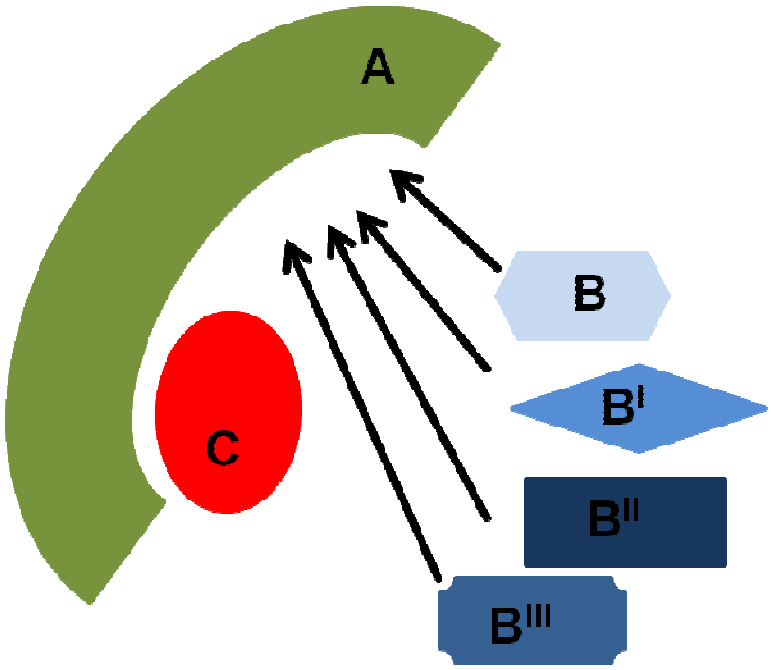

Figure 5: Structure of the protein phosphatase 2A

The PP2A holoenzyme consists of three subunits: a structural subunit (A), a catalytic subunit (C) and a regulatory subunit (B). So far four different families of regulatory subunits have been identified, termed the B, B^{I}, B^{II} and B^{III} families. The association of the regulatory subunit with the PP2A core enzyme is mutually exclusive and likely determines substrate specificity of PP2A. (Figure is adapted from Janssens and Goris, 2001)

Although PP2A was found to localize to synapses in the developing nervous system, little is known about the role of PP2A in synaptic development.

In *Drosophila* a B^{I} regulatory subunit (Figure 5) of PP2A, named well-rounded (Wrd) was identified. Wrd is widely expressed in *Drosophila*, but was shown to be enriched in the synaptic neuropil of the ventral nerve cord (VNC) and at the NMJ (Viquez et al., 2006). Presynaptically, Wrd is required for normal synaptic growth and morphology at the *Drosophila* NMJ and regulation of the cytoskeleton by promoting PP2A activity. Postsynaptic expression of Wrd is required for normal levels of evoked neurotransmitter release (Viquez et al., 2006).

While it has been shown that PP2A plays an important role in the development and function of the *Drosophila* NMJs, further investigations are required to elucidate a role of PP2A in the formation and development of individual synapses at the *Drosophila* NMJ. Therefore, aspects of this thesis were undertaken to gain greater insight into these mechanisms.

2.3 *Drosophila melanogaster* as a model for the SPG10 subtype of the neurodegenerative disorder Hereditary Spastic Paraplegia

2.3.1 *Drosophila* in the study of human neurodegeneration

In addition to its expedient role in studies of development and function of the nervous system, during the last two decades *Drosophila* has established as a valuable model organism in the study of human neurodegeneration. Most of the genes implicated in the heritable forms of neurodegenerative diseases have at least one fly homolog (Reiter et al., 2001) and often there is no redundancy in the *Drosophila* genes, thereby facilitating functional analysis of the gene products (Reiter et al., 2001). *Drosophila* has proven a reliable model in the study of a variety of neurodegenerative disorders including Alzheimer´s (Greeve et al., 2004, Carmine-Simmen et al., 2009, Goguel et al., 2011), Parkinson´s (Fernandes and Rao, 2011, Liu et al., 2011a, Liu et al., 2011b), motor-neuron diseases such as amyotrophic lateral sclerosis (ALS) (Ratnaparkhi et al., 2008, Chen et al., 2011, Wang et al., 2011), HSP (Sherwood et

al., 2004, Wang et al., 2007, Lee et al., 2009, Du et al., 2010), and others (Venkatachalam et al., 2008, Lorenzo et al., 2010).

2.3.2 Hereditary Spastic Paraplegia

Hereditary Spastic Paraplegias are a group of clinically and genetically heterogeneous neurological disorders with the cardinal feature of progressive spasticity and weakness of the lower extremities (Salinas et al., 2008). HSP prevalence is estimated to be 3-10 cases per 100.000 people in Europe (Silva et al., 1997, McMonagle et al., 2002, Erichsen et al., 2009). Onset can occur in early childhood up to 70 years of age (Salinas et al., 2008). HSPs can be classified into pure and complex forms. In pure HSP spasticity and weakness of the lower extremities are the main symptoms. In complex forms symptoms can also include cerebellar ataxia, epilepsy, thinning of the corpus callosum and mental retardation (Salinas et al., 2008). HSP can be inherited in an autosomal dominant, autosomal recessive, or X-linked recessive way. Autosomal dominant HSP is the most prevalent form and represents around 70% of cases. Most cases of pure HSP are autosomal dominant, whereas complicated forms tend to be autosomal recessive. So far 48 different genetic loci (spastic paraplegia gene (SPG) 1–48) (Slabicki et al., 2010, Blackstone et al., 2011) and 25 identified genes have been reported (Schule and Schols, 2011). A list of 20 identified genes and the cell biological function of their products is shown in Table 1 (Blackstone et al., 2011).

Gene symbol	Protein name	Main phenotype	Cell biological function
Membrane traffic-related			
SPG3A[101]	Atlastin-1	AD Pure	• ER morphogenesis • BMP signalling
SPG4 (also known as *SPAST*)[11]	Spastin	AD Pure	• ER morphogenesis • Endosomal traffic • BMP signalling • Cytokinesis • Cytoskeletal regulation
SPG6 (also known as *NIPA1*)[102]	NIPA1	AD Pure	• Endosomal traffic • BMP signalling
SPG8 (also known as *KIAA0196*)[47]	Strumpellin	AD Pure	• Endosomal morphogenesis • Cytoskeletal regulation
SPG10 (also known as *KIF5A*)[82]	KIF5A	AD Complex	• Microtubule-based motor protein
SPG11 (REF. 103)	Spatacsin	AR Complex	• Membrane traffic?
SPG15 (also known as *ZFYVE26*)[104,105]	Spastizin (also known as ZFYVE26 or FYVE-CENT)	AR Complex	• Membrane traffic? • Cytokinesis
SPG17 (also known as *BSCL2*)[106]	Seipin	AD Complex	• ER membrane protein • Lipid droplet biogenesis
SPG20 (REF. 107)	Spartin	AR Complex	• Endosomal traffic • BMP signalling • Lipid droplet biogenesis • Mitochondrial?
SPG21 (REF. 108)	Maspardin	AR Complex	• Endosomal traffic
SPG31 (also known as *REEP1*)[109]	REEP1	AD Pure	• ER morphogenesis
Mitochondrial			
SPG13 (also known as *HSPD1*)[110]	HSP60	AD Pure	• Mitochondrial chaperone
SPG7 (REF. 111)	Paraplegin	AR Complex	• Mitochondrial protease
Myelination			
SPG2 (also known as *PLP1*)[112]	PLP	XLR Complex	• Myelin protein
SPG35 (also known as *FA2H*)[113,114]	Fatty acid 2-hydroxylase	AR Complex	• Hydroxylation of myelin lipids
Miscellaneous			
SPG1 (also known as *L1CAM*)[115]	L1CAM	XLR Complex	• Cell adhesion and signalling
SPG5 (also known as *CYP7B1*)[116]	CYP7B1	AR Pure	• Cholesterol metabolism
SPG39 (REF. 117)	Neuropathy target esterase	AR Complex	• Phospholipid homeostasis • Target of organophosphates
SPG42 (also known as *SLC33A1*)[118]	SLC33A1	AD Pure	• Acetyl-CoA transporter
SPG48 (also known as *KIAA0415*)[119]	KIAA0415	AR Complex	• DNA repair

Table 1: List of 20 known HSP genes, divided into functional groups.

SPG, spastic paraplegia gene; AD, autosomal dominant; AR, autosomal recessive; BMP, bone morphogenetic protein; ER, endoplasmic reticulum. (Table is taken from Blackstone et al., 2011)

The common pathological feature of HSPs is a progressive retrograde axonopathy of the longest corticospinal motor-neurons (Salinas et al., 2008). Thus, to understand the mechanisms of pathophysiology in HSP, it seems crucial to gain insight into

molecular mechanisms underlying axonal function, maintenance and degeneration. The identification of 20 of the SPGs and of the cell biological function of their products provides important insight into these mechanisms. Several of these indentified proteins can be combined into functional groups (Table 1), highlighting different processes as crucial to the maintenance of axonal health (Blackstone et al., 2011).

2.3.3 Mechanisms in the pathophysiology of HSPs

2.3.3.1 Membrane modeling and shaping

Four HSP-associated proteins, including Spastin, Atlastin1, receptor expression enhancing protein 1 (REEP1) and Strumpellin, are involved in membrane shaping and modeling events. Mutations in these genes cause up to 60% of HSP cases in North America and northern Europe (Blackstone et al., 2011). Spastin, Atlastin1 and REEP1 interact in corticospinal neurons to coordinate endoplasmic reticulum (ER) shaping and microtubule dynamics (Park et al., 2010). Strumpellin was shown to be part of an endosomal complex that is necessary for sorting certain cargos from endosomes into the *trans*-Golgi network (Derivery et al., 2009, Gomez and Billadeau, 2009). Mutations in Strumpellin impair trafficking of cargo through early endosomal compartments, thereby resulting in dysfunction such as impaired recycling of the transferrin receptor (Derivery et al., 2009, Gomez and Billadeau, 2009).

The exact mechanisms that link defects in membrane modeling to axonopathy remain unclear. There is a multitude of possible explanations including the proposal that defects in membrane modeling and shaping events within the axon might interfere with axonal functions such as synaptic plasticity or with specific signaling

pathways important for axonal function or with efficient axonal transport (Blackstone et al., 2011).

2.3.3.2 Mitochondria and neurodegeneration

Mitochondrial dysfunction, changes in mitochondrial dynamics and mobility, and perturbation of mitochondrial turnover are involved in the pathology of some neurodegenerative and neurological disorders, such as Alzheimer´s disease, Parkinson´s, Huntington´s and ALS (reviewed in Schon and Przedborski, 2011).

Two HSP genes, Paraplegin and HSP60, are implicated in mitochondrial function and quality control (Blackstone et al., 2011). Mitochondria are the main site of ATP (adenosine triphosphate) production and play an essential role in Ca^{2+} buffering within cells. Therefore, dysfunctional mitochondria fail to produce ATP and to efficiently buffer Ca^{2+} levels. This energy depletion might contribute to disturbances in the highly ATP-dependent process of axonal transport. Further energy depletion at the synapses as well as toxic Ca^{2+} levels might initiate synaptic dysfunction and eventually loss of synapses (Sheng and Cai, 2012). As a result of synaptic loss or dysfunction the degeneration of the axons might be triggerd.

2.3.3.3 Alterations of bone morphogenetic protein signaling in motor-neuron disorders

2.3.3.3.1 Bone morphogenetic protein signaling

Bone morphogenetic proteins (BMPs) are morphogenes that belong to the TGFβ superfamily. To date over 20 different BMPs have been described in humans (Bragdon et al., 2011). These BMPs play crucial roles in many developmental and cellular processes such as embryogenesis, skeletal formation, hematopoiesis and neurogenesis (Bragdon et al., 2011). In *Drosophila* BMP signaling is essential for the appropriate growth of the NMJ and synaptic transmission (Aberle et al., 2002, Marques et al., 2002).

The BMP signaling pathway is activated upon binding of the ligand, and subsequently, type I and type II BMP-receptors are joined. The type II receptor, which is a constitutively active kinase, activates the type I receptor by phosphorylation. The activated type I receptor then phosporylates one of the several receptor-regulated Smads (R-Smads e.g. Smad 1 or Smad 5). Phosporylated R-Smads bind to the common Smad (Co-Smad, Smad 4) and the complex translocates to the nucleus, where it acts as a transcription factor. Inhibitory Smads (I-Smads) can further regulate the pathway.

In *Drosophila* the components of the BMP signaling pathway are structurally and functionally conserved (Padgett et al., 1993, Sampath et al., 1993).

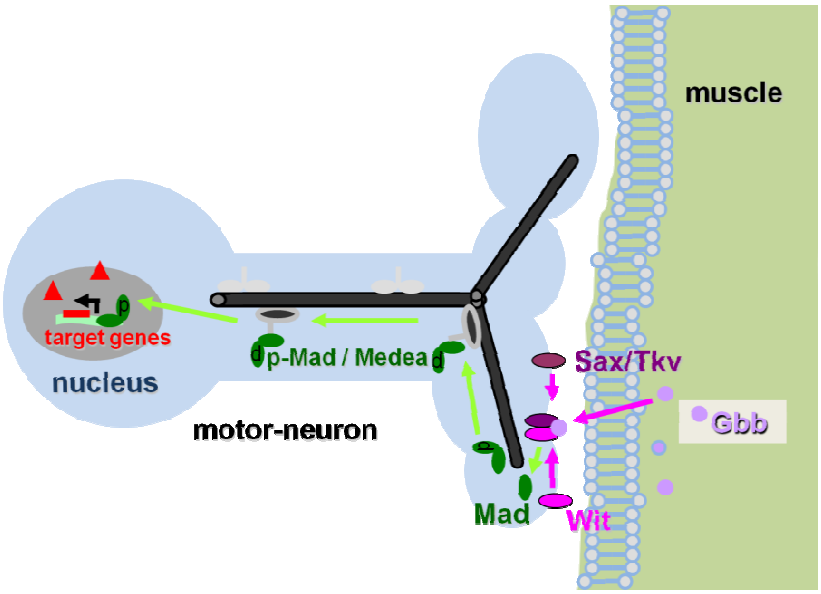

Figure 6: Bone morphogenetic signaling in the *Drosophila* motor neuron.
Upon binding of the postsynaptically released ligand Gbb, type I (Sax or Tkv) and type II (Wit) BMP-receptors dimerize. This dimer then phosphorylates the receptor-regulated Smad Mad. Phosphorylated Mad (pMad) binds to a Co-Smad (Medea) and the complex translocates to the nucleus, where it acts as a transcription factor. Figure is adapted from T. Rasse.

Wishful thinking (Wit) has been described as the *Drosophila* ortholog of vertebrate type II BMP-receptor (Aberle et al., 2002, Marques et al., 2002). Saxophone (Sax) und Thick veins (Tkv) are the *Drosophila* orthologs to the vertebrate type I BMP-receptors. The protein mothers against decapentaplegic (Mad) is the *Drosophila* R-Smad, while Medea has been described as a Co-Smad. Glass bottom boat acts as a ligand in the *Drosophila* BMP signaling pathway. It is expressed at the *Drosophila* NMJ presynaptically and postsynaptically (McCabe et al., 2003). Postsynaptic release of Gbb by the muscle activates the presynaptically located type II receptor Wit (McCabe et al., 2003), which in turn activates the type I receptors Tkv or Sax. Upon phosphorylation of Mad (pMad) by activated Tkv or Sax, pMad forms a

complex with Medea and translocates to the nucleus to act as a transcription factor (Raftery and Sutherland, 1999).

Alterations in BMP signaling have been implicated as a possible pathogenic mechanism in animal models of motor-neuron diseases such as HSP (Wang et al., 2007, Tsang et al., 2009, Fassier et al., 2010), spinal bulbar muscular atrophy (SBMA) (Katsuno et al., 2010) and ALS (Nakamura et al., 2008).

2.3.3.3.2 Alterations of BMP signaling in HSP

The HSP-associated proteins Atlastin, Spastin, NIPA1 and Spartin have all been shown to be negative regulators of BMP signaling. Knockdown or loss of the proteins Atlastin (Fassier et al., 2010), Spastin (Tsang et al., 2009), NIPA1 (Wang et al., 2007, Tsang et al., 2009), and Spartin (Tsang et al., 2009) lead to an upregulation of BMP signaling in vertebrates (Tsang et al., 2009, Fassier et al., 2010) and invertebrates (Wang et al., 2007). Interestingly two of these proteins, Atlastin and Spastin, are involved in membrane modeling events. These proteins might cause changes in BMP signaling via altered BMP receptor trafficking (Blackstone et al., 2011). Alterations of BMP signaling might be a unifying mechanism of axonopathy in some classes of HSP (Blackstone et al., 2011).

2.3.3.4 Motor-neurons critically depend on efficient axonal transport

2.3.3.4.1 Axonal transport and axonopathy

Motor-neurons are highly specialized cells with long axons, which can reach up to 1 m in humans. The axon connects the soma of the cell to the distant synaptic site. As syntheses of proteins and lipids takes place almost exclusively in the soma, the motor-neuron depends on anterograde transport to supply the axon and the synapses with the synthesized material and organelles (Holzbaur, 2004). Retrograde transport is required to return damaged organelles to the cell body and to transport signaling molecules from the synapses to the soma of the cell. Maintenance and function of the axons of motor-neurons critically depend on efficient axonal transport.

Several studies identified mutations that affect axonal transport as the cause for different hereditary forms of motor-neuron diseases, thereby linking defects in axonal transport to motor-neuron degeneration (Ikenaka et al., 2012). As a result of disturbed axonal transport diverse cargos of motor proteins are accumulated in degenerated motor-neurons and are a pathological hallmark of various motor-neuron diseases.

In ALS patients, abnormal accumulation of neurofilaments, damaged mitochondria, and the presence of autophagosomes in motor-neurons suggest a role for axonal transport defects in disease pathogenesis (Ikenaka et al., 2012). In the spinal motor-neurons of SBMA patients and transgenic model mice *Dynactin-1*, an activator complex necessary for efficient axonal transport, is down regulated; in addition abnormal accumulations of neurofilaments and synaptic proteins were observed in the distal part of the axons of the SBMA model mice (Katsuno et al., 2006). From autopsies of human SPG4 HSP patients (Kasher et al., 2009) and mouse models of

SPG4 (Spastin) (Kasher et al., 2009) and SPG7 (Paraplegin) (Ferreirinha et al., 2004) axonal swellings have been reported. Thus axonal transport defects also emerge as a possible pathogenic mechanism in HSPs (see next paragraph).

Axonal swellings and an accumulation of cargo of anterograde and retrograde transport were also found in *Drosophila* larvae that carried mutations in the kinesin heavy chain (Khc) of the motor protein kinesin-1. In addition the diameter of an individual axon was found to be increased in diameter up to 10-fold within a micron (Hurd and Saxton, 1996b). These Khc mutations did not only disturb anterograde and retrograde transport, but also impaired development of the NMJs (Hurd and Saxton, 1996b). Furthermore, they caused distal paralysis of the *Drosophila* larvae, presumably due to a reduction in transmission, which was more severe in the longer axons, innervating the distal ventral muscles of the larvae (Hurd and Saxton, 1996b).

Thus, the function and viability of motor-neurons in vertebrates as well as in invertebrates critically depend on efficient axonal transport.

2.3.3.4.2 A role of axonal transport in the pathophysiology of HSP

In HSP disturbed axonal transport is also hypothesized as a possible mechanism of pathology. The most direct evidence comes from *SPG10* (see paragraph 2.3.4), encoding the motor protein KIF5A. Almost all HSP-associated mutations found in *SPG10* are located to the motor domain of the protein (Reid et al., 2002, Schule et al., 2008). Therefore, it has been proposed that the mutations may impair axonal transport because the affected kinesins have lower microtubule binding affinity, move slower along the microtubules and compete for cargo with unaffected motors (Ebbing et al., 2008), thereby reducing net cargo transport along the axon to the synapses. It was shown that a HSP-related mutation in KIF5A reduced the transport frequency of

neurofilaments along axons in both the anterograde and retrograde direction in cultured mouse cortical neurons (Wang and Brown, 2010). In cultured cortical neurons derived from mice lacking Spastin (SPG4) (Tarrade et al., 2006, Kasher et al., 2009), a reduction of anterograde transport frequency of mitochondria was observed. Furthermore, mutations in other *SPGs* that cause disturbed membrane modeling or mitochondrial dysfunction are postulated to affect axonal transport (Blackstone et al., 2011).

2.3.4 Spastic Paraplegia Gene 10

One of the HSP-associated genes identified is *Kif5a*, encoded by *SPG10* (Reid et al., 2002). KIF5A is the kinesin heavy chain of a neuron-specific form of kinesin-1, a motor protein involved in intracellular long-distance anterograde transport (see paragraph 2.3.4.1).

Mutations in the *SPG10* locus account for 3% of autosomal dominant HSP cases in European families (Schule et al., 2008). *SPG10* mutations can emerge in a clinically pure and complicated form of HSP (Schule et al., 2008) and the age of onset can vary from early childhood to the third decade of life (Schule et al., 2008).

To date, 21 mutations in *SPG10* have been described (Reid et al., 2002, Fichera et al., 2004, Blair et al., 2006, Lo Giudice et al., 2006, Schule et al., 2008, Tessa et al., 2008, Goizet et al., 2009, Crimella et al., 2011, Musumeci et al., 2011) 19 of which localize to the motor domain of KIF5A. One mutation was shown to localize to the neck region (Lo Giudice et al., 2006), adjacent to the globular motor domain. Recently the first HSP-associated *SPG10* mutation, located in the stalk domain of KIF5A was identified (Crimella et al., 2011).

2.3.4.1 The motor protein Kinesin-1

Kinesins are molecular motors primarily responsible for anterograde microtubule-based transport in neuronal and in non-neuronal cells. Within neurons kinesins transport cargo from the soma along the plus end of the microtubules to the synapse. Retrograde transport from the synapse to the soma is accomplished mainly by dyneins. During movement along microtubules ATP is hydrolyzed by the motor proteins and the released energy is used to generate movement force. In mammals, the kinesin superfamily consists of approximately 45 members (KIFs) grouped into 14 subfamilies (Duncan and Goldstein, 2006).

Kinesin-1/KIF5, formerly referred to as conventional kinesin, was the first member of the kinesin superfamily that was discovered and is responsible for anterograde transport in neuronal and non-neuronal cells. Kinesin-1/KIF5 motors are heterotetramers that are composed of two kinesin heavy chains (Khc), which are responsible for motor activity, and two kinesin light chains (Klc), which are involved in cargo association. The kinesin heavy chain is comprised of an N-terminal head domain, an α-helical stalk domain and a C-terminal tail domain (Bloom et al., 1988, Yang et al., 1989). The globular N-terminal head domain contains the ATP-binding motif and a microtubule binding domain. It is attached via a neck region to an α-helical stalk, that is responsible for dimerization with another heavy chain. The C-terminal tail domain interacts with the Klcs (Vale and Fletterick, 1997).

The vertebrate genome contains three Khc isoforms (KIF5A, KIF5B and KIF5C) and three Klc isoforms (KLC1, KLC2, KCL3). KIF5B, KLC1 and KLC2 are expressed ubiquitously, whereas KLC3 is expressed in a testis specific manner (Junco et al., 2001). KIF5A and KIF5C are expressed specifically in neurons (Niclas et al., 1994, Kanai et al., 2000).

The *Drosophila* genome contains one Khc isoform and one isoform of Klc, which are ubiquitously expressed (Yang et al., 1988). The *Drosophila* Khc shows high structural similarities to the vertebrate Khc. Alignment of the Khc protein across species (*Danio rerio* (Dr), *Tribolium castaneum* (Tc), *Xenopus tropicalis* (Xt), *Drosophila melanogaster* (Dm), *Homo sapiens* (Hs) and *Rattus norvegicus* (Rn)) shows unique conservation of the amino acids spanning from the ATP-(β-sheet 7: Figure 7, blue arrow) to the microtubule-binding site (α-helix 4: Figure 7, green box) of Khc (Kozielski et al., 1997). HSP-associated pathological mutations (red dots) are highly enriched in this sequence, termed loop 11 (L11) (Figure7). Given the essentially 100% conservation of this structure between human KIF5A and *Drosophila* Khc, we suggest that *Drosophila* is a suitable model for the analysis of *SPG10* mutations. The human mutations at position 253 (blue star) and position 256 (red star) of the protein were selected for this purpose.

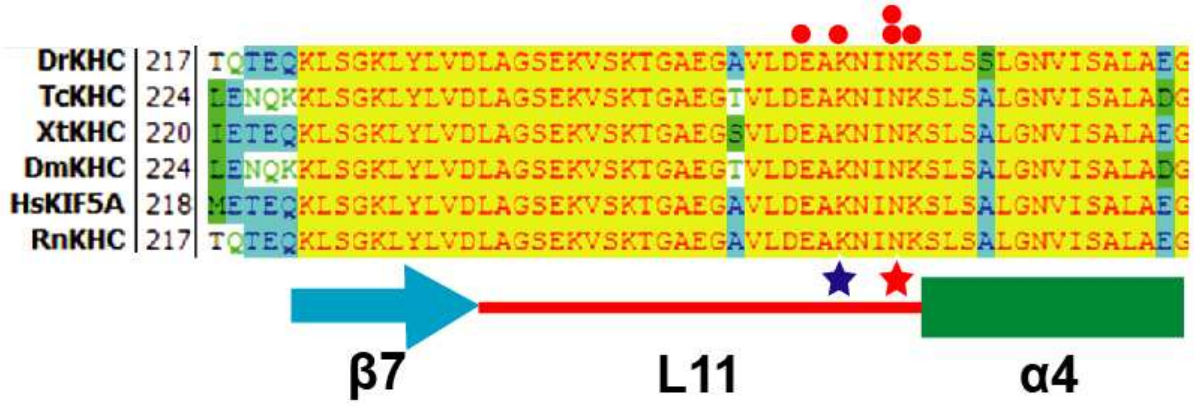

Figure 7: Alignment of loop 11 of kinesin heavy chain across species

Khc protein alignment across species shows high conservation of loop 11. (Figure was kindly provided by V. Sreekumar)

The amino acid exchange K253N in human KIF5A corresponds to the amino acid exchange K259N in *Drosophila* Khc (Figure 7, blue star) and the amino acid

exchange N256S in KIF5A to the amino acid exchange N262S in *Drosophila* Khc (Figure 7, red star). In the following the mutations will be named according to their position in the *Drosophila* Khc (Khc^{N262S} and Khc^{K259N}).

2.4 Previous work

To generate the Khc constructs UAS-Khc^{K259N} and UAS-Khc^{N262S}, the amino acid lysine (K) was exchanged to asparagine (N) at position 259 (K259N) and asparagine (N) was exchanged to serine (S) at position 262 (N262S) in a full-length wild-type *Drosophila* Khc. To this, site-directed mutagenesis was used to exchange the nucleotides 777G>T (corresponding to amino acid exchange K259N) and 785A>G (corresponding to amino acid exchange N262S) in a full-length wild-type *Drosophila khc* cDNA (SD02406), which was then inserted into a modified pUAST attB vector. To generate the control construct UAS-Khc^{wt}, full-length wild-type *khc* was also inserted into the vector. For generation of UAS-$Khc^{truncwt}$ and UAS-$Khc^{truncN262S}$, wild-type and mutated (containing nucleotide exchange 785A>G) full-length *Drosophila khc* cDNA, were truncated and inserted into the modified pUAST attB vector. The truncated constructs contain only the 401 N-terminal amino acids of Khc and lack the C-terminal tail and most of the stalk domain. Truncated Khc_{401} is still able to dimerize and move processively along microtubules, but unable to bind cargo (Seitz and Surrey, 2006, Sung et al., 2008).

Transgenic flies were created by BestGene (Chino Hills, USA) using integrase-mediated site-specific transgenesis at cytological position 86F (Fly strain BDSC 23648). Site-specific integration assures equal expression levels of the different constructs, thereby enabling comparative analysis of different mutations in the same protein.

2.5 Objectives

In this thesis the *Drosophila melanogaster* NMJ is used as a model system to study mechanisms of neurodevelopment and degeneration. The work of this thesis can be divided into two parts. In the first part the impact of PP2A on the development of individual synapses at the *Drosophila* NMJ is investigated. This was done in collaboration with the group of Prof. A. DiAntonio, Department of Developmental Biology, Washington University School of Medicine, St. Louis, Missouri, USA.

The second and central part of this thesis focuses on the establishment of a *Drosophila* model to study the degenerative motor-neuron disease HSP. The aim is to establish a *Drosophila* model of the HSP subtype SPG10. Therefore, the HSP-related point mutation N256S in human KIF5A (N262S in *Drosophila* Khc) is selected to characterize synaptic and axonal phenotypes, gain insight into potential pathogenic mechanisms that cause degeneration and decipher possible pathways involved in disease progression. To model SPG10 in *Drosophila* two approaches are used. Ectopic expression of mutated Khc (Khc^{N262S}) is induced either alone or in combination with wild-type Khc ($Khc^{wt+N262S}$) in the wild-type background. In the former model the amount of mutated Khc^{N262S} exceeds the endogenous wild-type Khc, due to the over-expression of Khc^{N262S}. In the latter model the ratio of mutated Khc to wild-type Khc is shifted; in this model more wild-type Khc is available, due to the two copies of endogenous wild-type Khc and the additional expression of Khc^{wt}. The two approaches are chosen to study the impact of the ratio of mutated Khc to wild-type Khc in the establishment and progression of HSP pathology-like characteristics in the *Drosophila* model.

Furthermore a comparative analysis of the SPG10 mutations K253N (K259N in *Drosophila* Khc) and N256S (N262S in *Drosophila* Khc) is started. These mutations

displayed different characteristics when analyzed *in vitro* (Ebbing et al., 2008). We want to clarify whether the differences in biophysical qualities of Khc *in vitro* caused by the two mutations might result in different phenotypic characteristics in the *Drosophila* model.

III. Materials and methods

3.1 Chemicals

All chemicals were purchased from Roth (Karlsruhe, Germany), Sigma (St. Louis, USA) or Aplichem (Darmstadt, Germany), if not stated otherwise.

3.2 *Drosophila melanogaster*

3.2.1 Maintenance of fly stocks

Flies were maintained at 25℃ in plastic bottles (G reiner Bio-One) on standard fly medium (0.8% agar, 14.3% dried yeast, 10% soy flour, 21.3% treacle, 8% malzin, 8% corn meal, 0.63% propionic acid) seeded with fresh yeast. For fly strains used in this study, see Table 2. The transgenic stocks UAS-Khc^{wt}, UAS-Khc^{N262S}, UAS-Khc^{K259N}, UAS-Khc^{truncwt} and UAS-Khc^{truncN262S} were created by BestGene (Chino Hills, USA) using integrase mediated site-specific transgenesis at cytological position 86F (Fly strain BDSC 23648).

The strain white^{1118} (w^{1118}) is a null mutant of the *white* gene. To obtain the *white* null, exon 1of the gene was deleted. This strain is a common strain used for germ line transformation of *Drosophila melanogaster*. In this study the strain w^{1118} is used for control crosses to the Gal4-driver lines.

Wild-type	Genetics	Donor/ BDSC number	Reference
w^{1118}	$w^{-}/w^{-};+/+;+/+$		(Castiglioni, 1951)
Allele	**Chromosome**		
khc^{8}	III	BL 1607	(Saxton et al., 1991)
khc^{13314}	III	BL 11084	(Spradling et al., 1999)
Gal4-Driver			
D42-Gal4	III	BL 8816	(Gustafson and Boulianne, 1996)
D42-Gal4, UAS-mito-GFP	III	B. Saxton	
elav^{C155}-Gal4; tub-gal80^{ts}	X;II		(Lin and Goodman, 1994) (McGuire et al., 2004)
IIA-C-GFP-genomic;elav-Gal4	II, III		(Rasse et al., 2005)
UAS-Construct			
UAS-dnMts	III		(Hannus et al., 2002)
UAS-mito-GFP	II	BL 8442	(Horiuchi et al., 2005)
UAS-Khc^{wt}	III		This study
UAS-Khc^{N262S}	III		This study
UAS-Khc^{K259N}	III		This study
UAS-Khc^{truncwt}	III		This study
UAS-Khc^{truncN262S}	III		This study
Exon-Trap Line			
dlg-GFP	X	Flytrap CC01936	(Buszczak et al., 2007)

Table 2: Fly strains used in this study.

3.2.2 Flies used for Western Blot analysis

Transgenic male flies carrying either UAS-Khc^{N262S} or UAS-Khc^{wt} were crossed to female flies carrying the pan-neural elav^{C155}-Gal4 driver and a ubiquitously driven temperature sensitive Gal80 construct (tub-Gal80^{ts}). Flies of the following genotypes (y/elav^{C155}-Gal4;tub-Gal80^{ts}/+;+/+, y/elav^{C155}-Gal4;tub-Gal80^{ts}/+;Khc^{N262S}/+ and y/elav^{C155}-Gal4;tub-Gal80^{ts}/+;Khc^{wt}/+) were raised and allowed to hatch at a permissive temperature of 18℃, preventing the expr ession of the UAS-constructs. Within 24 hours after hatching male flies (to guarantee equal expression levels of x-chromosomal elav^{C155}-Gal4) were transferred to a restrictive temperature of 29℃, enabling the expression of the UAS-constructs. Flies were kept at 29℃ for 13 days and subsequently frozen at -80℃.

3.2.3 *Drosophila* larvae used for analysis

For all experiments UAS-Khc^{wt}, UAS-Khc^{N262S} or UAS-Khc^{N262S} combined with UAS-Khc^{wt} (UAS-Khc$^{wt+N262S}$), UAS-Khc^{K259N}, UAS-Khc^{truncwt} and UAS-Khc^{truncN262S} were expressed in a wild-type background using the motor-neuron specific driver D42-Gal4 (Sanyal, 2009). As an additional control D42-Gal4 was crossed into a wild-type (w^{1118}) background. Flies carrying the *khc* mutant alleles *khc*^{8} and *khc*^{13314} were used to create *khc* null heterozygous (*khc*^{8}/+) and homozygous (*khc*^{8}/*khc*^{13314}) larvae. The *khc*^{8} (Saxton et al., 1991) allele carries an ethylmethansulfonat (EMS) induced point mutation (C948T) introducing an early stop codon into the *khc* gene (R210STOP). In *khc*^{13314} the *khc* gene is disrupted by the introduction of the transposon P{lacWkhc13314} at position 2R:12159268 in minus orientation. The cytological map location is 53A3-5. This allele was created in the Berkley Drosophila Gene Disruption Project (Spradling et al., 1999).

In Table3 the genotypes of the flies and the abbreviations used in this thesis are listed.

Genotype	Named as
w^{-}/w^{-};+/+;D42-Gal4/+	D42
w^{-}/w^{-};+/+;D42-Gal4/UAS-Khc^{wt}	D42>Khc^{wt}
w^{-}/w^{-};+/+;D42-Gal4,UAS-Khc^{wt}/UAS-Khc^{N262S}	D42>$Khc^{wt+N262S}$
w^{-}/w^{-};+/+;D42-Gal4/UAS-Khc^{N262S}	D42>Khc^{N262S}
w^{-}/w^{-};+/+;D42-Gal4/UAS-Khc^{K259N}	D42>Khc^{K259N}
w^{-}/w^{-};+/+;D42-Gal4/UAS-$Khc^{truncN262S}$	D42>$Khc^{truncN262S}$
w^{-}/w^{-};+/+;D42-Gal4/UAS-$Khc^{truncwt}$	D42>$Khc^{truncwt}$
w-/w-;khc^{8}/+;+/+	$Khc^{+/-}$
w-/w-;khc^{8}/khc^{13314};+/+	$Khc^{-/-}$

Table 3: Genotypes of flies used for analysis in this study.

3.3 Behavior Analysis

3.3.1 Imaging of tail-flipping phenotype

(Imaged by Vrinda Sreekumar)

To monitor the tail-flipping phenotype, individual larvae were placed on a thin slice of apple juice agar. Tail-flipping was examined at 25°C at 50% humidity by using a DCM510 (ScopeTek, P.R. China) camera integrated in a custom-built stereomicroscope. Videos were recorded at a frame rate of 30 frames per second (fps) for 5 min and then converted into avi format by using a Prism Video Converter, v 1.61 (NCH Software Inc., Australia). Next, images were cropped and compressed by using VirtualDub 1.9.10 (http://www.virtualdub.org/).

3.3.2 Larval locomotion assay

For imaging and quantification of larval locomotion behavior, an algorithm was developed in our lab by the diploma student Michael Knopp on the basis of the software Worm tracker & Track Analyzer (Miriam B. Goodman Daniel Ramot. Worm Tracker & Track Analyzer. Department of Molecular and Cellular Physiology at Stanford University).

This algorithm can be divided into two parts. (1) The larval tracker, which identifies and tracks individual larvae within a movie. (2) The track analyzer, which analyzes the movies and returns the area and the velocity of single larvae. For detailed information about larval tracking and track analysis see (Systematische Identifizierung von Genen, die zur Stabilisierung von Synapsen beitragen; Diploma Thesis, Michael Knopp, HIH 2008) (Knopp, 2008).

3.3.2.1 Quantification of larval size and locomotion speed

Analysis of the movies returns the area and the velocity of single larvae. The area of the larvae is given in [pixel] and the velocity in [pixel/sec]. For comparative analysis of the different genotypes the larval length in [mm] (Formula 2) and the velocity in [mm/s] (Formula 1) are to be calculated.

For these calculations the following formulas were used:

(1) $Velocity\ [mm/sec] = velocity\ [pixel/sec] * pixel\ width\ [mm]$

(2) $Larval\ lenght\ [mm] = \sqrt{3.5 * larval\ area\ [pixel]} * pixel\ width\ [mm]$

The pixel width [mm] required for both formulas is calculated from the known resolution of the detected region by the camera and the defined height of the camera (see Figure 9A).

For calculation of larval length from larval area the width to length ratio of filmed larvae had to be determined first. To this larvae of a defined length were filmed. From this a width to length ratio of 1:3.5 was determined on average (Figure 8). Using this ratio formula 2 was established.

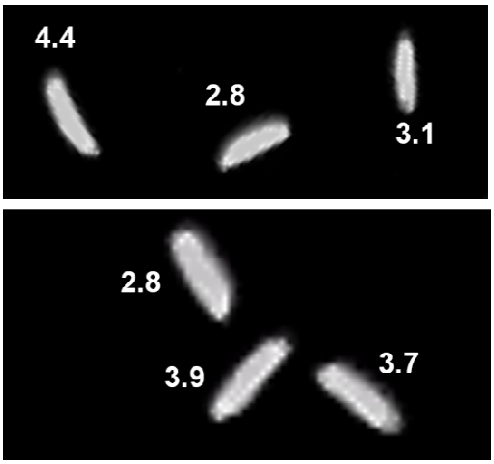

Figure 8: Width to length ratio of filmed larvae
Width to length ratio of filmed larvae was determined to calculate the length of the larvae from the larval area returned after analysis of the movies. Illustrated are six larvae.

For analysis the length and the average velocity of the larvae were calculated and larvae were grouped according to their size (small (1-3 mm) and large (3-5 mm)) for each movie. To eliminate dead or injured larvae from analysis, larvae whose velocity was less than 10% of average velocity of the respective genotype and size group were excluded from analysis. Eight movies per genotype were analyzed. For statistical analysis n was defined as the number of movies analyzed.

3.3.2.2 Performance of larval locomotion assay

For the larval locomotion assay larvae were raised at 25℃ and 3 and 4-days old larvae were combined for analysis. Larvae were cleaned by using a 15% sucrose solution. After washing, larvae were kept in a closed petri dish, containing agar, for 45 minutes at a room temperature of 25℃ and 50% hu midity, to adapt larvae to test conditions. To analyze larval locomotion speed, around 100 larvae were placed on a 15 × 15 cm agar plate and a 10min movie was recorded with a frame rate of 5 fps and a resolution of 1280 x 960 pixels (Figure 9A). After recording, the movies were compressed to a frame rate of 1 fps using VirtualDub 1.9.10 (http://www.virtualdub.org/). Finally the movies were tracked (Figure 9 B, B^{I}-E^{I}) and tracks were analyzed, returning the area and the velocity of single larvae. If larvae collided tracking of these larvae stopped and new tracks were started after larvae separated again.

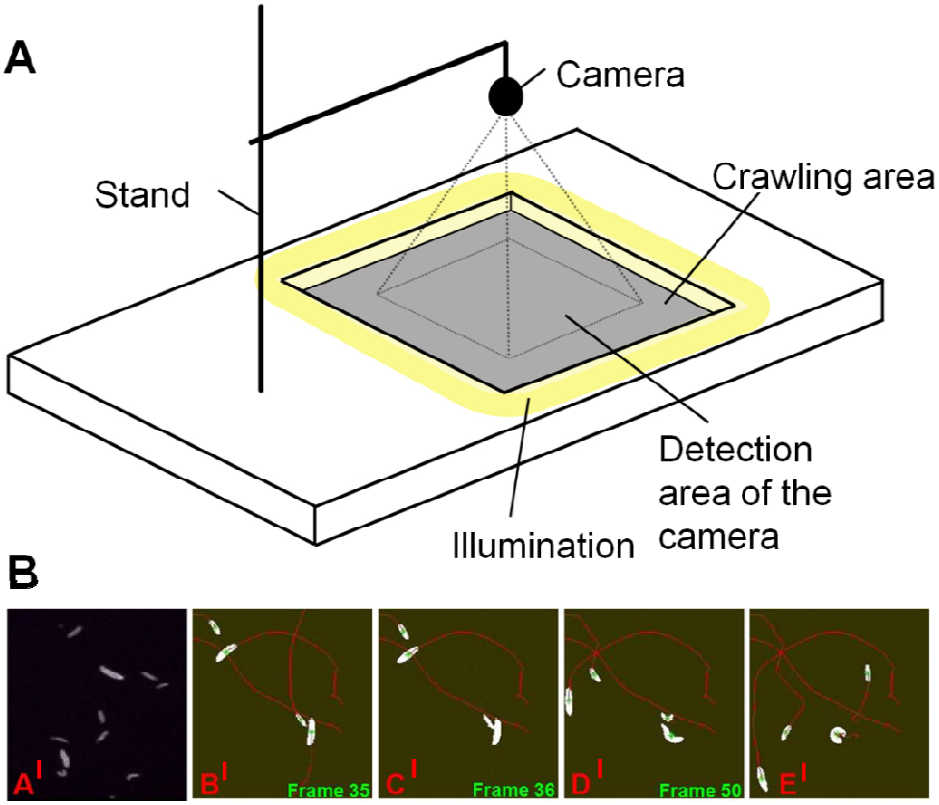

Figure 9: Recording and tracking of larval locomotion.

(A) Assembly to record larval locomotion. Figure is adapted from (Knopp, 2008). (B) Tracking of larval locomotion after compression of the movies. For details on performance see main text.

3.4 Biochemical analysis

3.4.1 Sample preparation for Western Blot

For sample preparation whole flies were frozen at -80℃ for at least 4 h. Fly heads were removed on ice and collected in a 1.5 ml Eppendorf tube on ice. Fly heads were homogenated in buffer (65 mM Tris pH 6.8, 5% (w/v) SDS, 1x Protease Inhibitor (Roche)) (2 µl/head) using a plastic pistil (Roth, Karlsruhe, Germany). Samples were extracted at room temperature for 10 min, boiled at 95℃ for 15 min and subsequently centrifuged for 10 min at 4℃ at 10.000 g. The supernatant was transferred into a new Eppendorf tube and Laemmli sample buffer (240 mM Tris-Cl,

pH 6.8, 6% SDS, 30% Glycerol, 16% β-Mercaptoethanol, 0.06% Bromphenol Blue) was added to a 1x final concentration. Samples were stored at -20℃.

3.4.2 Western Blot analysis

For Khc detection, samples were boiled at 95℃ for 5 minutes before loading on the gel. Khc expression was analyzed by standard SDS-PAGE on a 7.5 % acryl amide gel. Gel run was performed at 100 V for around 90 minutes. Proteins were transferred onto nitrocellulose membrane (Millipore, Eschborn, Germany) by semi-dry blotting and visualized by chemiluminescence (1 ml Solution A + 100 µl Solution B + 0.3 µl H_2O_2, incubated for 2 min). Chemiluminescence was visualized using a film (Kodak XAR) or an image acquisition system (Fusion FX7, Vilber Lourmat, Marne-la-Vallée, France).

The following buffers and solutions were used:

2x Stacking gel buffer, pH 6.8: 250 mM Tris, pH 6.8; 7 mM SDS

5x Separation gel buffer, pH 8.8: 1.86 M Tris, pH 8.8; 17 mM SDS

10x Running buffer: 192 mM glycine; 25 mM Tris; 0.1% SDS

1x Transfer buffer, pH 8.5: 192 mM glycine; 25 mM Tris; 10% methanol

Solution A: 50mg of Luminol to 200 ml of 0,1 M Tris HCl pH 8,6

Solution B: 11mg p-Hydroxycumarinsäure in 10 ml DMSO

For protein detection the following antibodies were used (Table 4):

Primary Antibodies

Antigen	*Antibody*	*Host*	*Dilution*	*Donor*	*Reference*
Khc	SUK4	mouse	1:100	DSHB*	(Ingold et al., 1988)
β-Tubulin	E7	mouse	1:500	DSHB	(Klymkowsky et al.,

Secondary Antibodies				
Antigen	***Coupled to***	***Host***	***Dilution***	***Source***
Mouse	HRP	goat	1:2000	Santa Cruz Biotechnology

*DSHB Developmental Studies Hybridoma Bank

Table 4: Primary and secondary antibodies used for western blot analysis.

3.5 Immunohistochemical analysis

3.5.1 Larval body-wall preparation

Third-instar larvae were fixed on a rubber dissection pad with fine insect pins (0.1x10mm, Austerlitz, Slavkov, Czech Republic) and covered with a drop of cold Ca^{2+}-free hemolymph-like solution (HL-3) (NaCl 70 mM, KCl 5 mM, $MgCl_2$ 20 mM, $NaHCO_3$ 10 mM, trehalose 5 mM, sucrose 115 mM, HEPES 5mM, pH adjusted to 7.2). Larvae were opened dorsally along the midline from the posterior to the anterior end with dissection spring scissors (NO.15005-08, Fine Science Tools, Vancouver, Canada). Subsequently, the gut was removed (leaving the ventral nerve cord and segmental nerves if required for analysis) with fine forceps (A1 231-20, Fine Science Tools, Vancouver, Canada), the epidermis was stretched and pinned down with two pins on each side. Larvae were fixed in 4% formaldehyde in phosphate buffered saline (PBS) or Bouin´s fixative respectively (For details see Table 5). After removing the fixative with PBS-T (0.05% Triton-X 100 in PBS) larval body wall preparations were kept in PBS-T.

3.5.2 Immunostaining

After 30 min of blocking with 5% normal goat serum (NGS) in PBS-T, the PBS-T/NGS solution was refreshed; primary antibodies were added and incubated over night at 4℃. The next day the samples were washed twice shortly and three times for 20 min with PBS-T. Secondary antibodies were applied in PBS-T with 5% NGS and incubated at room temperature for two hours. Larval preparations were washed again (twice shortly and three times for 20 min) and mounted on a glass object slide using VectaShield Mounting Medium (Vector Laboratories, Burlingame, USA).

For immunohistochemistry the following antibodies were used (Table 5):

Primary Antibodies

Antigen	*Antibody*	*Host*	*Dilution*	*Fixation*	*Donor*	*Reference*
Bruchpilot	Nc82	mouse	1:100	10min PFA	DSHB*	(Wagh et al., 2006)
CSP	DCSP-2	mouse	1:50	10min PFA	DSHB	(Zinsmaier et al., 1994)
Even-skipped	3C10	mouse	1:10	30min PFA	DSHB	(Doe et al., 1988)
Futsch	22C10	mouse	1:150	2min Bouin´s	DSHB	(Hummel et al., 2000)
GFP	3E6	mouse	1:500	10min PFA	Molecular Probes	
GluRIIC		rabbit	1:2000	10min PFA	S. Sigrist	(Qin et al., 2005)
Khc	SUK4	mouse	1:20	10min PFA	DSHB	(Ingold et al., 1988)
pMad	PS1	rabbit	1:500	30min PFA	P. ten Dijke	(Persson et al., 1998)
α-Tubulin	12G10	mouse	1:10	2min Bouin´s	DSHB	(Thazhath et al., 2002)
acetylated–α –Tubulin	6-11B-1	mouse	1:250	2min Bouin´s	Sigma-Aldrich	
Synapsin	3C11	mouse	1:5	3min PFA	DSHB	(Klagges et al., 1996)

Secondary Antibodies				
Antigen	***Coupled to***	***Host***	***Dilution***	***Source***
HRP**	Cy3	goat	1:500	DiAnova
HRP**	Cy5	goat	1:500	DiAnova
mouse	Alexa488	goat	1:500	Molecular Probes
mouse	Alexa568	goat	1:500	Molecular Probes
rabbit	Alexa488	goat	1:500	Molecular Probes
rabbit	Alexa568	goat	1:500	Molecular Probes

Table 5: Primary and secondary antibodies used for immunohistochemistry.
* DSHB Developmental Studies Hybridoma Bank

** Anti-horseradish peroxidase (HRP) is an antibody raised against a plant glycoprotein, which was shown to specifically stain neural tissue in *Drosophila melanogaster* (Paschinger et al., 2009).

3.6 Imaging

3.6.1 *In vivo* imaging

In vivo imaging was essentially performed as described (Rasse, 2004, Rasse et al., 2005, Fuger et al., 2007, Zhang et al., 2010).

3.6.1.1 *In vivo* imaging of glutamate receptor clustering

Imaging of GluR clustering (Results, paragraph 4.1.2) was performed using a Zeiss Axiovert 200M equipped with a LSM510 scanhead and a 40x Plan-Neofluar oil objective (1.3 NA).

To mark GluR clusters for *in vivo* imaging a GFP-tagged *Drosophila* glutamate receptor subunit IIA (GluRIIA-GFP) expressed under the native GluRIIA promoter (Rasse et al., 2005) was used. For neuronal inhibition of PP2A a dominant negative isoform of the catalytic subunit microtubule star (UAS-dnMts) of PP2A was expressed using the pan-neuronal driver elav-Gal4. Larvae were raised at 25℃ and early L3 stage larvae were used for *in vivo* imaging. Time points of imaging were 0 and 6 hours. For analysis formation and retraction of glutamate receptor clusters within these 6 hours of development were quantified.

3.6.1.2 Animal sorting for *in vivo* imaging of axonal transport

For *in vivo* imaging of axonal transport of mitochondria, *Drosophila* larvae expressing mito-GFP, were sorted using a binocular fluorescence microscope (Olympus SZX16, Olympus, Hamburg, Germany) equipped with a GFP filter.

3.6.1.3 *In vivo* imaging of axonal transport of mitochondria

Imaging of axonal transport of mitochondria (Results, paragraph 4.2.1.7) was performed using a Zeiss LSM 710 confocal microscope equipped with a 40x Plan Apochromat objective (1.3 NA).

In *Drosophila* the axons of motor-neurons are bundled in segmental nerves and expand from the motor-neuron cell bodies, located in the ventral nerve cord, to their respective target muscles in the abdominal segments of the larva. These axon bundles are optically easily accessible through the larval body wall.

As density of mitochondria in motor axons is very high, it is difficult to identify and trace single mitochondria. Thus to trace single mitochondria a part of a segmental

nerve was bleached (30µm in length). Subsequently mitochondria moving through this area were imaged. Confocal Z-stacks (Z-planes: 10; voxel size: 100 nm × 100 nm × 1500 nm, pinhole: 1.6 AU, average: 2) were recorded at a frame rate of 2.4 Hz. Movies with residual movement of the segmental nerves were not excluded from the analysis, but aligned using the ImageJ plugin *StackReg* (Philippe Thevenaz, Biomedical Imaging Group, Swiss Federal Institute of Technology Lausanne; www.epfl.ch/thevenaz/stackreg/). This plugin applies a recursive alignment to a stack of images. Each slice is used as the template, with respect to which the next slice is aligned, thus the alignment proceeds by propagation. When the plugin is launched, the current slice acts as a global anchor (www.epfl.ch/thevenaz/stackreg/).
Subsequent quantification of anterograde and retrograde transport rates and speeds was done semi manually, using ImageJ.

3.6.1.4 Generation of Kymographs

Kymographs were extracted from representative movies for each genotype using ImageJ. In case residual movement of the larvae was observed, movies were aligned with the StackReg plugin. Next, the Multiple Kymograph plugin was used to build kymographs.

Kymographs were generated by Josephine Ng.

3.6.2 Imaging of immunostainings

Immunostainings were imaged using a Zeiss LSM 710 confocal microscope equipped with a 40x Plan Apochromat oil objective (1.3 NA). The resolution was adjusted to the size of the objects imaged, but kept constant within one data set. The settings used

were: voxel size: 100 nm × 100 nm × 500 nm for imaging of NMJ and segmental nerves and 200 nm x 200 nm x 500 nm for imaging of the VNC; pinhole: 1 AU, line averaging: 4, if not stated otherwise. Laser intensities were adjusted to one genotype, depending on the analysis to be performed, and kept constant within one data set.

For analysis z-stacks of whole NMJs of muscle 6 and 7 of abdominal segment A2 and A5 (Figure 10), VNCs (Figure 10, light gray structure) or sections of segmental nerves, passing trough segment A4 (Figure 10, arrow) were imaged.

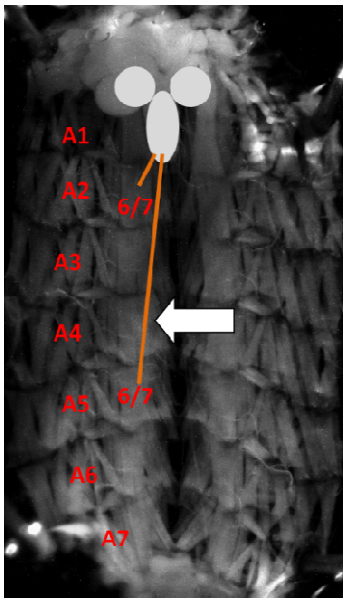

Figure 10: Exemplary picture of a larval body wall preparation.
Highlighted are the structures imaged for different analyses: VNCs (light gray), segmental nerves (orange), NMJs of muscle 6 and 7 of abdominal segments A2 and A5.
(Image of larval body wall preparation was kindly provided by Josephine Ng.)

3.7 Data Analysis

3.7.1 Data Processing

For data processing and analysis ImageJ 1.41o (US National Institutes of Health; http://rsb.info.nih.gov/ij/download.html) was used.

Images, used for illustration purposes only, were processed as follows: (1) A Gaussian filter (radius=2) was applied to the raw data stack. Brightness and contrast were appropriately adjusted (constant within one data set). The relevant slices of the modified stacks were maximum-projected. Projected images were scaled by 2, and gamma adjustment (gamma=0.75) was applied. If necessary, brightness and contrast were adjusted again (constant within one data set).

3.7.2 Quantification of glutamate receptor field size

For the quantification of GluR field sizes data were kindly provided by our collaboration partner Prof. DiAntonio. GluR fields were marked by staining for the GluR subunit IIC. The maximum z-projections of the confocal z-stacks of the IIC channel (Figure 11A) were scaled by a factor of 2 and then used to produce a binary mask (structure of interest is set to 255, background is set to 0) by applying a threshold. This binary mask was then used for manual segmentation to define single GluR fields (Figure 11B). Finally, the binary mask was superimposed (minimum overlay) with the original maximum projections. This returned the original fluorescence intensity values and the signals were analyzed (Figure 11C). The following measurement parameters were therefore activated: area, mean gray value, limit to threshold, minimum size: 10 pixel, maximum size: not restricted, show outlines, display results, exclude on edge particles. The area, denoted in pixels, was converted to μm^2. Finally GluR fields positive and negative for the presynaptic marker Brp (Figure 11D) were determined.

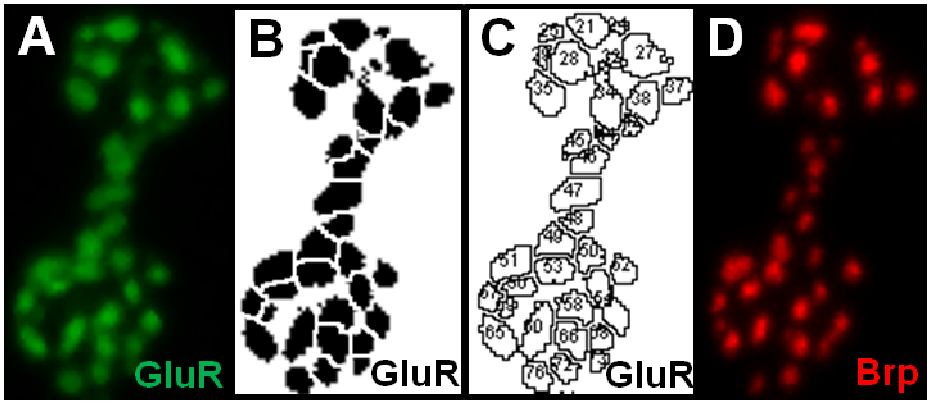

Figure 11: Illustration of quantification of glutamate receptor field sizes.
Sizes of GluR fields, positive and negative for the presynaptic marker Brp were quantified. A section of a NMJ is shown. Maximum z-projections of the confocal z-stacks of the IIC channel (A) were transferred into a binary mask and manually segmented (B).The binary mask (B) was superimposed with the original maximum projections (A) and analyzed (C). Finally Brp positive and negative GluR clusters were determined by comparing quantified GluR clusters to Z-projections of the Brp channel of the same NMJ (D).

3.7.3 Quantitative data analysis

Quantitative image analysis was carried out semi manually using ImageJ 1.41o. Before analysis raw data stacks were filtered, stacks were then maximum projected and projections were scaled by a factor of 2.

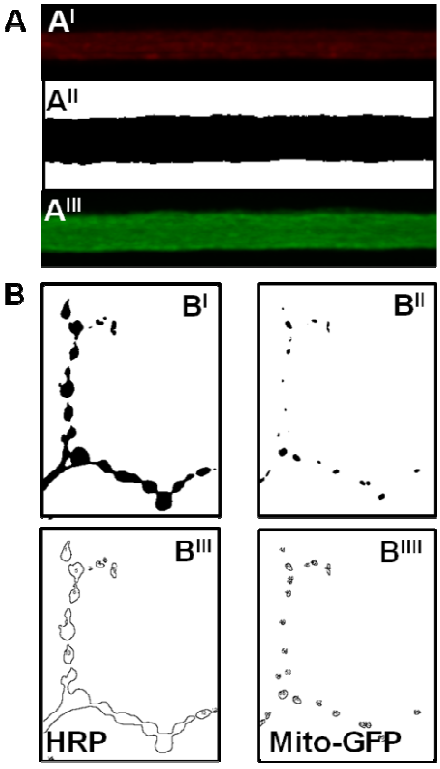

Figure 12: Illustration of quantitative data analysis.
(A) Quantification of total tubulin levels. Projections of the HRP channel (A^{I}) were used to create a binary mask (A^{II}). The binary mask (A^{II}) was then superimposed with the maximum projections of the tubulin (A^{III}) and the resulting image was analyzed.
(B) Quantification of mitochondrial content at the NMJ. To this, maximum projections of the HRP channel as well as the mito-GFP were converted into binary masks ($13B^{I}$ and $13B^{II}$). The areas of the structures were calculated (B^{III} and B^{IIII}) and the ratio of mito-GFP to HRP area was determined.

Quantification of fluorescence intensities in segmental nerves

For quantification of total tubulin (Figure 12A), acetylated tubulin levels and pMad levels in segmental nerves the maximum z-projections of the HRP image stacks (Image 1) (Figure $12A^{I}$) were used to create a binary mask (Image 2) (Figure $12A^{II}$) (structure of interest is set to 255, background is set to 0) by applying a threshold. During the process of thresholding, the individual pixels in the image are marked as "structure of interest" and assigned a value of 255, if their original value equates or is greater than the threshold value applied. If the original value of a pixel is below the threshold value, the pixel is assigned a value of 0 and set to be "background".

The binary masks (Image 2) were then superimposed (minimum overlay) with the maximum z-projections of the tubulin (Figure $12A^{III}$) or pMad channels (Image 3) respectively. This returned the original intensity values of tubulin and pMad (Image 4). Finally, Image 4 was used to analyze the signals using the following parameters:

area, mean gray value, limit to threshold, show outlines, display results. For details on image processing see Table 6.

Channel	*Filter*	*Radius*	*Projected*	*Scaled*	*Threshold value applied to create binary mask*
Quantification of total tubulin levels in segmental nerves					
HRP	mean	3	max*	-	15*
α-tubulin	mean	3	max	-	-
Quantification of acetylated tubulin levels in segmental nerves					
HRP	mean	3	max	-	10
Acetylated α-tubulin	mean	3	max	-	-
Quantification of pMad levels in segmental nerves					
HRP	mean	3	max	-	20
pMad	mean	3	max	-	-

Table 6: Pre processing details for quantification of total tubulin, acetylated tubulin and pMad in segmental nerves.

*max = maximum projection

*****pixels with a value of 15 or greater are marked as "structure of interest" and assigned a value of 255. Pixels with a value below 14, the pixel is assigned a value of 0 and set to be "background".

Quantification of pMad fluorescence intensities in motor-neuron cell bodies

For quantification of pMad levels in motor-neuron cell bodies the Even-skipped (Eve) channel (Image 1) was used to create a three-dimensional binary mask (Image 2), which was subsequently superimposed (minimum overlay) with the pMad channel stack (Image 3). As to avoid misallocation of fluorescence signals from different cell bodies located in differing planes in the z-stack, which might occur in a projected

image, the superimposition was done using a three-dimensional binary mask (Image 2) and the z-stack of the original channel (Image 3). The resulting stack (Image 4) was then maximum projected and pMad fluorescence intensities of aCC and RP2 motor-neurons were analyzed. For details on image processing see Table 7.

Channel	*Filter*	*Radius*	*Projected*	*Scaled*	*Threshold value applied to create binary mask*
Even-skipped	GB*	2	-	-	30
pMad	GB	2	-	-	-

Table 7: Pre processing details for quantification of pMad in motor-neuron cell bodies.
*GB = Gaussian Blur filter

Quantification of mitochondrial density and Futsch innervation at the NMJ

For quantification of mitochondrial density and Futsch area fraction of the NMJ, areas of the respective structures were determined. To this, maximum projections of the HRP (Figure 12B^{I}) channel as well as the mito-GFP (Figure 12B^{II}) and Futsch channel were converted into binary masks. The area of the structures was calculated (Figure 12, B^{III} and B^{IIII}) and the ratio of mito-GFP to HRP (total NMJ) area, as well as Futsch to HRP (total NMJ) area was determined. For details on image processing see Table 8.

Channel	*Filter*	*Radius*	*Projected*	*Scaled*	*Threshold value applied to create binary mask*
Quantification of mitochondrial content at NMJ					
HRP	mean	3	max*	-	25
Mito-GFP	GB*	2	max	-	12
Quantification of Futsch content at NMJ					
HRP	mean	3	max	-	35
Futsch	mean	3	max	-	70

Table 8: Pre processing details for quantification of mitochondrial and Futsch content at the NMJ.

*GB = Gaussian Blur filter. *max = maximum projection

3.7.4 Quantification of synapses

For quantification of synapses, Brp puncta were counted using the Delta 2D software (Decodon GmbH, Germany), that was originally designed to identify spots on 2D gels. The applicability of this software to our objects and the adequate pre processing of the images was tested before, by the rotation student Nina Dräger in our lab (Impact of different kinesins on synaptic plasticity in *Drosophila*, Lab report by Nina Draeger (Draeger, 2009)). To find the adequate way of pre processing confocal z-stacks were maximum projected and different pre processing steps were tried out (Figure 13).

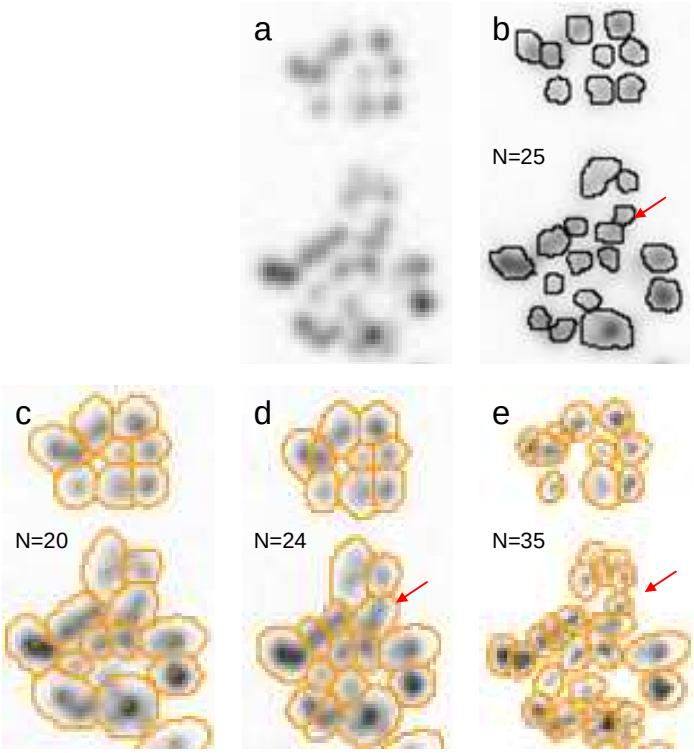

Figure 13: Automated counting of synapses

Analysis of Brp puncta with Delta-2D software differently pre-processed in scale, Gaussian blur filter, and threshold, n = number of counted Brp puncta. **(a)** Gaussian blur filter 1 **(b)** Scale 2, Gaussian blur filter 2, manual analysis **(c)** Scale 2, Gaussian blur filter 1, analysis with Delta2D **(d)** Scale 2, Gaussian blur filter 2, analysis with Delta2D **(e)** Scale 2, threshold 20, analysis with Delta2D

Figure is taken from (Draeger, 2009).

The automated analysis of Brp with Delta2D software differed from manual counting, depending on the pre processing steps applied (Figure 13). The pre processing steps used for the image shown in Figure 13D rendered nearly the same results than manual counting. Thus datasets for automated Brp counting were pre processed in the following way using Image J: Z-stacks were maximum projected, scaled by a factor of two and Gaussian blur filter (radius two) was applied. In the Delta2D software the following parameters were adjusted: background 100; spot size 10; sensitivity 20.

To account for possible differences in larval size counted synapses were normalized to the surface of muscle 6/7 of segment A2 and A5, respectively (Formula 1).

$$(1) Normalized\ synapse\ number = \frac{synapse\ number}{muscle\ surface\ [\mu m^2]} * average\ muscle\ surface\ w^{1118}\ [\mu m^2]$$

Normalization to the muscle surface was also applied to the quantification of NMJ area (Formula 2).

$$(2) Normalized\ NMJ\ area = \frac{NMJ\ area\ [\mu m^2]}{muscle\ surface\ [\mu m^2]} * average\ muscle\ surface\ w^{1118}\ [\mu m^2]$$

3.7.5 Quantification of presynaptic degeneration

To quantify presynaptic degeneration the synaptic footprint assay was used (Introduction, paragraph 2.1.2) and the analysis was modified (see next paragraph). The ratio of presynaptic Synapsin (Syn) area to Dlg area, as well as presynaptic neuronal membrane area (HRP) to Dlg was determined. Importantly no widening of Dlg in any of the analyzed genotypes was observed (Figure 14), which might have introduced a bias into analysis.

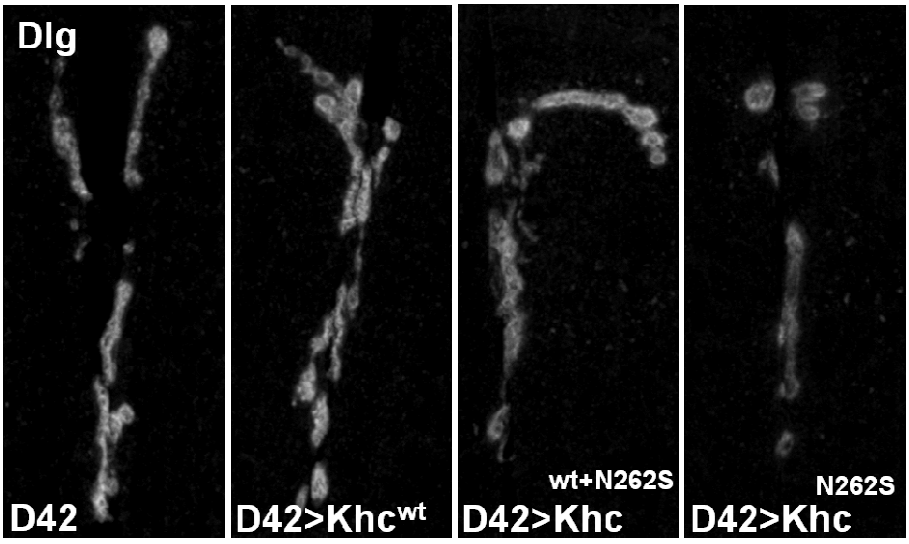

Figure 14: Postsynaptic discs large.
Discs large is not widened in D42>Khc$^{wt+N262S}$ and D42>Khc^{N262S} animals compared to controls.

Performance of analysis

For quantification of the ratio of presynaptic Syn and neuronal membrane area to Dlg maximum z-projections of the image stacks of all three channels were converted into binary masks. The Syn and neuronal membrane binary mask were superimposed (AND overlay) with the Dlg binary mask, to eliminate presynaptic structures which did not co-localize with Dlg. From these resulting binary masks (Figure 15A - B, Dlg, HRP, Syn), the area of the respective structures was calculated and the ratio of Syn to Dlg area, as well as neuronal membrane to Dlg area was determined. An exemplary overlay of the HRP and Dlg mask, as well as of the Syn mask with the Dlg mask for a control and a mutant genotype (Figure 15A - B) shows that there is a change in the ratio of presynaptic Syn and neuronal membrane area to Dlg area in D42>Khc^{N262S} animals compared to D42 and that the method is suited for analysis of degeneration. For details on image processing see Table 9.

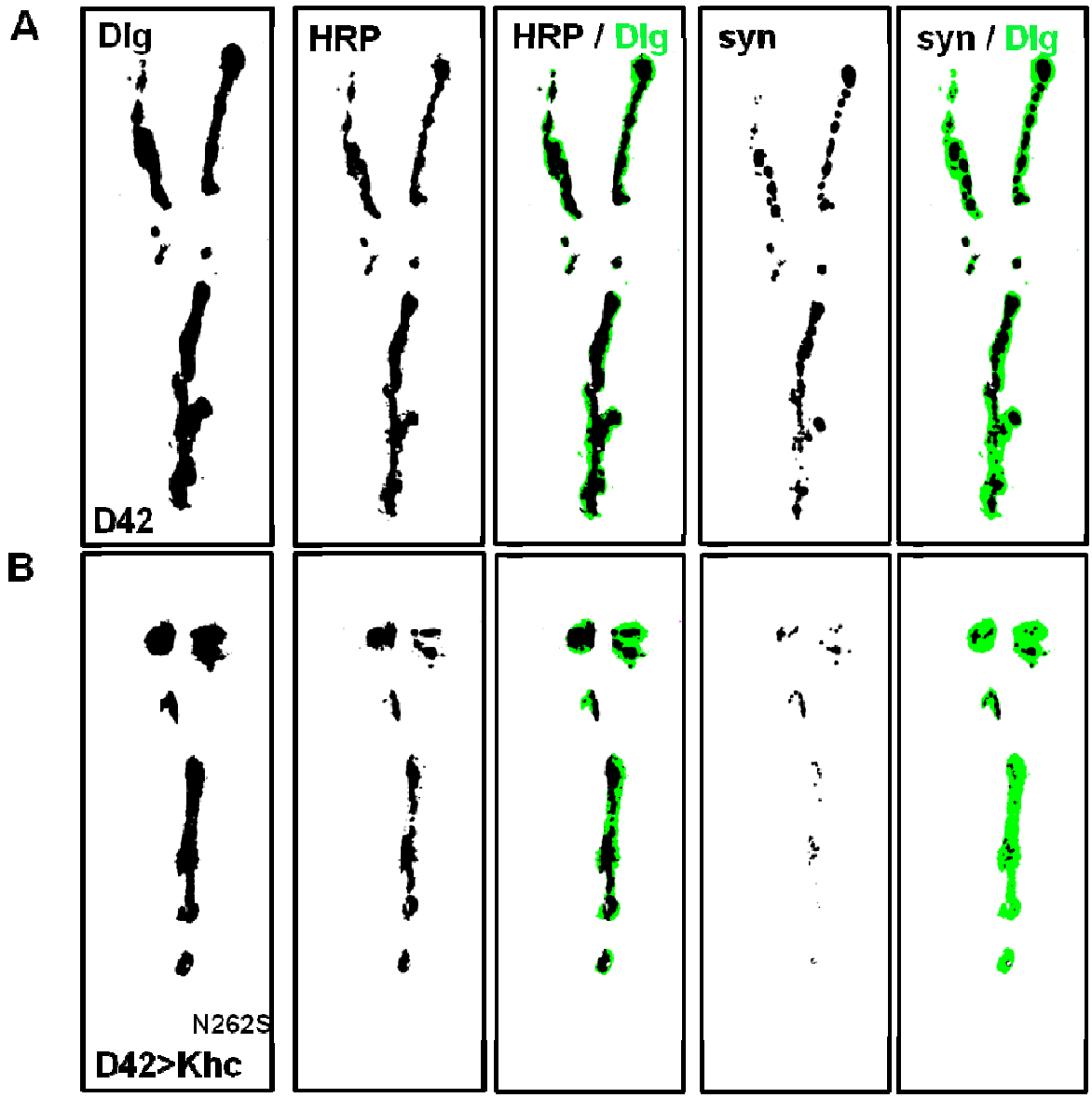

Figure 15: Illustration of quantification of presynaptic degeneration.

For quantification of the ratio of presynaptic Syn and neuronal membrane area to Dlg maximum z-projections of the image stacks all three channels were converted into binary masks. The Syn and neuronal membrane binary mask were superimposed with the Dlg binary mask, to eliminate presynaptic structures which did not co-localize with Dlg. From these resulting binary masks the respective area was calculated and the ratio of presynaptic area to Dlg area was determined.

Channel	*Filter*	*Radius*	*Projected*	*Scaled*	*Threshold value applied to create binary mask*
HRP	GB*	2	max*	-	35
Syn	GB	2	max	-	13
Dlg	GB	2	max	-	18

Table 9: Pre processing details for quantification of presynaptic degeneration.
*GB = Gaussian Blur filter. *max = maximum projection

3.7.6 Quantification of motor-neuron cell loss

For quantification of motor-neuron cell loss, a subset of motor-neuron cell bodies was marked by staining for the transcription factor Eve. Eve is expressed in the medially located aCC and RP2 motor-neurons (Figure 16A) as well as in the lateral U/CQs motor-neurons. It is also expressed in other neuronal cells, such as the medially located pCC interneurons and the EL interneuron cluster (Landgraf et al., 2003). To score motor-neuron cell loss the aCC (innervating abdominal muscle 1) and RP2 (innervating abdominal muscle 2) motor-neurons (Figure 16A) that are located in the ventral nerve cord middle line and innervate segments A1-A3 (anterior segments) and A5-A7 (posterior segments) (Figure 16B), were quantified.

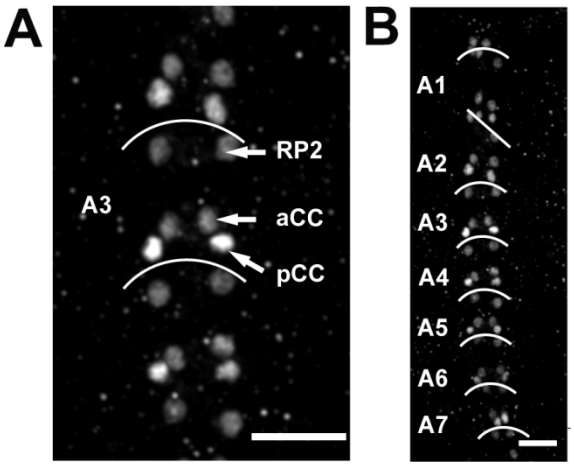

Figure 16: Illustration of motor-neuron cell bodies used for motor-neuron cell body quantification.

(A) The transcription factor Eve marks the medially located motor-neurons RP2 and aCC, as well as the pCC interneurons. For quantification the motor-neuron cell bodies innervating the abdominal segments A1-A3 and A5-A7 (B) were scored.

Scale bars 20 µm

3.7.8 Quantification of presynaptic pMad

The transcription factor pMad is abundant at the NMJ as well as in motor-neuron and muscle nuclei suggesting that the pathway is bidirectional, with some pMad being generated both pre- and postsynaptically at the NMJ (Collins and DiAntonio, 2007; Dudu et al., 2006). As we were interested in presynaptic pMad levels, staining for the active zone protein Brp (Wagh et al., 2006) was used to mark the presynaptic area of the synapses (Figure 17A - B). Figure 17A shows partial co-localization of pMad and presynaptic Brp. Brp staining (Image 1) was then used to create a three-dimensional binary mask (Image 2) that was applied to the confocal stacks of the pMad channel (Image 3) (total pMad Figure 17C). pMad signal that co-localized with Brp was defined as presynaptic (Image 4) (Figure 17D). Postsynaptic pMad signal (Figure 17E) was obtained by subtracting presynaptic pMad (Figure 17D) from total pMad signal (Figure 17C). Thereby pre- and postsynaptic pMad (Figure 17D - E) were separated. Subsequently presynaptic pMad (Image 4) fluorescence intensities were quantified using ImageJ. Postsynaptic pMad was not quantified.

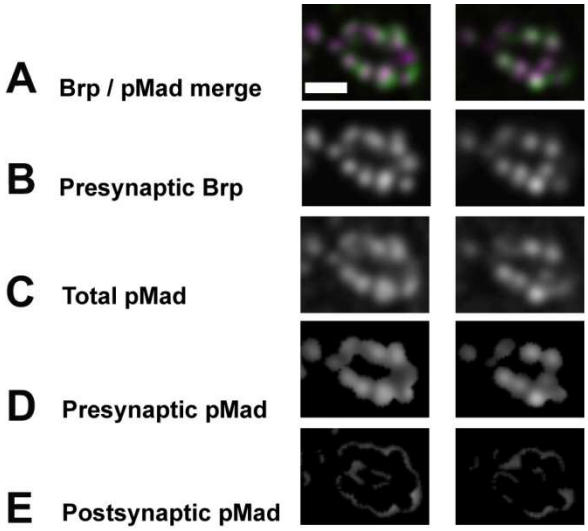

Figure 17: Illustration of quantification of presynaptic pMad.
pMad is generated both pre- and postsynaptically at the NMJ (A + C). To distinguish pre- and postsynaptic pMad the presynaptic marker Brp was used (B) to create a three-dimensional binary mask and pMad colocalizing with Brp was defined as presynaptic (D). Postsynaptic pMad (E) was obtained by subtracting presynaptic pMad (D) from total pMad (C). Scale bar 2 µm

Channel	*Filter*	*Radius*	*Projected*	*Scaled*	*Threshold value applied to create binary mask*
Brp	GB*	2	-	-	22
pMad	GB	2	-	-	-

Table 10: Pre processing details for quantification of presynaptic pMad.
*GB = Gaussian Blur filter

3.8 Statistics

Statistical tests were performed using the software PAST.exe (http://folk.uio.no/ohammer/past/index.html) unless otherwise noted. Sample errors are given as standard deviation (SD) and standard error of the mean (SEM). Data were first tested for normality by using the Shapiro-Wilk test (α=0.05). Normally distributed data were analyzed either by student's t-test (two groups) or by a one-way analysis of variance (ANOVA) followed by a Tukey-Kramer post-test for comparing multiple groups. Not normally distributed data were analyzed by using either a Mann-Whitney test (two groups) or a Kruskal-Wallis H-test followed by a post-test for

comparisons between multiple groups. Significance levels: * $p<0.05$; ** $p<0.01$; *** $p<0.001$.

For *in vivo* imaging data of GluR clustering a stabilization of variance was performed. To this the ratios of new synapses were transformed to logits, i.e., the natural logarithms of the odds. The constant value 0.5 was added to all frequencies such that logarithms of zero were avoided. For the logitvalues we compared the groups by a multifactorial ANOVA with the fixed factor group and the random factor animal that is nested under the factor group. The model parameters were estimated according to restricted maximum likelihood (REML). The estimates together with their 95% confidence intervals were back transformed into percentages. We used the statistics package JMP Version 7.0.2.

IV. Results

4.1 A role of PP2A in synapse development in *Drosophila melanogaster*

The following analyses were performed in collaboration with the group of Prof. A. DiAntonio, Department of Developmental Biology, Washington University School of Medicine, St. Louis, Missouri, USA

The following chapters (4.1.1-4.1.2) are taken from: "PP2A and GSK-3β Act Antagonistically to Regulate Active Zone Development", N.M. Viquez, P. Füger et al., Journal of Neuroscience, 2009.

In collaboration with the group of Prof. DiAntonio we investigated the role of the serine-threonine protein phosphatase 2A in the development of individual synapses at the *Drosophila* NMJ. Mature and functional synapses at the *Drosophila* NMJ are characterized by a precise apposition of the presynaptic AZs and the AZ protein Brp to the postsynaptic GluR clusters (Zhai and Bellen, 2004, Rasse et al., 2005). The group of Prof. DiAntonio showed that neuronal inhibition of PP2A resulted in abnormal presynaptic development: about 30% of GluR clusters were unapposed to AZs and the AZ protein Brp when PP2A was inhibited, whereas in the control larvae only 0.1% of the GluR clusters were found to be unapposed to presynaptic Brp.

To gain first insights into the impact of neuronal PP2A inhibition on synapse formation and maturation we measured the size of GluR fields apposed and unapposed to Brp and performed *in vivo* imaging to examine the dynamics of GluR clustering.

4.1.1 Neuronal inhibition of PP2A impairs presynaptic maturation

The dataset of confocal images for the quantification of GluR cluster size in larvae with inhibited PP2A function was kindly provided by the group of Prof. DiAntonio. To inactivate PP2A in neurons a dominant negative allele of the PP2A catalytic subunit microtubule star (UAS-dnMts) was expressed under the control of the pan-neuronal elav-Gal4 driver (dnPP2A). Larvae carrying only elav-Gal4 were used as a control. For details see N. M. Viquez, P. Füger et al., 2009. The analysis was performed on the NMJs innervating muscle 4 in segments A2 and A3.

	GluR cluster size [µm²]	
	+Brp	***-Brp***
control	0.37 ± 0.21	0.16 ± 0.06
dnPP2A	0.62 ± 0.32	0.23 ± 0.15

Table 11: Neuronal inhibition of PP2A leads to an increase of GluR cluster size.
Quantification of the size of GluR clusters apposed (+Brp) and unapposed (-Brp) to presynaptic Brp in larvae with neuronal inhibition of PP2A (dnPP2A) and control larvae. Data shown are mean ± SD.

Neuronal PP2A-inactivation resulted in an increase of the size of GluR clusters in dnPP2A larvae compared to control larvae (Table11). GluR clusters apposed as well as unapposed to presynaptic Brp were around 1.5-fold broader in the dnPP2A larvae.

In the dnPP2A animals the size of the GluR clusters apposed to Brp compared to the GluR clusters unapposed to Brp was increased 3.7-fold ($p<0.001$). In the control larvae a similar difference in size (2.3-fold) was observed between GluR clusters apposed and unapposed to Brp ($p<0.001$). It was shown before that newly formed

GluR clusters are quite small and precede the localization of Brp at the presynaptic site of the synapse (Rasse et al., 2005).

Our data show that neuronal inhibition of PP2A leads to abnormal GluR clustering. Furthermore the finding that GluR clusters unapposed to Brp are significantly smaller than GluR clusters apposed to Brp in the dnPP2A larvae suggests that the absence of Brp from these synapses is due to a failure of delivery of Brp to these synapses rather than maintenance of Brp at the synapses.

4.1.2 Neuronal inhibition of PP2A additionally impairs postsynaptic GluR clustering

To examine the dynamics of GluR clustering, *in vivo* imaging was performed. To this GluRs were marked by expression of the GFP-tagged GluRIIA subunit under its endogenous promoter, in larvae with PP2A inhibition and control larvae.

The following genotypes were used for *in vivo* imaging: xy;DGluRIIA-GFP/+;elav-Gal4/dnMts (dnPP2A) and xy;DGluRIIA-GFP/+;elav-Gal4/+ (Control). Larvae were raised at 25℃ and early L3 stage larvae were used for *in vivo* imaging. Imaging was done at two time points (0 and 6 hours) and the changes to the receptor clusters within these six hours of development were quantified.

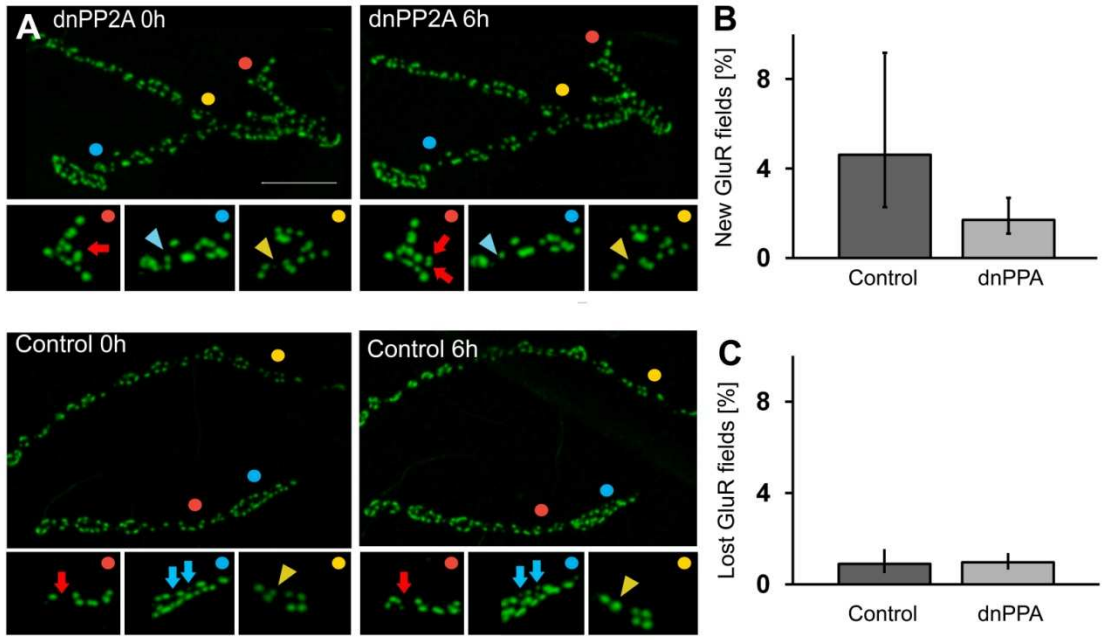

Figure 18: Neuronal inhibition of PP2A causes defects in GluR clustering.
(*A*) *In vivo* imaging of GFP-labeled DGluRIIA at larval NMJs. Shown are two time points of imaging (0 and 6 h) of individual NMJs from a larva in which PP2A is inhibited (dnPP2A) (top) and a control larva (bottom). Regions of formation and loss of GluR fields within the NMJs are marked by colored dots. Enlargements of the areas marked are shown beneath the corresponding NMJs. Newly formed GluR fields are marked with arrows, lost GluR fields are marked with arrowheads. Scale bar: 5 µm. (B) Quantification of formation of GluR fields. (C) Quantification of loss of GluR fields. For B and C, 13 control junctions (from five different larvae) were compared with 42 mutant junctions (from 13 different larvae). Error bars show the SEM.

In vivo imaging of GluR dynamics revealed that a small proportion of the GluR clusters were lost in both genotypes within 6 hours of development (loss of synapses: dnPP2A 0.96%; control 0.90%) (Figure 18A, arrowheads and 18C). Quantification of the newly formed GluR fields showed a ~3-fold reduction in the number of newly formed GluR clusters in dnPP2A larvae (1.71%) compared to control animals (4.62%) (Figure 18A, arrows and 18B) Thus, the net addition of GluR clusters in the dnPP2A animals was strongly reduced compared to the controls. These results demonstrate

that presynaptic inhibition of PP2A at the NMJ does not only impair presynaptic active zone development, but also causes defects in postsynaptic GluR clustering.

4.2 *Drosophila melanogaster* in the study of the SPG10 subtype of the neurodegenerative disorder Hereditary Spastic Paraplegia

Parts of the following chapters are taken from

"Spastic paraplegia mutation N256S in the neuronal microtubule motor KIF5A disrupts axonal transport in a Drosophila HSP model", P. Füger, V. Sreekumar et al., Manuscript accepted for publication

4.2.1 Establishment of a *Drosophila* model for the HSP subtype SPG10

4.2.1.1 The mutation N262S does not affect stability of Khc when expressed pan-neuronal in *Drosophila*

To establish a *Drosophila* model for the HSP subtype SPG10 and gain insight into the associated pathogenic mechanisms, site-directed mutagenesis was used to exchange the nucleotides 785A>G (corresponding to amino acid exchange N262S) in a full-length wild-type *Drosophila khc* cDNA (SD02406), which was then inserted into a modified pUAST attB vector (UAS-Khc^{N262S}). To generate the control construct UAS-Khc^{wt}, full-length wild-type *khc* was also inserted into the vector. (Previous work; for details see paragraph 2.4)

To examine expression of the proteins, pan-neuronal conditional expression was used. Thereby the expression of UAS-constructs by the elav^{C155}-Gal4 driver is only enabled at the restrictive temperature of 29℃. To this, transgenic flies carrying either UAS-Khc^{N262S} or UAS-Khc^{wt} were crossed to flies carrying the pan-neuronal elav^{C155}-

Gal4 driver and a ubiquitously driven temperature-sensitive Gal80 construct (tub-Gal80^{ts}). Flies of the following genotypes (y/elav^{C155}-Gal4;tub-Gal80^{ts}/+;+/+ (elav), y/elav^{C155}-Gal4/tub-Gal80^{ts}/+;UAS-Khc^{N262S}/+ (elav>Khc^{N262S}) and y/elav^{C155}-Gal4;tub-Gal80^{ts}/+;Khc^{wt}/+ (elav>^{Khcwt})) were raised and allowed to hatch at a permissive temperature of 18°C. 24 hours after hatching the male flies were transferred to a restrictive temperature of 29°C. The flies were kept at 29°C for 13 days to induce expression of Khc^{N262S} and Khc^{wt}. Then protein extraction from the whole fly heads and western blot analysis was performed.

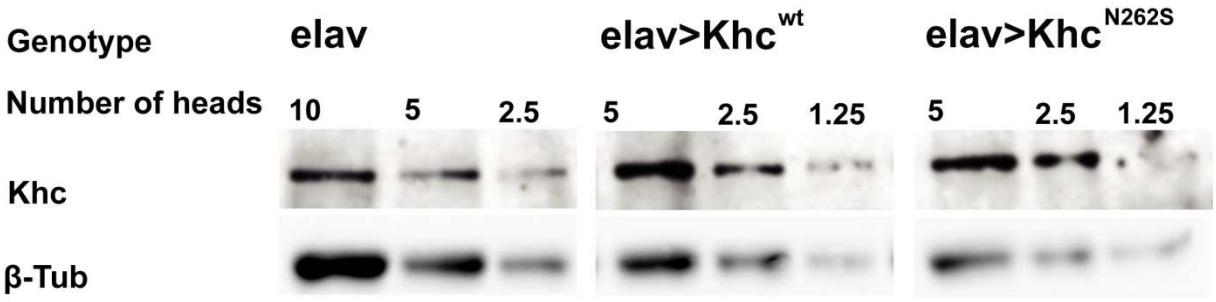

Figure 19: Khc^{N262S} and Khc^{wt} are stably expressed in *Drosophila.*
Genotypes: y/elav^{C155}-Gal4;tub-Gal80^{ts}/+;+/+ (elav), y/elav^{C155}-Gal4/tub-Gal80^{ts}/+;UAS-Khc^{wt}/+ (elav>Khc^{wt}) and y/elav^{C155}-Gal4;tub-Gal80^{ts}/+;Khc^{N262S}/+ (elav>Khc^{N262S}). 14 days old male flies were used for western blot analysis. The number of heads loaded per lane is indicated. β-Tubulin was used as a loading control.

In 14 days old male flies the levels of endogenous Khc from the 10 heads of the control flies (elav) were comparable to the Khc levels in 2.5 heads from flies over-expressing Khc^{N262S} or Khc^{wt} under the elav^{C155}-Gal4 driver (Figure 19). A ~3-fold excess of ectopic Khc to endogenous Khc was determined using the ImageJ Gel Analyzer. Similar protein levels of Khc were detected in elav>Khc^{wt} and elav>Khc^{N262S} flies, showing that N262S does not affect protein stability. Therefore mutated Khc (Khc^{N262S}) exceeds the endogenous wild-type Khc in flies expressing ectopic Khc^{N262S} only. In contrast, in flies expressing Khc^{N262S} together with an

additional copy of Khc^{wt} the ratio of wild-type Khc to mutated Khc is shifted; more wild-type Khc is available, due to the two copies of endogenous wild-type Khc and the additional expression of Khc^{wt}.

4.2.1.2 Motor-neuron expression of Khc^{N262S} causes distal paralysis of *Drosophila* larvae

In *khc* null mutant larvae a characteristic tail-flipping phenotype has been described (Hurd and Saxton, 1996a). This tail-flipping is caused by a distal paralysis, that is more pronounced in the ventral distal part of the larvae and reflects the more severe effects of Khc mutations on the structure and function of the long axons that innervate the posterior segments (Hurd and Saxton, 1996b).

Upon motor-neuron specific expression of Khc^{N262S} and $Khc^{wt+N262S}$ (D42>Khc^{N262S} and D42>$Khc^{wt+N262S}$) third-instar larvae also displayed the tail-flipping phenotype (Figure 20).

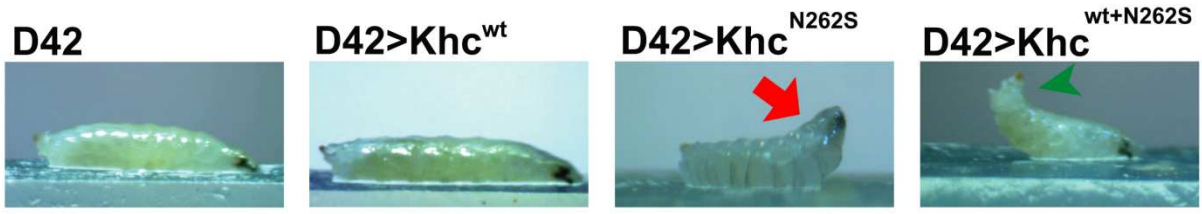

Figure 20: Motor-neuron specific ectopic expression of Khc^{N262S} in the wild-type background causes tail-flipping of *Drosophila* larvae.
The tail-flipping of D42>Khc^{N262S} and D42>$Khc^{wt+N262S}$ larvae is due to a distal paralysis. This phenotype is more pronounced in D42>Khc^{N262S} larvae and precedes a complete paralysis of the distal part of these larvae.

In D42>Khc^{N262S} larvae the distal paralysis was more pronounced compared to D42>Khc$^{wt+N262S}$ larvae. In D42>Khc^{N262S} larvae the tail-flipping phenotype was followed by an almost complete paralysis of the posterior parts of the larvae. Eventually these larvae could only move their heads (Figure 20, red arrow). As a result of complete paralysis, D42>Khc^{N262} larvae died at second or third instar stages. Third-instar D42>Khc$^{wt+N262S}$ larvae exhibited the tail-flipping phenotype but were still able to crawl (Figure 20, green arrowhead). Expression of Khc$^{wt+N262S}$ under the D42-Gal4 driver did not cause larval lethality. In D42>Khc^{wt} animals no defects became obvious.

In *Drosophila*, axons innervating the posterior segments are considerably longer than those innervating anterior segments. In *Drosophila* larvae expressing Khc^{N262S}, longer motor-neuron axons seem to be primarily affected in their function. Thus the distal paralysis of D42>Khc^{N262S} and D42>Khc$^{wt+N262S}$ *Drosophila* larvae, resembles HSP pathological symptoms that are characterized predominantly by affection of the lower limbs caused by a particular vulnerability of the long axons of the descending spinal tracts.

4.2.1.3 Khc^{N262S} acts as a dominant-negative allele in *Drosophila* larvae

From *in vitro* analyses it was suggested that KIF5A^{N256S} is not a loss-of-function mutant, but a dominant-negative allele (Ebbing et al., 2008). This is consistent with the autosomal dominant inheritance of the HSP subtype SPG10.

To test whether Khc^{N262S} interferes with the function of wild-type Khc in a dominant-negative way *in vivo*, the impact of motor-neuron specific ectopic expression of

Khc^{N262S} in a wild-type background was compared to the impact caused by the loss of one ($Khc^{+/-}$) or two endogenous copies ($Khc^{-/-}$) of *khc*. The following genotypes were used for the larval locomotion assay D42, D42>Khc^{wt}, D42>Khc^{N262S}, D42>$Khc^{wt+N262S}$, $Khc^{+/-}$ and $Khc^{-/-}$. Larvae were raised at 25℃ and second and third-instar larvae were used for analysis.

The size and average speed of the larvae was calculated and larvae were grouped according to their size (small, 1-3 mm; large, 3-5 mm; Figure 21).

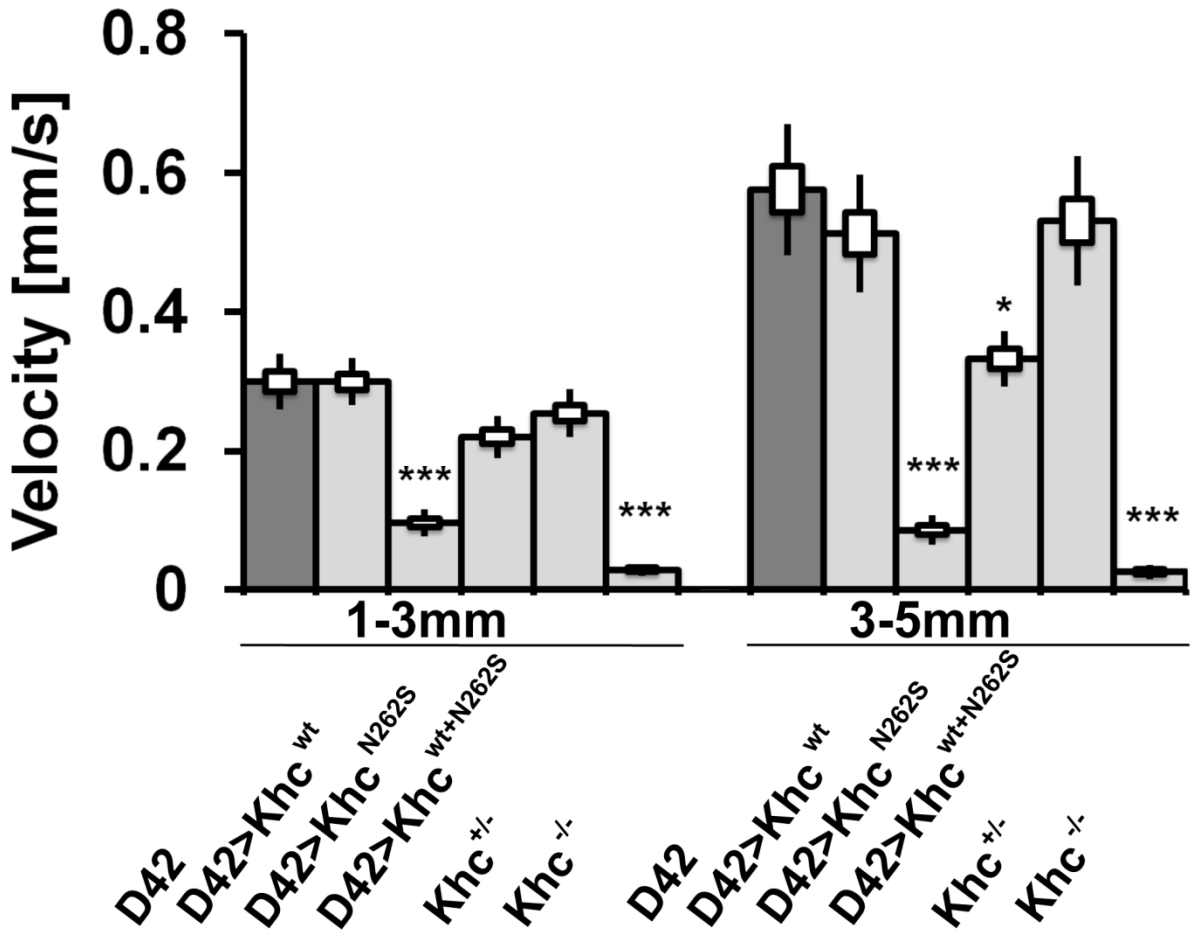

Figure 21: Motor-neuronal expression of Khc^{N262S} in the wild-type background strongly impairs locomotion of *Drosophila* larvae.

Boxes indicate SEM; black lines indicate SD. Kruskal-Wallis H-tests for multiple comparisons were performed. All genotypes within a single size group were compared to the D42 larvae (dark gray bare). Eight movies per genotype were analyzed.

	Larval size 1-3 mm		*Larval size 3-5 mm*	
	velocity [mm/s]	***p-value***	***velocity [mm/s]***	***p-value***
D42	0.30 ± 0.04	-	0.58 ± 0.09	-
D42>Khc^{wt}	0.30 ± 0.04	n.s	0.51 ± 0.08	n.s
D42>Khc^{N262S}	0.10 ± 0.02	< 0.001	0.09 ± 0.02	< 0.001
D42>Khc$^{wt+N262S}$	0.22 ± 0.03	n.s	0.33 ± 0.04	< 0.05
Khc$^{+/-}$	0.25 ± 0.03	n.s	0.53 ± 0.09	n.s
Khc$^{-/-}$	0.03 ± 0.009	< 0.001	0.03 ± 0.01	< 0.001

Table 12: Quantification reveals severe impairment of *Drosophila* larval locomotion upon motor-neuronal expression of Khc^{N262S}.
Data are means ± SD. Statistical significance was determined using a Kruskal-Wallis H-test for multiple comparisons. The p-values shown are when compared to D42 larvae.

The locomotion of small and large D42>Khc^{N262S} and *khc* null (Khc$^{-/-}$) larvae was strongly impaired compared to the D42 and D42>Khc^{wt} larvae, which exhibited no significant difference between each other (Figure 21 and Table 12). The locomotion of the small D42>Khc$^{wt+N262S}$ larvae was indistinguishable from that of control animals (D42 and D42>Khc^{wt}), while the large larvae displayed a reduction in locomotion speed (Figure 21 and Table 12). No difference was observed in the locomotion speed between the D42 larvae and the larvae lacking one copy of *khc* (Khc$^{+/-}$) (Figure 21 and Table 12).

The obvious differences in the locomotion of D42>Khc^{N262S} and Khc$^{+/-}$ larvae show that Khc^{N262S} acts as a dominant-negative *in vivo*.

4.2.1.4 Motor-neuron expression of Khc^{N262S} causes axonal swellings and disturbs axonal transport in *Drosophila* larvae

The occurrence of axonal swellings has been reported from autopsies of human SPG4-associated HSP patients (Kasher et al., 2009) and mouse models of SPG4 (Spastin) (Kasher et al., 2009) and SPG7 (Paraplegin) (Ferreirinha et al., 2004) Within these swellings the accumulation of axonal transport cargo was observed, suggesting an impairment of axonal transport. Axonal swellings have also been observed in *Drosophila khc* null mutant larvae (Hurd and Saxton, 1996b). In the *khc* null mutant larvae axonal swellings, showed increased immunoreactivity for the synaptic vesicle-associated Cysteine-string protein (CSP), a kinesin-1 cargo (Hurd and Saxton, 1996a, Barkus et al., 2007).

For analysis of axonal transport *in vitro*, D42, D42>Khc^{wt}, D42>Khc^{N262S}, D42>Khc$^{wt+N262S}$ and Khc$^{-/-}$ larvae were used. Larvae were raised at 29°C and third-instar larvae were dissected and stained for the kinesin-1 cargo CSP and the kinesin-3 cargo Brp as well as the neuronal membrane marker anti-HRP.

In *Drosophila* the axons that project from the motor-neuron cell bodies, located in the VNC, to the abdominal segmental muscles are bundled within segmental nerves. A segmental nerve contains 60-80 motor and sensory axons. Structures marked by anti-HRP staining and shown in Figure 22 represent segmental nerves.

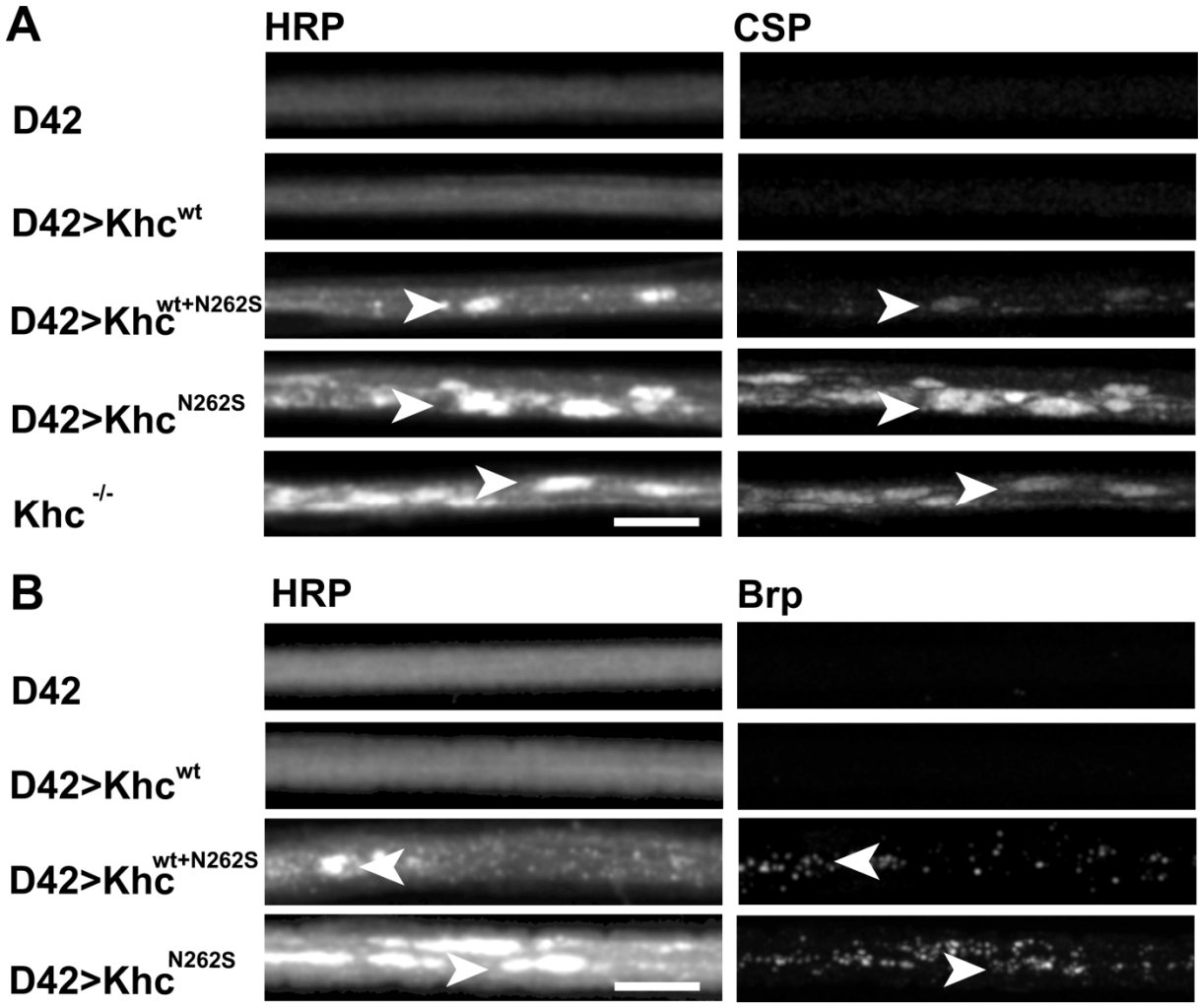

Figure 22: The kinesin-1 cargo CSP and the kinesin-3 cargo Brp accumulate in segmental nerves of Khc^{N262S} expressing *Drosophila* larvae.

Anti-HRP and CSP (A) and anti-HRP and Brp (B) staining in segmental nerves of *Drosophila* larvae. Axonal swellings (arrowheads in A-B) are characterized by a bright anti-HRP staining and an accumulation of the kinesin-1 cargo CSP or the kinesin-3 cargo Brp. Scale bars, 10 µm.

Motor-neuron specific expression of Khc^{N262S} and Khc$^{wt+N262S}$ under the D42-Gal4 driver caused a distinct inhomogeneity in anti-HRP staining in segmental nerves of these larvae compared to D42 and D42>Khc^{wt} larvae (Figure 22A - B, arrowheads). Similar inhomogeneity in anti-HRP staining was also found in Khc$^{-/-}$ animals (Figure 22A, arrowheads). As anti-HRP is a marker of neuronal membranes the areas of increased anti-HRP intensities should mark areas of increased neuronal membrane

accumulation. In *khc* null mutants the occurrence of axonal swellings has been reported, that are characterized by an accumulation of membrane-bounded organelles such as mitochondria, small vesicles, cisternal membranes and multivesicular bodies (Hurd and Saxton, 1996b). Thus we concluded that the areas of increased anti-HRP intensities within the segmental nerves of D42>Khc^{N262S}, D42>Khc$^{wt+N262S}$ and Khc$^{-/-}$ larvae would mark sites that exhibit an accumulation of structures rich in membranes within single axons of the nerves and thus axonal swellings. Electron microscopic analysis of segmental nerves of Khc^{N262S} expressing animals confirmed that axonal swellings, containing multivesicular bodies, prelysosomal vacuoles and autophagosomes occur in these animals (data by J. Kern).

Axonal swellings were more prevalent in D42>Khc^{N262S} compared to D42>Khc$^{wt+N262S}$ larvae and were characterized by an increase in CSP fluorescence intensity (Figure 22A), indicating an accumulation of CSP within axonal swellings. Hence, motor-neuron specific expression of Khc^{N262S} impairs the axonal transport of CSP by kinesin-1. Axonal swellings were absent in D42 and D42>Khc^{wt} larvae.

Next, staining for the kinesin-3 cargo Brp (Barkus et al., 2007, Pack-Chung et al., 2007) was used to investigate whether the expression of Khc^{N262S} also affects kinesin-1 independent axonal transport. Accumulation of Brp within axonal swellings revealed that axonal transport by kinesin-3 was also disturbed in D42>Khc^{N262S} and D42>Khc$^{wt+N262S}$ larvae (Figure 22B). This suggests that ectopic expression of mutated Khc does not selectively disturb axonal transport by kinesin-1, but also impairs kinesin-1 independent axonal transport.

4.2.1.5: Axonal swellings in motor-neurons of Khc^{N262S} expressing *Drosophila* larvae do not represent sites of abnormal Khc accumulation

One question to be answered was whether Khc accumulates abnormally in axonal swellings of Khc^{N262S} expressing larvae. To answer this, immunohistochemical staining of segmental nerves of D42, D42>Khc^{wt}, D42>Khc^{N262S} and D42>Khc$^{wt+N262S}$ larvae was performed. Larvae were raised at 29℃ and third-instar larvae were dissected and stained for neuronal membranes and Khc.

A

Genotype	D42	D42>Khc^{wt}	D42>Khc$^{wt+N262S}$	D42>Khc^{N262S}
Mean ± SD	1.08 ± 0.04	1.76 ± 0.13	8.77 ± 3.21	2.35 ± 0.69
p-value	-	0.311	0.182	0.085

B

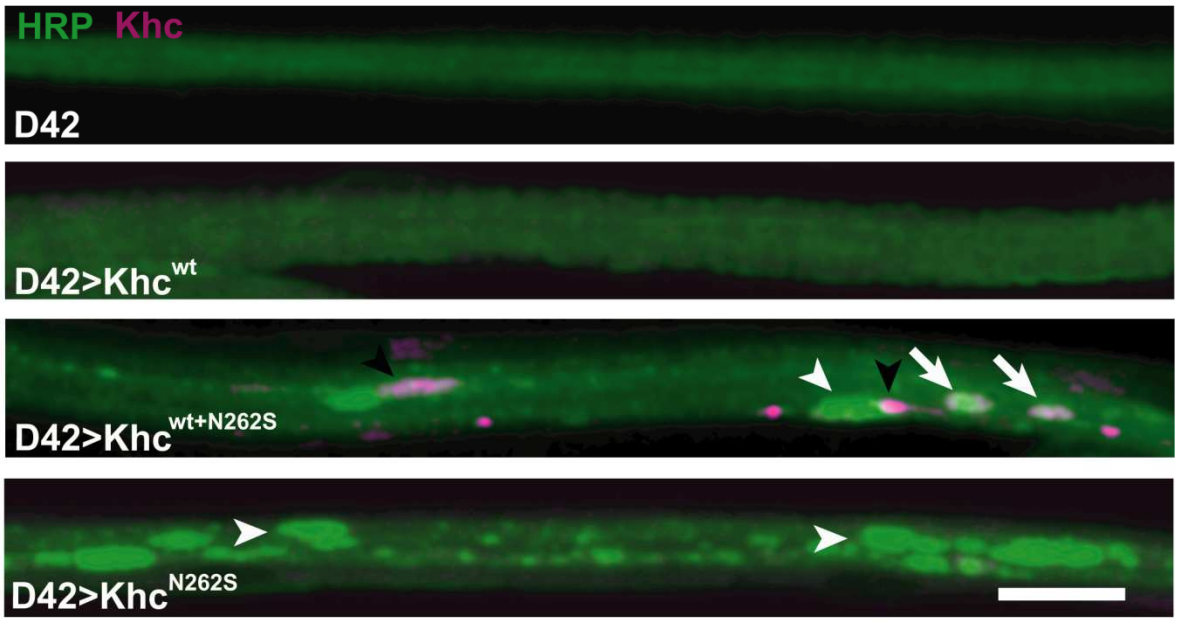

Figure 23: Motor-neuron specific expression of Khc^{N262S} does not cause abnormal accumulation of Khc in axonal swellings in *Drosophila* larvae.

(A) Motor-neuron expression of Khc^{N262S} increased Khc levels in segmental nerves of *Drosophila* larvae. For statistical analysis Kruskal-Wallis H-tests for multiple comparisons were used. p-values shown are when compared to D42 (B) Khc staining in segmental nerves of third-instar *Drosophila* larvae. Larvae were stained for anti-HRP to mark neuronal membranes. In D42>Khc$^{wt+N262S}$ larvae some axonal swellings (green) co-localized with Khc

accumulations (white arrow), while other axonal swellings did not show increased Khc fluorescence intensity (white arrowhead). Furthermore Khc accumulations were also found outside of axonal swellings (black arrowhead) in these larvae. In D42>Khc^{N262S} larvae no Khc accumulations were found within axonal swellings. Scale bar, 10 µm

Expression of Khc^{wt} as well as of Khc^{N262S} in motor-neurons of *Drosophila* larvae caused a trend towards an increase of Khc levels in segmental nerves, that was most pronounced in D42>Khc$^{wt+N262S}$ larvae (Figure 23A). However it was not statistically significant different compared to D42 larvae. The increase in Khc levels observed in the D42>Khc$^{wt+N262S}$ larvae resulted from abnormal Khc accumulations present in segmental nerves of these animals. These Khc accumulations (31 Khc accumulations from 5 segmental nerves of 5 larvae; Figure 23B, white arrows and black arrowheads), partially co-localized with axonal swellings (9 out of 31 Khc accumulations; Figure 23B, white arrows). However, there were also axonal swellings that did not show increased Khc immunoreactivity (7 axonal swellings from 5 segmental nerves of 5 larvae). In the D42>Khc^{N262S} animals no abnormal Khc accumulations were observed, except for one that co-localized with an axonal swelling (72 axonal swellings from 5 segmental nerves of 5 larvae; Figure 23, white arrowheads). In control animals (D42 and D42>Khc^{wt}), no Khc accumulations were detected within segmental nerves.

The presence of the Khc accumulations in the D42>Khc$^{wt+N262S}$ larvae is most likely due to a strong expression of Khc in these animals. Since there is not any Khc accumulation in axonal swellings of D42>Khc^{N262S} larvae it is unlikely that axonal swellings are caused by blockage of axons due to abnormal Khc accumulation.

4.2.1.6 The full-length Khc protein is necessary for the dominant negative effects exerted by Khc^{N262S}

As the degeneration of the long motor-neurons in HSP starts from the synapses it seems likely that a gradual diminishment of cargo arriving at the synapses is the reason for the degeneration. Two mechanisms were proposed how mutations in KIF5A would diminish cargo arriving at the synapses. First, homo- or heterodimeric mutant kinesin-1 motors might block microtubules or act as brakes for the transport of cargo particles (Ebbing et al., 2008). Second, mutant kinesin-1 motors, incompetent for microtubule binding or efficient processing along microtubules, might compete for cargo binding sites that are then inaccessible for intact motors (Ebbing et al., 2008).

To investigate the second hypothesis the impact of motor-neuron expression of truncated wild-type and mutant Khc proteins in *Drosophila* larvae was analyzed. These truncated proteins are still able to dimerize *in vitro*, but lack the C-terminal tail and a part of the stalk that is necessary for cargo binding (Seitz and Surrey, 2006). Thus they will not compete for cargo binding with the endogenous full-length wild-type Khc.

For immunohistochemical analysis D42, D42>Khc^{wt}, D42>$Khc^{truncwt}$ and D42>$Khc^{truncN262S}$ larvae were raised at 29℃ and third-instar larvae were dissected and stained for neuronal membranes (anti-HRP) and Khc or CSP. For the larval crawling assay larvae were raised at 25℃.

A

Genotype	D42	D42>Khc^{wt}	D42>Khc^{truncwt}	D42>Khc^{truncN262S}
Mean ± SD	21.31 ± 1.34	38.68 ± 3.71	25.72 ± 2.49	33.49 ± 2.14
p-value	-	0.00022	0.204	0.00087

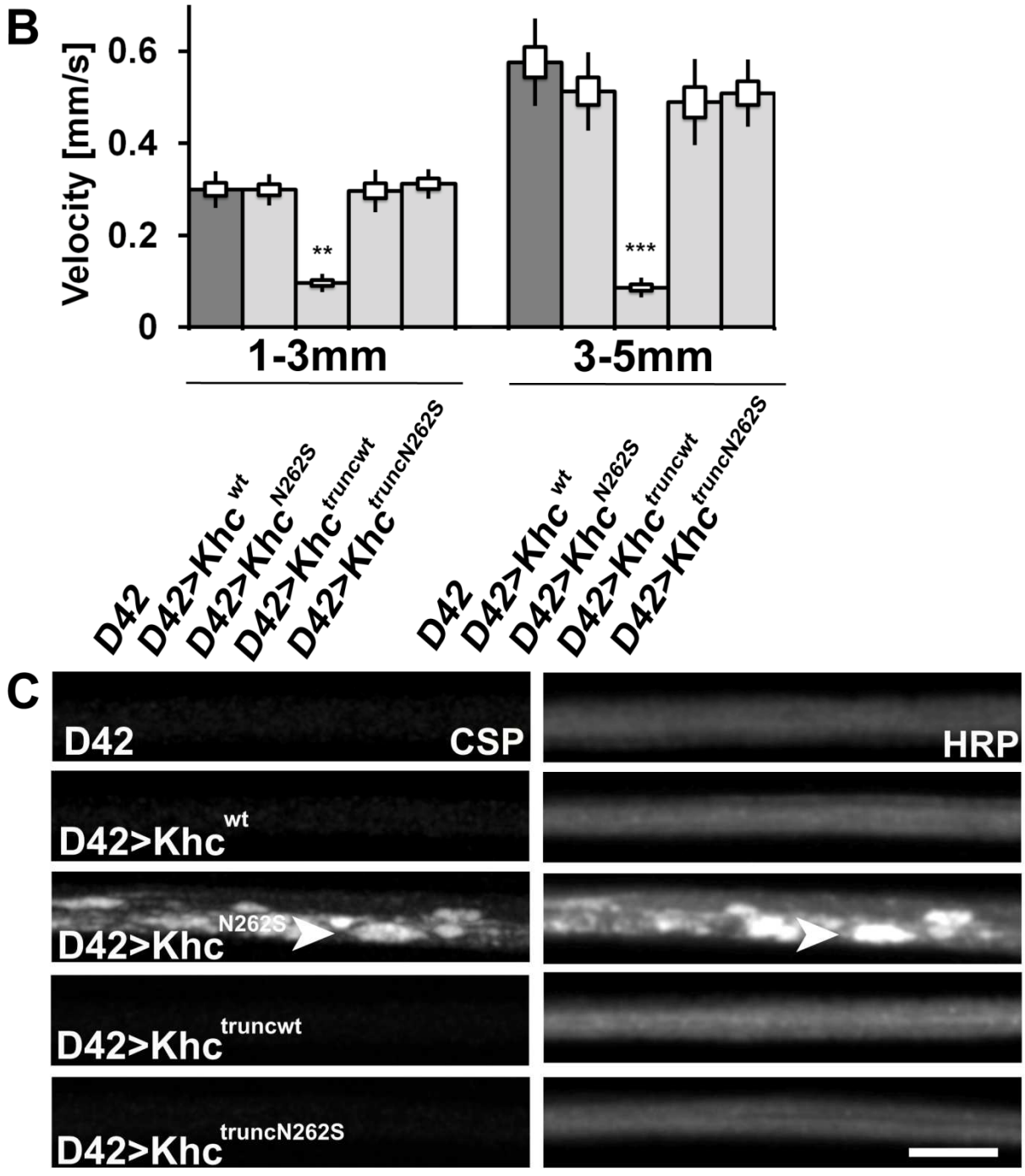

Figure 24: Full-length Khc^{N262S} is necessary for the dominant negative impact in *Drosophila* larvae.

(A) Motor-neuron expression of full length or truncated Khc caused increased levels of Khc within segmental nerves of *Drosophila* larvae. Statistical significance was determined by a

ONE-Way ANOVA for multiple comparisons. The p-values shown are when compared to D42. (B) Quantification of larval locomotion. Boxes indicate SEM; black lines indicate SD. For statistical analysis Kruskal-Wallis H-tests for multiple comparisons were used. All genotypes within one size group were compared to D42 (dark gray bar). Eight movies per genotype were analyzed. (C) CSP staining of segmental nerves of *Drosophila* larvae. Anti-HRP staining was used to mark neuronal membranes. Scale bar, 10 µm.

	Larval size 1-3 mm		***Larval size 3-5 mm***	
	velocity [mm/s]	***p-value***	***velocity [mm/s]***	***p-value***
D42	0.30 ± 0.04	-	0.58 ± 0.09	-
D42>Khc^{wt}	0.30 ± 0.04	n.s	0.51 ± 0.08	n.s
D42>Khc^{N262S}	0.10 ± 0.02	< 0.01	0.09 ± 0.02	< 0.001
D42>Khc^{truncwt}	0.30 ± 0.05	n.s	0.49 ± 0.09	n.s
D42>Khc^{truncN262S}	0.31 ± 0.03	n.s	0.51 ± 0.07	n.s

Table 13: Expression of truncated Khc proteins has no impact on the locomotion of *Drosophila* larvae.

Values are means ± SD. Statistical significance was determined using a Kruskal-Wallis H-test for multiple comparisons. The p-values shown are when compared to D42 larvae.

Quantification of Khc fluorescence levels in segmental nerves indicates that the truncated Khc proteins are stably expressed, as fluorescence levels of Khc were significantly increased in D42>Khc^{truncN262S} larvae and showed a trend towards an increase in D42>Khc^{truncwt} compared to D42 animals (Figure 24A). Fluorescence levels of Khc in D42>Khc^{truncwt} and D42>Khc^{truncN262S} larvae in segmental nerves were lower than fluorescence levels detected in the D42>Khc^{wt} animals (Figure 24A).

Furthermore an interaction of the truncated Khc proteins with full-length Khc is indicated by motor-neuron specific co-expression of Khc^{N262S} and $Khc^{truncwt}$. Co-expression of Khc^{N262S} and $Khc^{truncwt}$ at 29°C rendered no larvae. Upon expression of each of the proteins alone at 29°C, the animals sur vived to the L2 or L3 larval stage (Khc^{N262S}) or adulthood ($Khc^{truncwt}$). The non-viability of the D42>Khc^{N262S} larvae upon co-expression of $Khc^{truncwt}$, indicates an additional impact of the truncated Khc. This is most likely due to the interaction of the truncated Khc with full-length wild-type Khc. Thereby the availability of intact full-length Khc homodimers, ensuring axonal transport, is further decreased in D42>$Khc^{N262S+truncwt}$ animals. This might impair larval fitness and thereby viability more severely. When $Khc^{truncwt}$ alone is expressed the reduction of available full-length Khc homodimers, caused by the truncated Khc protein, presumably is not that severe and therefore does not cause lethality of D42>$Khc^{truncwt}$ animals.

Analysis of larval locomotion upon ectopic expression of truncated Khc proteins ($Khc^{truncwt}$ or $Khc^{truncN262S}$) showed no difference in locomotion of these animals compared to animals expressing no ectopic Khc (D42) or animals expressing an additional copy of full-length wild-type Khc (D42>Khc^{wt}) (Figure 24B and Table 13). D42>$Khc^{truncwt}$, as well as D42>$Khc^{truncN262S}$, larvae were considerably faster than the D42>Khc^{N262S} larvae (Figure 24B and Table 13). Anti-HRP and CSP staining in the segmental nerves showed that neither D42>$Khc^{truncwt}$ nor D42>$Khc^{truncN262S}$ larvae exhibited axonal swellings (Figure 24C), which were present in the D42>Khc^{N262S} animals (Figure 24C, arrowheads).

In conclusion, truncated Khc^{N262S} does not seem to act as a dominant-negative allele *in vivo*. This indicates that cargo binding by homodimeric or heterodimeric mutant motors and detaining it from the synapses might be responsible for the dominant-

negative effect exerted by Khc^{N262S}. However, the stable expression and interaction of the truncated proteins by western blot and co-immunoprecipitation assays need to be confirmed.

4.2.1.7 Analysis of axonal transport of mitochondria

To directly address the effects of the expression of Khc^{N262S} and $Khc^{wt+N262S}$ on anterograde and retrograde cargo transport, *in vivo* imaging was performed. Kinesin-1 has been described as the primary motor for anterograde transport of mitochondria in *Drosophila* (Pilling et al., 2006). In order to quantify the axonal transport of mitochondria, mitochondria were visualized using a green fluorescent protein (GFP) fused to a mitochondrial targeting sequence (mito-GFP) (Pilling et al., 2006). For the assay, D42, D42>Khc^{wt}, D42>Khcwt+^{N262S} and D42>Khc^{N262S} larvae co-expressed mito-GPF under the D42-Gal4 driver were used. Larvae were raised at 29℃ and third-instar larvae were used for analysis.

4.2.1.7.1 Expression of Khc^{N262S} reduces mitochondrial transport frequency in motor-neuron axons of *Drosophila* larvae

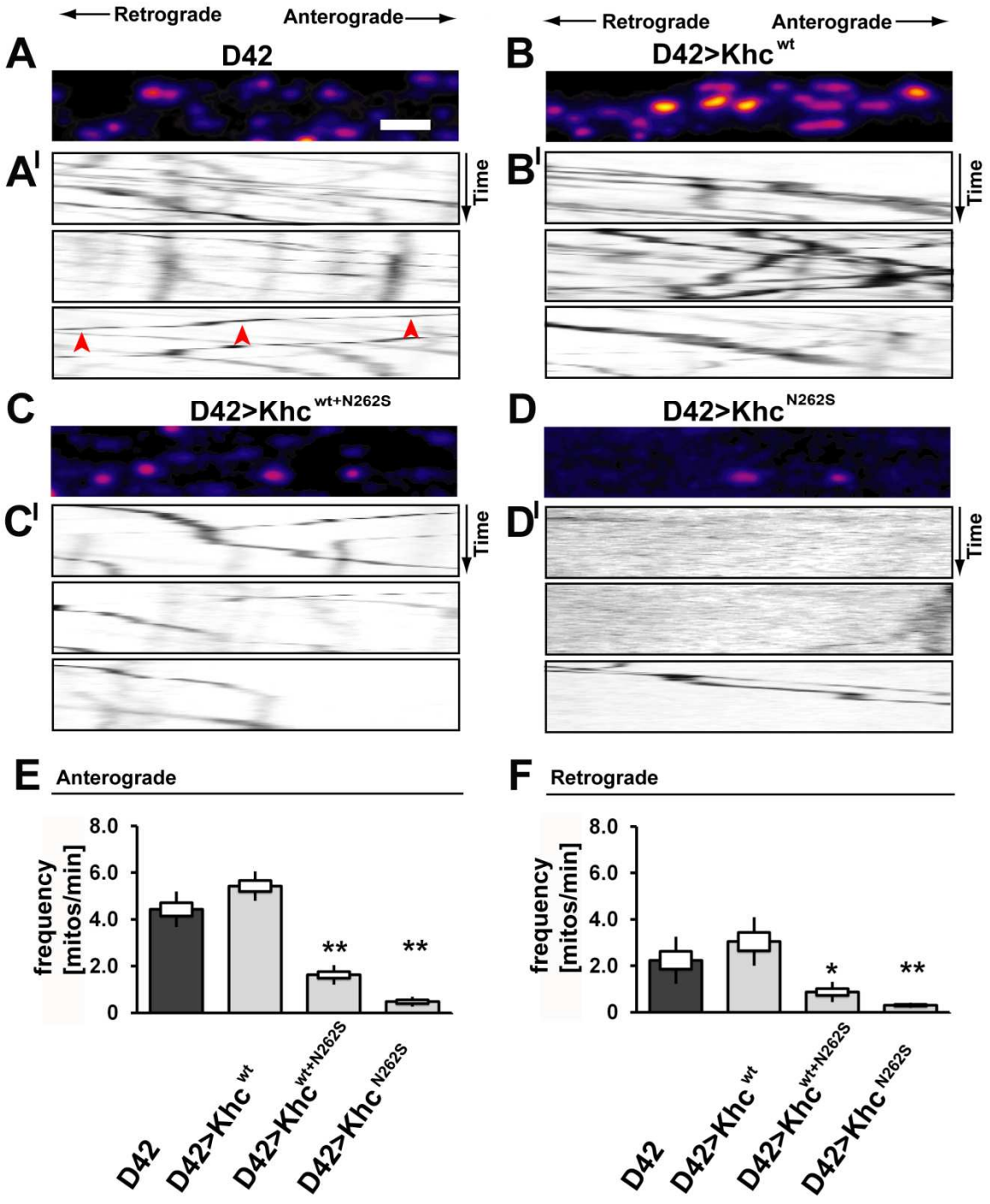

Figure 25: Motor-neuron expression of Khc^{N262S} reduces mitochondrial transport frequency in axons of *Drosophila* larvae.

The movement of mitochondria was recorded in anesthetized larvae after bleaching a section of the segmental nerve. (A-D) A representative frame of a movie for each genotype is shown.

(A^I, B^I) Kymographs of mitochondrial movement in axons of *Drosophila* larvae. Mitochondria moving in the anterograde and retrograde direction appear as oblique lines. Red arrowheads in A^I highlight the movement of one mitochondrion in the retrograde direction. Scale bar: 5 µm. (E-F) The transport frequency of mitochondria is significantly reduced in D42>$Khc^{wt+N262S}$ and D42>Khc^{N262S} larvae compared to the controls (D42 and D42>Khc^{wt}). For quantification 7-9 movies of individual larvae per genotype were analyzed. Statistical significance was determined by using a Kruskal-Wallis H-test for multiple comparisons. Stars indicate statistical significance compared to D42 (dark gray bar). The SEM is shown as a box, the SD as a black line. * $p < 0.05$; ** $p < 0.01$

	Anterograde		***Retrograde***	
	Frequency [mitos/min]	***p-value***	***Frequency [mitos/min]***	***p-value***
D42	4.43 ± 0.76	-	2.24 ± 1.01	-
D42>Khc^{wt}	5.43 ± 0.63	0.313	3.05 ± 1.04	0.937
D42>$Khc^{wt+N262S}$	1.62 ± 0.42	0.006	0.87 ± 0.44	0.024
D42>Khc^{N262S}	0.48 ± 0.21	0.008	0.3 ± 0.11	0.007

Table 14: Quantification of transport frequency of mitochondria along motor-neuron axons in *Drosophila* larvae.

Data represent the mean ± SD. Statistical significance was determined using a Kruskal-Wallis H-test for multiple comparisons. The p-values shown are when compared to D42.

Motor-neuron specific expression of Khc^{wt} slightly increased the mitochondrial transport frequency in the anterograde and retrograde direction, but this was not significantly different to D42 larvae (Figure 25E - F and Table 14). In D42>$Khc^{wt+N262S}$ larvae the mitochondrial transport frequency was significantly decreased in both directions compared to D42 animals (Figure 25E - F and Table 14). The expression of Khc^{N262S} without an additional copy of Khc^{wt} in the wild-type background reduced the transport frequency of mitochondria even further (Figure 25E - F and Table 14).

The more pronounced reduction in mitochondrial transport frequency in D42>Khc^{N262S} animals compared to D42>Khc$^{wt+N262S}$ larvae, is consistent with an expected lower number of Khc^{wt}-homodimers and thus fully functional kinesin-1 motor proteins in the D42>Khc^{N262S} animals. A decrease in the number of functional motor proteins would be expected to also decrease the transport frequency of kinesin-1 cargo.

4.2.1.7.2 Khc^{N262S} expression does not affect total amount of mitochondria in motor-neuron cell bodies in the VNC of *Drosophila* larvae

In order to exclude that the observed reduction in mitochondrial transport frequency resulted from a decrease in the amount of mitochondria in the VNC of D42>Khc$^{wt+N262S}$ and D42>Khc^{N262S} animals, the VNCs of D42, D42>Khc^{wt}, D42>Khcwt+^{N262S} and D42>Khc^{N262S} larvae were stained for mito-GFP, a marker of mitochondria.

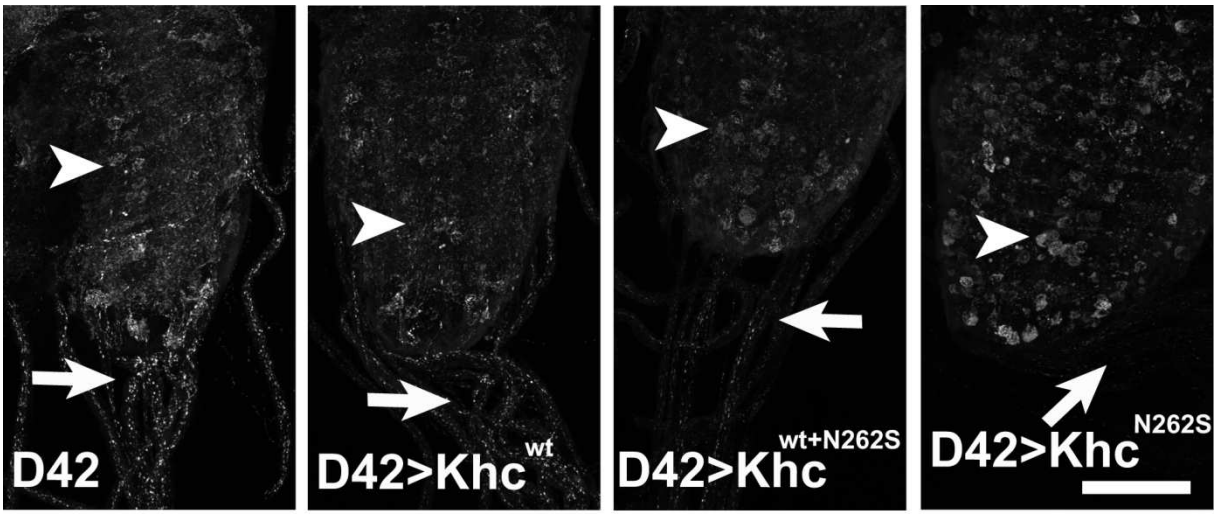

Figure 26: Expression of Khc^{N262S} does not affect total amount of mitochondria in the motor-neuron cell bodies in the VNC of *Drosophila* larvae.
Anti-GFP staining of mito-GFP in the VNC of *Drosophila* larvae, to mark mitochondria. Scale bar, 50 µm.

The amount of mitochondria was not reduced in the VNC of D42>Khc$^{wt+N262S}$ and D42>Khc^{N262S} animals compared to controls, as indicated by fluorescence intensities of mito-GFP in the VNCs of the four genotypes. In fact, fluorescence intensities were slightly increased in D42>Khc$^{wt+N262S}$ and D42>Khc^{N262S}, suggesting an accumulation of mitochondria in motor-neuron cell bodies of the VNC of these animals (Figure 26, arrowheads). A decrease in fluorescence intensities of mito-GFP in the segmental nerves exiting the VNC in D42>Khc$^{wt+N262S}$ and D42>Khc^{N262S} larvae (Figure 26, arrows) was evident. This reduction was more distinct in D42>Khc^{N262S} animals than in D42>Khc$^{wt+N262S}$, which is consistent with the observed reduction in the transport frequency of mitochondria, that was also more severe in D42>Khc^{N262S} larvae.

4.2.1.7.3 Khc^{N262S} expression in motor-neurons does not affect the velocity of wild-type kinesin-1 motors in *Drosophila* larvae

The transport velocity of mitochondria was determined during periods of uninterrupted runs. Movement of mitochondria was recorded in anesthetized larvae after bleaching a section of the nerve. For quantification, 7-9 movies of individual larvae were analyzed per genotype. From each movie the speed of 5-10 mitochondria per direction was quantified.

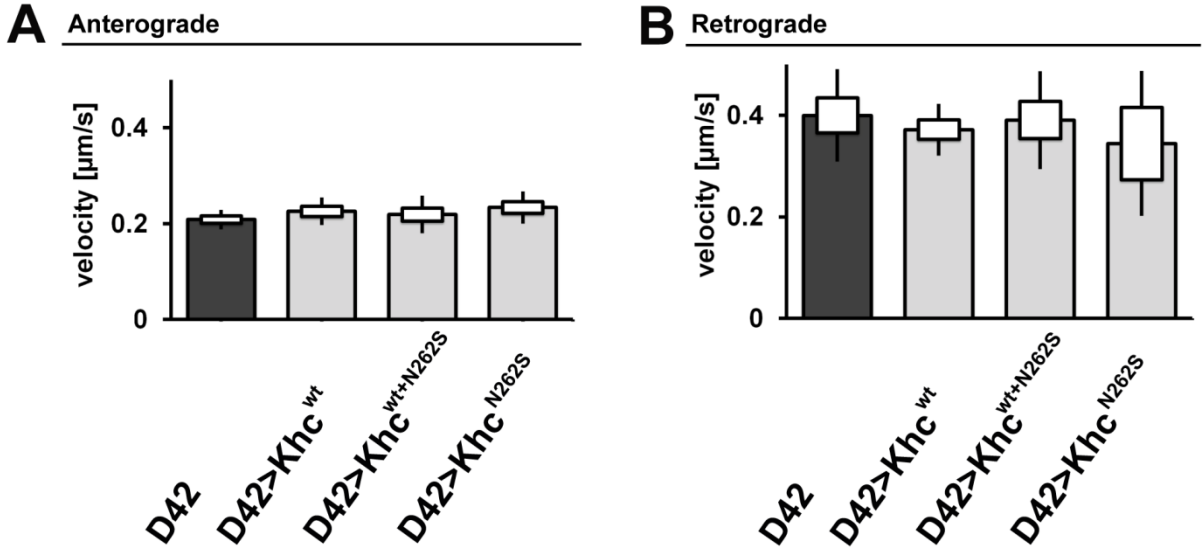

Figure 27: Expression of Khc^{N262S} does not affect the transport velocity of mitochondria in motor-neuron axons of *Drosophila* larvae.

(A-B) There is no difference in the velocity of mitochondrial transport among the four genotypes analyzed. Statistical significance was determined by using a Kruskal-Wallis H-test for multiple comparisons. The SEM is shown as a box, the SD as a black line.

	Anterograde		*Retrograde*	
	Velocity [µm/s]	***p-value***	***Velocity [µm/s]***	***p-value***
D42	0.21 ± 0.02	-	0.40 ± 0.09	-
D42>Khc^{wt}	0.23 ± 0.03	1	0.37 ± 0.05	1
D42>Khc$^{wt+N262S}$	0.22 ± 0.04	1	0.39 ± 0.10	1
D42>Khc^{N262S}	0.23 ± 0.03	0.520	0.34 ± 0.14	1

Table 15: Quantification of transport velocities of mitochondria in motor-neuron axons of *Drosophila* larvae. No difference is observable in the velocity of transport mitochondria among the four genotypes analyzed. Data given are means ± SD. Statistical significance was determined using a Kruskal-Wallis H-test for multiple comparisons. The p-values shown are when compared to D42.

There was no significant difference in either anterograde or retrograde transport velocity among the four genotypes (Figure 27 and Table 15). The transport velocities in the anterograde and retrograde direction determined in D42 larvae in this study (Table 15) are similar to transport velocities previously described for mitochondria in wild-type *Drosophila* larvae (Pilling et al., 2006).

4.2.1.7.4 Khc^{N262S} expression does not change number or duration of pauses between mitochondrial runs in *Drosophila* motor-neuron axons

To further address the impact of ectopic Khc^{N262S} expression on axonal transport, the number and duration of pauses between mitochondrial runs were determined. For evaluation of the number of pauses, we assessed the mitochondria that completely

traversed the bleached area (around 30 µm) of the segmental nerve. For analysis of the duration of the pauses, we analyzed the mitochondria that entered the bleached zone and completely traversed it or paused till the end of the movie, but were traceable for at least 50 frames.

These analyses were performed in the genotypes D42, D42>Khc^{wt} and D42>Khc$^{wt+N262S}$. In D42>Khc^{N262S} larvae too few moving mitochondria were available for analyses.

For analysis of the number of pauses, pauses were defined as follows: (1) the particle did not move for at least two consecutive frames, and (2) the particle jittered back and forth before moving in its original direction again. Using these specifications, there was no difference in the number of pauses observed when a mitochondrion traversed a 30 µm part of the nerve, in either the anterograde or retrograde direction (Table 16).

	Anterograde		***Retrograde***	
	median	***mean***	***median***	***Mean***
D42	2	2.1	1	1.6
D42>Khc^{wt}	2	1.9	2	1.4
D42>Khc$^{wt+N262S}$	2	1.8	1	1.6

Table 16: Khc^{N262S} expression does not change number of pauses between mitochondrial runs in *Drosophila* motor-neuron axons.
The number of pauses was quantified for each mitochondrion that traversed a 30 µm part of the nerve. For quantification, the following numbers of mitochondria were analyzed: Anterograde: D42 (27 mitochondria from four larvae), D42>Khc^{wt} (16 mitochondria from four larvae), and D42>Khc$^{wt+N262S}$ (30 mitochondria from seven larvae); Retrograde: D42 (18 mitochondria from four larvae), D42>Khc^{wt} (18 mitochondria from four larvae), and D42>Khc$^{wt+N262S}$ (19 mitochondria from six larvae).

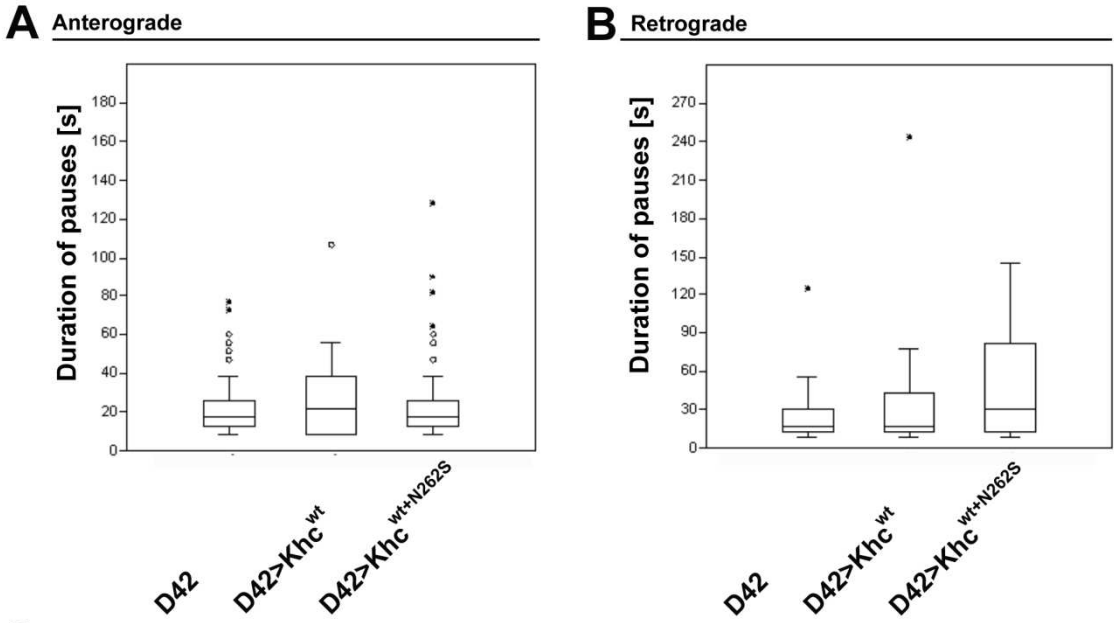

C

	Anterograde		*Retrograde*	
	median	***p-value***	***median***	***p-value***
D42	17.12	1	17.12	1
D42>Khc^{wt}	19.26	1	19.26	1
D42>Khc$^{wt+N262S}$	17.12	1	27.82	1

Figure 28: Khc^{N262S} expression does not change duration of pauses between mitochondrial runs in *Drosophila* motor-neuron axons.

(A-B) Boxplots of the durations of pauses. Distribution of the length of pauses in D42, D42>Khc^{wt} and D42>Khc$^{wt+N262S}$ larvae in the anterograde (A) and retrograde (B) direction. For quantification of the anterograde pause duration, a total of 27 mitochondria from four larvae were analyzed for D42, 16 mitochondria from four larvae for D42>Khc^{wt}, and 37 mitochondria from seven larvae for D42>Khc$^{wt+N262S}$. For quantification of the retrograde pause duration, a total of 21 mitochondria from four larvae were analyzed for D42, 18 mitochondria from four larvae for D42>Khc^{wt}, and 22 mitochondria from six larvae were analyzed for D42>Khc$^{wt+N262S}$. In the boxplot the 25-75 percent quartiles are shown as a box. The median is drawn as a horizontal line inside the box. The whiskers represent the upper and lower 1.5 times interquartile range (IQR). Values outside the 1.5 times IQR are defined as outliers. Values between the 1.5 IQR and 3 IQR and are shown as circles, values outside the 3 IQR, are shown as dark circles. (C) Determination of median value of duration of pauses. Statistical significance was determined by using a Kruskal-Wallis H-test for multiple comparisons. The p-values shown are when compared to D42.

Quantification revealed that there was no statistically significant difference in pause duration among the three genotypes, neither in the anterograde nor in the retrograde direction (Figure 28). In the retrograde direction, the proportion of pauses with a longer duration seemed slightly increased in D42>Khc$^{wt+N262S}$ animals; however this was not statistically significant.

4.2.1.8 The severity of NMJ defects caused by Khc^{N262S} expression depends on the length of the innervating axon

Behavioral experiments with D42>Khc$^{wt+N262S}$ and D42>Khc^{N262S} larvae, as well as data obtained from *khc* null mutants (Hurd and Saxton, 1996a) predict more severe defects in the posterior abdominal segments of the larvae. To address this NMJ structure was analyzed in the anterior abdominal segment A2 and the posterior abdominal segment A5.

To this D42, D42>Khc^{wt}, D42>Khc$^{wt+N262S}$ and D42>Khc^{N262S} larvae were raised at 29℃ and third-instar larvae were dissected and stained for neuronal membrane marker (anti-HRP; quantification of NMJ area) and the presynaptic marker Brp (quantification of synapse number). To account for possible differences in larval size, data were normalized to the area of muscle 6/7 of segment A2 and A5.

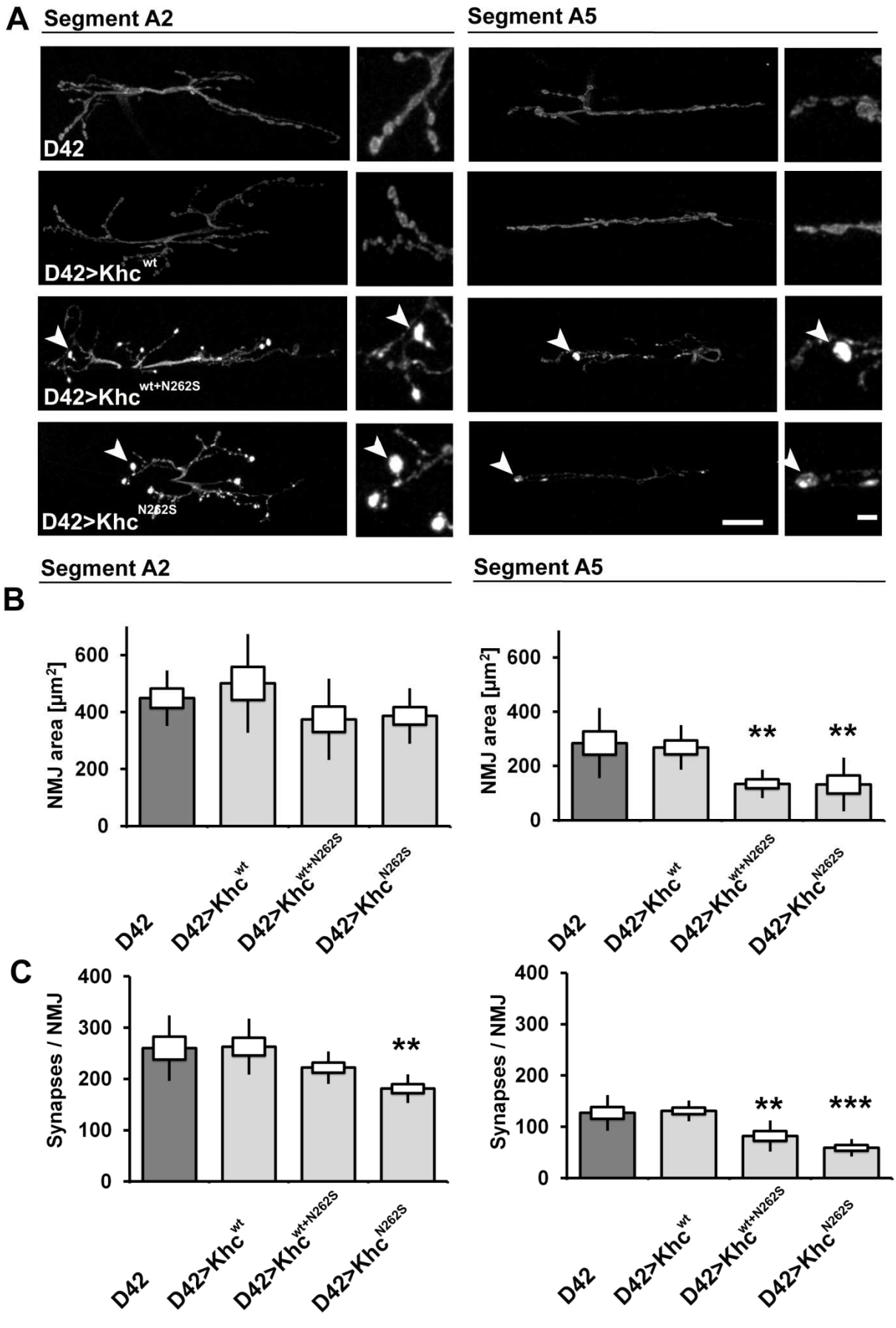
A
Segment A2
Segment A5
D42
D42>Khc wt
D42>Khc wt+N262S
D42>Khc N262S
B
Segment A2
Segment A5
NMJ area [µm²]
600
400
200
0
**
**
D42
D42>Khc wt
D42>Khc wt+N262S
D42>Khc N262S
C
Synapses / NMJ
400
300
200
100
0
**
**
***
D42
D42>Khc wt
D42>Khc wt+N262S
D42>Khc N262S

Figure 291: NMJ defects caused by expression of Khc^{N262S} depend on the length of the innervating axon.

(A) Confocal images of anti-HRP staining showing NMJs of muscle 6/7 in abdominal segments A2 and A5 of *Drosophila* larvae. Boutons with abnormal anti-HRP accumulation (A, arrowheads) were observed in D42>Khc^{N262S} and D42>Khc$^{wt+N262S}$ larvae. Scale bars: 20 µm, enlargement 20 µm. (B) Quantification of the NMJ area in the anterior segment A2 and in the posterior segment A5. (C) Quantification of synapse numbers in segment A2 and A5. For quantification, 8-10 larvae per genotype were analyzed. Statistical significance was determined using One-way ANOVA. ** $p < 0.01$; *** $p < 0.001$. The SEM is shown as a box, the SD as a black line.

	Segment A2		***Segment A5***	
	NMJ area [µm²/NMJ]	***p-value***	***NMJ area [µm²/NMJ]***	***p-value***
D42	449 ± 97	-	284 ± 129	-
D42>Khc^{wt}	500 ± 173	0.835	268 ± 82	0.982
D42>Khc$^{wt+N262S}$	375 ± 143	0.631	133 ± 52	0.007
D42>Khc^{N262S}	386 ± 97	0.745	132 ± 99	0.006
	Synapses [synapses/NMJ]	***p-value***	***Synapses [synapses/NMJ]***	***p-value***
D42	260 ± 64	-	127 ± 35	-
D42>Khc^{wt}	263 ± 55	0.998	131 ± 20	0.994
D42>Khc$^{wt+N262S}$	222 ± 31	0.306	82 ± 30	0.002
D42>Khc^{N262S}	181 ± 28	0.004	59 ± 17	0.0002

Table 17: Motor-neuron specific expression of Khc^{N262S} reduces area and synapse number of NMJs of muscles 6/7 in abdominal segments A2 and A5.

Data represent the mean ± SD. Statistical significance was determined using One-way ANOVA. The p-values shown are compared to D42 larvae.

The NMJs of the D42>Khc$^{wt+N262S}$ and D42>Khc^{N262S} larvae exhibited an inhomogeneity in anti-HRP staining. There was a strong increase in the anti-HRP intensity in terminal boutons of the NMJs (Figure 29A, arrowheads). This inhomogeneity in anti-HRP staining of the NMJs is comparable to that observed in segmental nerves, where axonal swellings in D42>Khc$^{wt+N262S}$ and D42>Khc^{N262S} animals are characterized by a strong increase in anti-HRP intensity, while outside of the swellings anti-HRP staining was dimmer (Figure 22).

	Segment A2	***Segment A5***	***Segment A2***	***Segment A5***
	HRP area [%]		***Synapse number [%]***	
D42	100	100	100	100
D42>Khc^{wt}	103	94	101	97
D42>Khc$^{wt+N262S}$	84	47	85	65
D42>Khc^{N262S}	85	46	70	46

Table 18: Motor-neuron expression of Khc^{N262S} results in a reduction of NMJ areas and synapse numbers.

Motor-neuron specific expression of Khc^{N262S} reduces percental NMJ areas and synapse numbers in D42>Khc$^{wt+N262S}$ and D42>Khc^{N262S} larvae more severely in the posterior segment A5.

Analysis revealed differences in the severity of NMJ defects caused by Khc^{N262S} expression that were dependent on the length of the innervating axon. In abdominal segment A2 there was a trend towards a reduction of the NMJ area (Table 17 and Figure 29B) in D42>Khc$^{wt+N262S}$ and D42>Khc^{N262S} animals; however this was not statistically significant. The synapse number at the NMJ of muscle 6/7 in segment A2 was significantly decreased in D42>Khc^{N262S} animals but not in D42>Khc$^{wt+N262S}$ larvae (Table 17 and Figure 29C). Only a trend towards a decrease in synapse numbers was present in these animals. In abdominal segment A5 both the NMJ area

as well as synapse number were significantly reduced in D42>Khc$^{wt+N262S}$ and D42>Khc^{N262S} animals (Table 17 and Figure 29B - C).The reduction in synapse numbers in abdominal segment A5 was more severe in the D42>Khc^{N262S} larvae. Motor-neuron specific expression of Khc^{wt} did not alter the NMJ area or synapse number in either of the two segments compared to D42 animals.

The decrease in the NMJ area and synapse number was proportional within the segments (Table 18) and was more distinct in the posterior segment A5, which is innervated by longer axons than segment A2. This reflects the more severe impairment of longer axons by the N262S mutation in Khc that also becomes obvious in the tail-flipping phenotype of the Khc^{N262S} expressing larvae (paragraph 4.2.1.2).

4.2.1.9 Motor-neuron specific expression of Khc^{N262S} causes presynaptic degeneration of neuromuscular structures in *Drosophila* larvae

HSP is a neurodegenerative disorder characterized by a progressive distal axonopathy, presumably triggered by the degeneration of the synapses. Thus, it was of interest, whether any signs of degeneration of the NMJs could be observed in the *Drosophila* model of SPG10.

To examine presynaptic degenerative alterations the synaptic footprint assay, initially described by G. Davis and colleagues (Eaton et al., 2002) was used.

To investigate degeneration occurring at the NMJs, the postsynaptic SSR was marked with a Discs-large-GFP (Dlg-GFP) fusion protein. GFP was inserted into the *dlg* locus (Buszczak et al., 2007) resulting in the expression of Dlg-GFP under the

control of the endogenous Dlg promoter (Flytrap: CC01936). In the assay D42, D42>Khc^{wt}, D42>Khc$^{wt+N262S}$ and D42>Khc^{N262S} larvae, that co-expressed Dlg-GFP under the endogenous Dlg promoter, were used. Larvae were raised at 29℃ and third-instar larvae were dissected and stained for presynaptic neuronal membranes (anti-HRP antibody) and synaptic vesicles (anti-Synapsin antibody). NMJs of muscles 6/7 of the posterior abdominal segment A5 were examined.

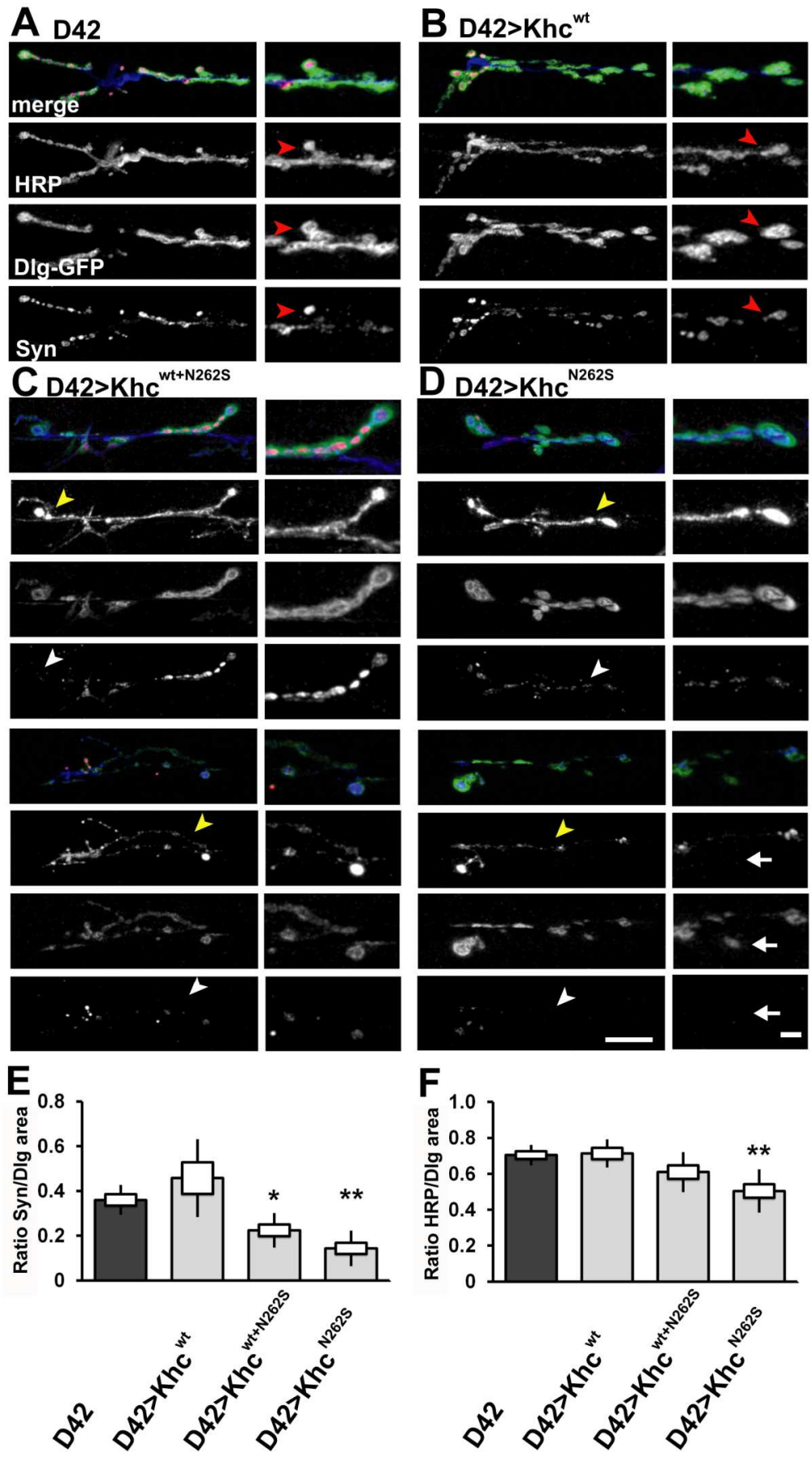
A D42
merge
HRP
Dlg-GFP
Syn
B D42>Khc^wt
C D42>Khc^wt+N262S
D D42>Khc^N262S
E
Ratio Syn/Dlg area
0.8
0.6
0.4
0.2
0
*
**
D42
D42>Khc^wt
D42>Khc^wt+N262S
D42>Khc^N262S
F
Ratio HRP/Dlg area
1.0
0.8
0.6
0.4
0.2
0
**
D42
D42>Khc^wt
D42>Khc^wt+N262S
D42>Khc^N262S

Figure 30: Motor-neuron specific expression of Khc^{N262S} results in presynaptic alterations at the NMJs of *Drosophila* larvae.

(A-D) Confocal images of NMJs innervating muscle 6/7 from segment A5 of *Drosophila* larvae that expresse Dlg-GFP. NMJs were additionally stained for HRP (neuronal membranes) and Syn (synaptic vesicles). In the control larvae (D42 and D42>Khc^{wt}, A-B) presynaptic neuronal membranes and Syn were almost completely apposed to Dlg (red arrowheads). In D42>Khc$^{wt+N262S}$ and D42>Khc^{N262S} larvae (C-D), the level of presynaptic Syn was reduced (white arrowheads) and the neuronal membranes showed abnormal organization (yellow arrowheads) Scale bar: 20 µm; enlargement 5 µm. (E-F) Quantification of the ratio of the presynaptic components, synaptic vesicles (E) and neuronal membranes (F), to the SSR marker Dlg in NMJs innervating muscles 6/7 of segment A5. For quantification, 6-10 NMJs per genotype were analyzed. Statistical significance was determined using One-way ANOVA or Kruskal-Wallis H-test for multiple comparisons * $p < 0.05$; ** $p < 0.01$. The SEM is shown as a box, the SD as a black line.

In the control animals (D42 and D42>Khc^{wt}), neuronal membranes (marked by HRP) and presynaptic vesicles (marked by Syn) showed almost complete apposition with the SSR marker Dlg (Figure 30A – B, red arrowheads). In contrast, the D42>Khc$^{wt+N262S}$ (Figure 30C) and D42>Khc^{N262S} (Figure 30D) larvae exhibited reduced abundance and altered distribution of synaptic vesicles (Figure 30C - D, white arrowheads) as well as alterations in neuronal membrane organization (Figure 30C - D, yellow arrowheads). The D42>Khc^{N262S} larvae were generally affected more severely compared to the D42>Khc$^{wt+N262S}$ larvae. However, synaptic footprints (Eaton et al., 2002), regions negative for both synaptic vesicles and neuronal membranes, and positive for Dlg were detected infrequently (Figure 30D, white arrow).

To investigate the presynaptic changes, observed in D42>Khc$^{wt+N262S}$ and D42>Khc^{N262S} larvae, in more detail the corresponding pre- and postsynaptic areas

were examined. To this the ratio of the presynaptic Syn area to the Dlg area, as well as of the presynaptic HRP area to the Dlg area was quantified.

	Syn/Dlg ratio		***HRP/Dlg ratio***		***Syn/HRP ratio***	
		p-value		***p-value***		***p-value***
D42	0.36 ± 0.07	-	0.70 ± 0.06	-	0.51 ± 0.09	-
D42>Khc^{wt}	0.46 ± 0.17	1	0.71 ± 0.08	0.998	0.54 ± 0.05	0.979
D42>Khc$^{wt+N262S}$	0.22 ± 0.08	0.049	0.61 ± 0.11	0.270	0.36 ± 0.09	0.105
D42>Khc^{N262S}	0.14 ± 0.08	0.0065	0.50 ± 0.12	0.0029	0.30 ± 0.19	0.013

Table 19: Motor-neuron specific expression of Khc^{N262S} alters the ratio of presynaptic to postsynaptic area at the NMJs of muscles 6/7 in abdominal segment A5 of *Drosophila* larvae.

Data represent mean ± SD. Statistical significance was determined using One-way ANOVA or Kruskal-Wallis H-Test for multiple comparison. The p-values show are when compared to D42.

The Syn/Dlg ratio was decreased in mutant larvae (Figure 30E and Table 19), showing that presynaptic Syn was lowered in these animals in relation to the postsynaptic SSR area. The decrease was more distinct in the D42>Khc^{N262S} larvae. The ratio of the presynaptic neuronal membrane (HRP) area to the Dlg area, was also decreased in D42>Khc^{N262S} larvae, but not in D42>Khc$^{wt+N262S}$ larvae (Figure 30F and Table 19). Generally, the alteration of the Syn/Dlg ratio was more pronounced than the alteration of the HRP/Dlg ratio in both mutant genotypes, implying a stronger decrease in the amount presynaptic vesicles (Syn) than neuronal membrane area (HRP) compared to the postsynaptic SSR. Determination of the ratio of presynaptic vesicles (Syn) to presynaptic neuronal membrane area (Syn/HRP) revealed that it was significantly reduced in D42>Khc^{N262S} animals, suggesting a

stronger decrease in presynaptic vesicles than neuronal membranes (Table 19). In the D42>Khc$^{wt+N262S}$ larvae there was a trend towards a decrease in Syn/HRP ratio; however this was not statistically significant.

4.2.1.10 Motor-neuron specific expression of Khc^{N262S} does not cause loss of motor-neuron cell bodies in *Drosophila* larvae

HSP is assumed to be a progressive distal axonopathy, presumably starting with degeneration of synapses. Interestingly, there is typically little neuronal cell death in HSP patients (Blackstone et al., 2011). So far nothing is known about motor-neuron cell loss in human SPG10 patients, as no autopsies have been reported. Thus, we were interested whether degeneration of synapses in the *Drosophila* SPG10 model is accompanied by a loss of motor-neuron cell bodies. Since the degeneration of synapses was more severe in D42>Khc^{N262S} animals, analysis of motor-neuron cell bodies was only performed in this genotype. For analysis D42 and D42>Khc^{N262S} larvae were raised at 29℃ and third-instar larvae were used.

To determine loss of motor-neuron cell bodies, a subset of motor-neuron cell bodies was marked by staining for the transcription factor Eve. Eve is, amongst others, expressed in the medially located aCC and RP2 motor-neurons, as well as in the pCC interneurons (Landgraf et al., 2003). To quantify motor-neuron cell loss the aCC (innervating abdominal muscle 1) and RP2 (innervating abdominal muscle 2) motor-neurons that are located in the VNC middle line and innervate segments A1-A3 (anterior segments) and A5-A7 (posterior segments) were quantified. For a more detailed description of the assay see Material and Methods, paragraph 3.7.6.

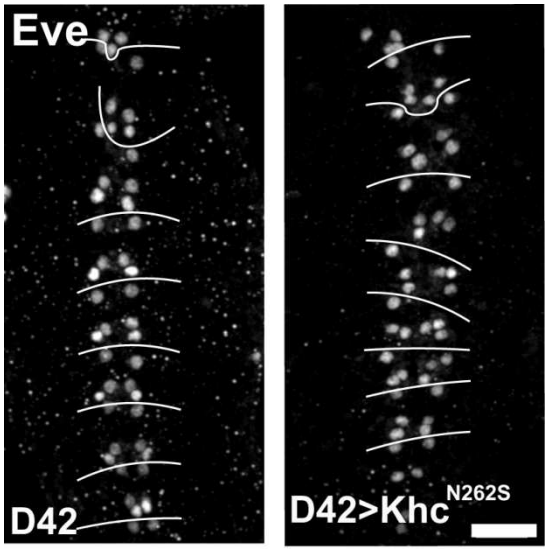

Figure 31: Motor-neuron specific expression of Khc^{N262S} does not cause loss of aCC and RP2 motor-neuron cell bodies in *Drosophila* larvae.

Even-skipped staining in the VNC of D42>Khc^{N262S} and D42 larvae. The white lines indicate the groups of neuronal cell bodies responsible for innervations of different abdominal segments. Scale bar: 20 µm.

No motor-neuron loss was detected in D42>Khc^{N262S} larvae (Figure 31) at a stage when degeneration at the NMJ was already pronounced (D42: 5 larvae; D42>Khc^{N262S}: 5 larvae). This is consistent with the concept that HSP is primarily caused by synaptopathy and axonopathy, whereas motor-neuron cell loss is neither causative for HSP nor an early feature of the pathological process.

4.2.2 Possible mechanisms contributing to pathology in the HSP subtype SPG10

4.2.2.1 The role of mitochondria in the pathology of SPG10

Mitochondrial dysfunction has been implicated in a number of neurodegenerative diseases, e.g. Parkinson´s or ALS (Schon and Przedborski, 2011) and genes associated with HSP have been linked to mitochondrial function (Blackstone et al., 2011). Kinesin-1, which is affected in SPG10, is the major motor protein for anterograde transport of mitochondria in vertebrates and *Drosophila* (Pilling et al., 2006). *In vivo* analysis of the axonal transport of mitochondria revealed that the

transport frequency of mitochondria was strongly decreased when Khc^{N262S} was expressed in motor-neurons of *Drosophila* larvae, in both the anterograde and retrograde direction (paragraph 4.2.1.7). We were therefore interested to assign mitochondrial densities at the NMJs of the SPG10 *Drosophila* model. Since mitochondria are the major site of ATP production, the amount of mitochondria at the NMJ is critical to maintain energy levels and thus proper synaptic function. In contrast, energy depletion, due to decreased amount of mitochondria at the NMJs, might initiate synaptic dysfunction and eventually loss of synapses (Sheng and Cai, 2012).

To study the impact of impaired mitochondrial transport in *Drosophila* larvae on the mitochondrial density at the NMJs, mitochondria were labeled with mito-GFP (Pilling et al., 2006). For the assay D42, D42>Khc^{wt}, D42>Khc^{N262S} and D42>$Khc^{wt+N262S}$ larvae, that co-expressed mito-GFP, were raised at 29℃ and third-instar larvae were analyzed. Quantification of mitochondrial density was performed at the NMJs of muscle 6 and 7 of segment A2 and the percentage of mitochondrial area per NMJ area was determined.

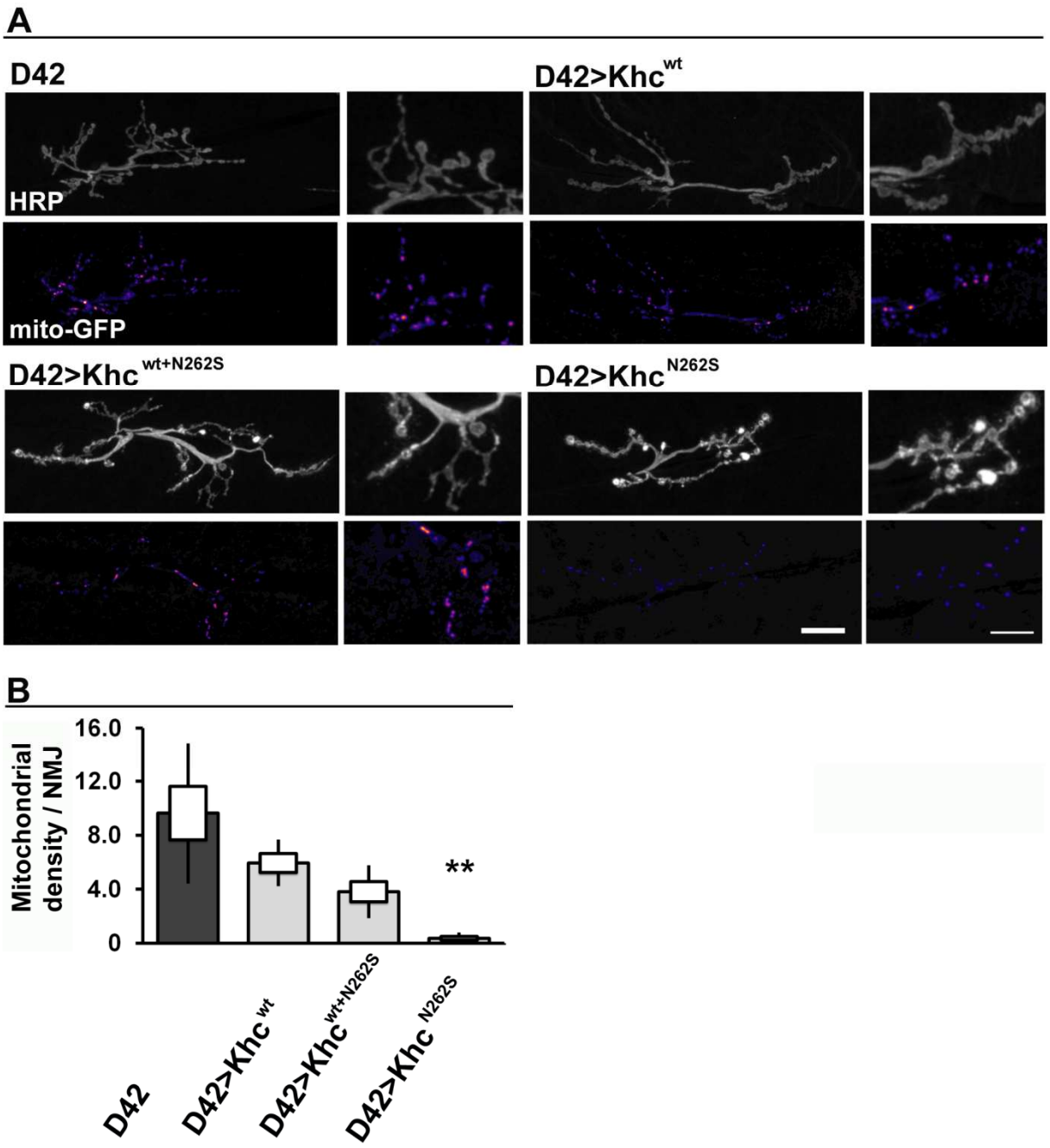

Figure 32: Motor-neuron specific expression of Khc^{N262S} reduces mitochondrial density at the NMJs of *Drosophila* larvae.

(A) Confocal images of NMJs of muscles 6 and 7 of segment A2 of *Drosophila* larvae. In mutant larvae (D42>Khc$^{wt+N262S}$ and D42>Khc^{N262S}), the mitochondrial density at the NMJs was lowered compared to that in the control larvae (D42 and D42>Khc^{wt}). Scale bar: 20 µm; enlargement, 10 µm. (B) Quantification of the mitochondrial density at NMJs of muscle 6/7 of segment A2. For quantification, 6-9 NMJs per genotype were analyzed. Statistical significance was determined using Kruskal-Wallis H-test for multiple comparisons ** $p < 0.01$. The SEM is shown as a box, the SD as a black line.

	Mitochondrial density / NMJ	*n*	*p-value*
D42	9.64 ± 5.23	7	-
D42>Khc^{wt}	5.95 ± 1.72	6	0.8017
D42>Khc$^{wt+N262S}$	3.81 ± 1.97	7	0.1287
D42>Khc^{N262S}	0.36 ± 0.43	9	0.0062

Table 20: Mitochondrial density per NMJs of muscles 6/7 in segments A2 is reduced when Khc^{N262S} is expressed in motor-neurons of *Drosophila* larvae.
Data represent mean ± SD. Statistical significance was determined using Kruskal-Wallis H-test for multiple comparisons. The p-values shown are when compared to D42.

Quantification revealed that the mitochondrial density at the NMJ was significantly reduced in the D42>Khc^{N262S} animals (Figure 32A - B and Table 20). These animals exhibited a 96% reduction in mitochondrial density per NMJ compared to D42 larvae ($p < 0.01$) and a 90% reduction compared to the D42>Khc$^{wt+N262S}$ larvae ($p < 0.05$). Although quantification revealed an almost 60% lower mitochondrial density per NMJ in the D42>Khc$^{wt+N262S}$ larvae compared to D42 (Figure 32A - B and Table 20), this was not statistically significant; probably due to the high variance in the D42 animals.

In conclusion, we observed a strong decrease in mitochondrial density at the NMJs of D42>Khc^{N262S} animals and a trend towards a decrease in the D42>Khc$^{wt+N262S}$ larvae.

4.2.2.2 BMP signaling is impaired in a *Drosophila* model of the HSP subtype SPG10

Alterations in BMP signaling have been suggested as a potential common pathological mechanism underlying some subtypes of HSP (Blackstone et al., 2011). In BMP signaling at the *Drosophila* NMJ, presynaptic BMP receptors are activated by postsynaptically released Gbb (Marques et al., 2003, McCabe et al., 2003) inducing the phosphorylation of Mad (pMad), which in turn translocates to the nucleus, where it act as a transcription factor.

To examine BMP signaling in the *Drosophila* SPG10 model, pMad levels in motor-neuron cell bodies (aCC and RP2 motor-neurons), at the NMJs and in segmental nerves were quantified. For the assays D42, D42>Khc^{wt}, D42>Khc^{N262S} and D42>Khc$^{wt+N262S}$ larvae were raised at 25℃ or 29℃ and third-insta r larvae were analyzed. For details on quantification of nuclear and presynaptic pMad levels see Material and Methods, paragraph 3.7.8.

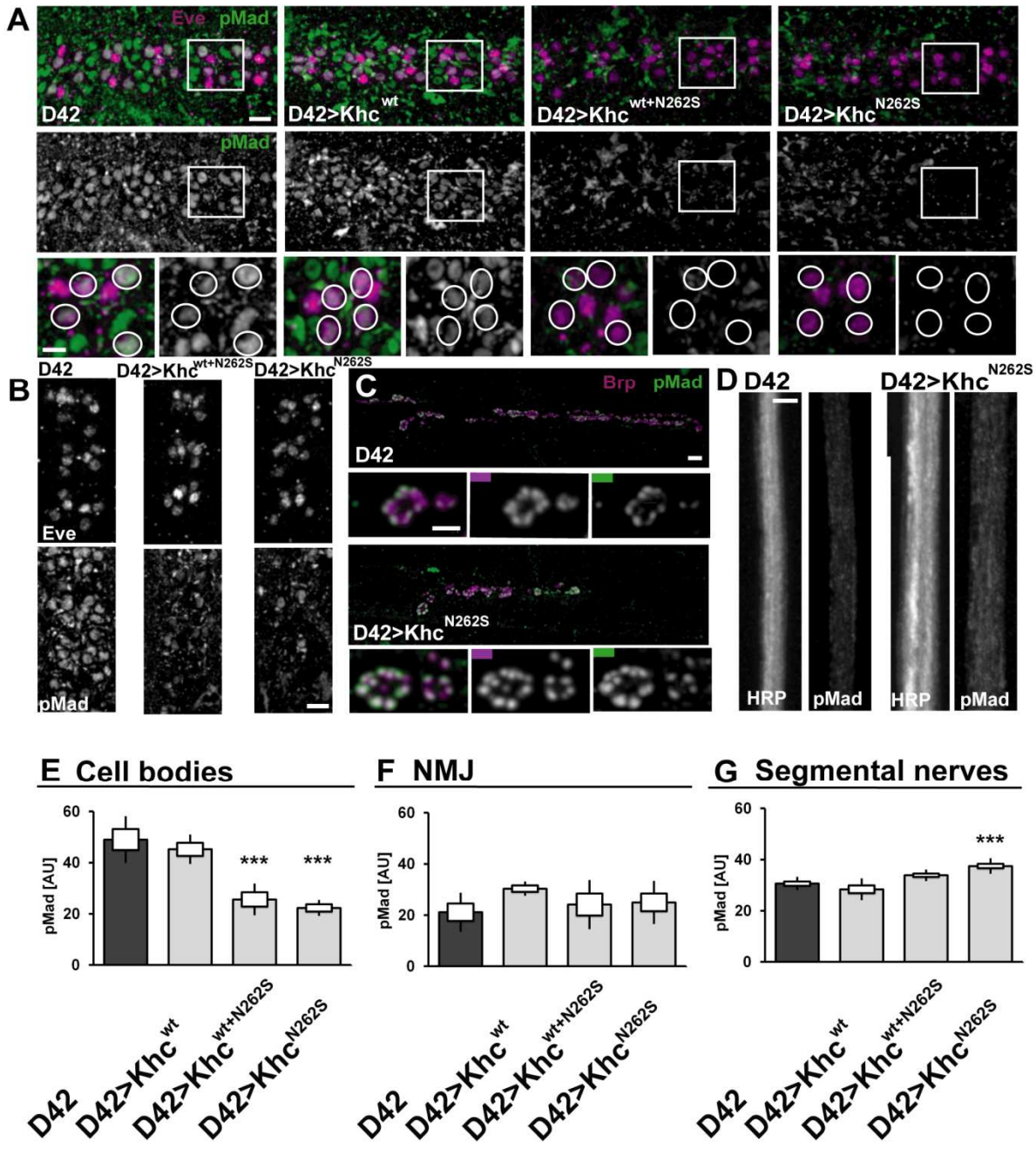

Figure 33: Motor-neuron specific expression of Khc^{N262S} impairs BMP signaling in motor-neurons of *Drosophila* larvae.

(A) Eve (magenta) and pMad (green) staining in the VNC of *Drosophila* larvae raised at 29℃. Motor-neurons innervating abdominal segments A3 to A7 are shown in the upper panels of (A). Squares indicate the magnification of motor-neurons innervating abdominal segment A6 shown in the bottom panels of (A). The aCC and RP2 motor-neurons, used for quantification of pMad (E), are encircled in the bottom panel to indicate their position. Scale bars: 10 µm. **(B)** Eve (magenta) and pMad (green) staining in the VNC of *Drosophila* larvae raised at 25℃. pMad levels were also lowered in D4 2>Khc$^{wt+N262S}$ and D42>Khc^{N262S} larvae if

they were kept at 25℃. Scale bar: 10µm. **(C)** Brp (magenta) and pMad (green) staining at NMJs innervating muscles 6/7 of segment A5 used for quantification shown in (F). Brp staining was used to mark the active zones of the NMJs. Scale bars: 5 µm. **(D)** pMad and anti-HRP staining in segmental nerves used for quantification shown in (G) Scale bar: 5 µm. **(E-G)** Quantification of pMad levels. **(E)** D42>Khc^{N262S} and D42>Khc$^{wt+N262S}$ larvae displayed significantly reduced levels of pMad in aCC and RP2 motor-neuron cell bodies compared to the control groups D42 and D42>Khc^{wt}. Five larvae were analyzed per genotype. **(F)** In the D42>Khc^{N262S} larvae no differences in pMad levels were observed at the NMJs innervating muscles 6/7 in segment A5. A minimum of five NMJs were analyzed per genotype. **(G)** The pMad level in the segmental nerves of D42>Khc^{N262S} larvae was significantly elevated compared to the control group D42. Per genotype, n = 8-12 segmental nerves were analyzed. Statistical significance was determined by using One-way ANOVA. ** $p < 0.01$; *** $p < 0.001$. The SEM is shown as a box, the SD as a black line.

	Motor-neuron cell bodies pMad		***NMJ***		***Segmental nerves***	
	[AU]	***p-value***	***pMad [AU]***	***p-value***	***pMad [AU]***	***p-value***
D42	49.03 ± 9.16	-	21.12 ± 7.68	-	30.62 ± 2.60	-
D42>Khc^{wt}	45.24 ± 5.76	0.782	30.33 ± 2.81	0.241	28.38 ± 4.26	0.380
D42>Khc$^{wt+N262S}$	25.62 ± 6.12	0.00032	24.11 ± 9.63	0.919	33.87 ± 2.24	0.104
D42>Khc^{N262S}	22.30 ± 3.14	0.00021	24.99 ± 8.45	0.844	37.49 ± 3.07	0.00024

Table 21: Motor-neuron specific expression of Khc^{N262S} alters pMad levels in motor-neuron cell bodies and segmental nerves of *Drosophila* larvae, but not at the NMJ.
Data represent mean ± SD. Statistical significance was determined using One-way ANOVA. The p-values show probability compared to D42.
Number of samples (n) used for quantification:
Motor neuron cell bodies: D42 5; D42>Khc^{wt} 5; D42>Khc$^{wt+N262S}$ 5; D42>Khc^{N262S} 5
NMJ: D42 5; D42>Khc^{wt} 5; D42>Khc$^{wt+N262S}$ 6; D42>Khc^{N262S} 6
Segmental nerves: D42 9; D42>Khc^{wt} 8; D42>Khc$^{wt+N262S}$ 11; D42>Khc^{N262S} 12

Motor-neuron specific expression of Khc$^{wt+N262S}$ and Khc^{N262S} at 29℃ resulted in a strong reduction of pMad levels in motor-neuron cell bodies (Figure 33A + E and

Table 21). In order to distinguish between a decreased activation of the BMP signaling pathway at the NMJ and impaired translocation of pMad to the nucleus, the pMad levels at the NMJ and within the segmental nerves were quantified. For these quantifications larvae were raised at 25°C, as for some unknown reason pMad staining at the NMJ did not work reasonably good in larvae raised at 29°C and could thus not be used for quantification. Although larvae raised at 25°C have a reduced expression level of Khc^{N262S}, they display ameliorated but similar HSP-pathology resembling characteristics and the nuclear pMad level in motor-neuron cell bodies was also decreased in these larvae (Figure 33B).

There were no significant differences in the presynaptic levels of pMad among the four genotypes analyzed (Figure 33C + F and Table 21). In contrast, quantification of the pMad levels in segmental nerves revealed an increase in pMad in the D42>Khc^{N262S} animals (Figure 33D + G and Table 21). In the D42>$Khc^{wt+N262S}$ larvae, a slight trend towards an increase was present, but this was not statistically significant compared to D42 larvae (Table 21). However the pMad level in segmental nerves of D42>$Khc^{wt+N262S}$ larvae was significantly higher than in the D42>Khc^{wt} larvae ($p = 0.0019$).

Taken together, these data indicate that the BMP signaling pathway is normally activated at the NMJ of D42>$Khc^{wt+N262S}$ and D42>Khc^{N262S} larvae. The observed decrease in nuclear pMad level is most likely due to impaired retrograde axonal transport of pMad, as indicated by the increased pMad level in segmental nerves of D42>Khc^{N262S} animals.

4.2.2.3 The cytoskeleton is disorganized in a *Drosophila* model of HSP subtype SPG10

Different studies suggest a role of BMP signaling in the maintenance of axonal microtubules. Down regulation of BMP signaling has been associated to a reduction of total and acetylated tubulin levels in axons of *Drosophila* (Wang, Shaw et al. 2007), as well as a loss of the microtubule associated protein Futsch from distal boutons of the NMJs (Wang, Shaw et al. 2007).

Since we observed reduced pMad levels in motor-neuron cell bodies in the *Drosophila* SPG10 model, implying a down regulation of BMP signaling, we were interested to investigate the cytoskeletal arrangement in motor-neuron axons and at the NMJs of these animals.

4.2.2.3.1 The axonal cytoskeleton is disturbed in a *Drosophila* model of SPG10

The axonal cytoskeleton is mainly comprised of the microtubules. For analysis of axonal microtubules D42, D42>Khc^{wt}, D42>Khc^{N262S} and D42>Khc$^{wt+N262S}$ larvae were raised at 29℃ and third-instar larvae were dissected. Microtubules were visualized using antibodies to total alpha-tubulin (recognizing free alpha-tubulin and microtubules) and acetylated alpha-tubulin (recognizing microtubules, but not free alpha-tubulin).

For analysis, the levels of total alpha-tubulin as well as acetylated alpha-tubulin were quantified. The fluorescence intensities of the alpha-tubulin channels were not normalized to a control channel (anti-HRP). Anti-HRP staining in segmental nerves of

Drosophila larvae, expressing Khc^{N262S}, was strongly inhomogeneous and anti-HRP fluorescence intensities were higher in segmental nerves of D42>Khc^{N262S} and D42>Khc$^{wt+N262S}$ larvae (Table 22), due to the high fluorescence intensity of anti-HRP staining in the axonal swellings. In D42>Khc^{N262S} animals anti-HRP fluorescence intensities were significantly higher compared to D42 larvae (Table 22). Thus for analysis total and acetylated alpha-tubulin levels were not normalized to anti-HRP fluorescence intensities as this would distort the results of the quantification.

	Anti-HRP fluorescence intensities in segmental nerves		
Genotype	***D42***	***D42>Khc$^{wt+N262S}$***	***D42>Khc^{N262S}***
1	39.535	42.303	52.603
2	38.297	47.711	48.586
3	29.394	47.381	49.947
4	31.726	40.479	46.220
5	33.839	39.422	37.214
6	38.170	37.210	44.940
7		34.310	46.857
8		25.734	
Mean ± SD	35.160 ± 4.119	39.319 ± 7.169	46.624 ± 4.869
p-value	-	0.3855	0.0043

Table 22: anti-HRP fluorescence intensities are increased in segmental nerves of *Drosophila* larvae expressing Khc^{N262S}. Statistical significance was determined using One-way ANOVA. The p-values shown are when compared to D42.

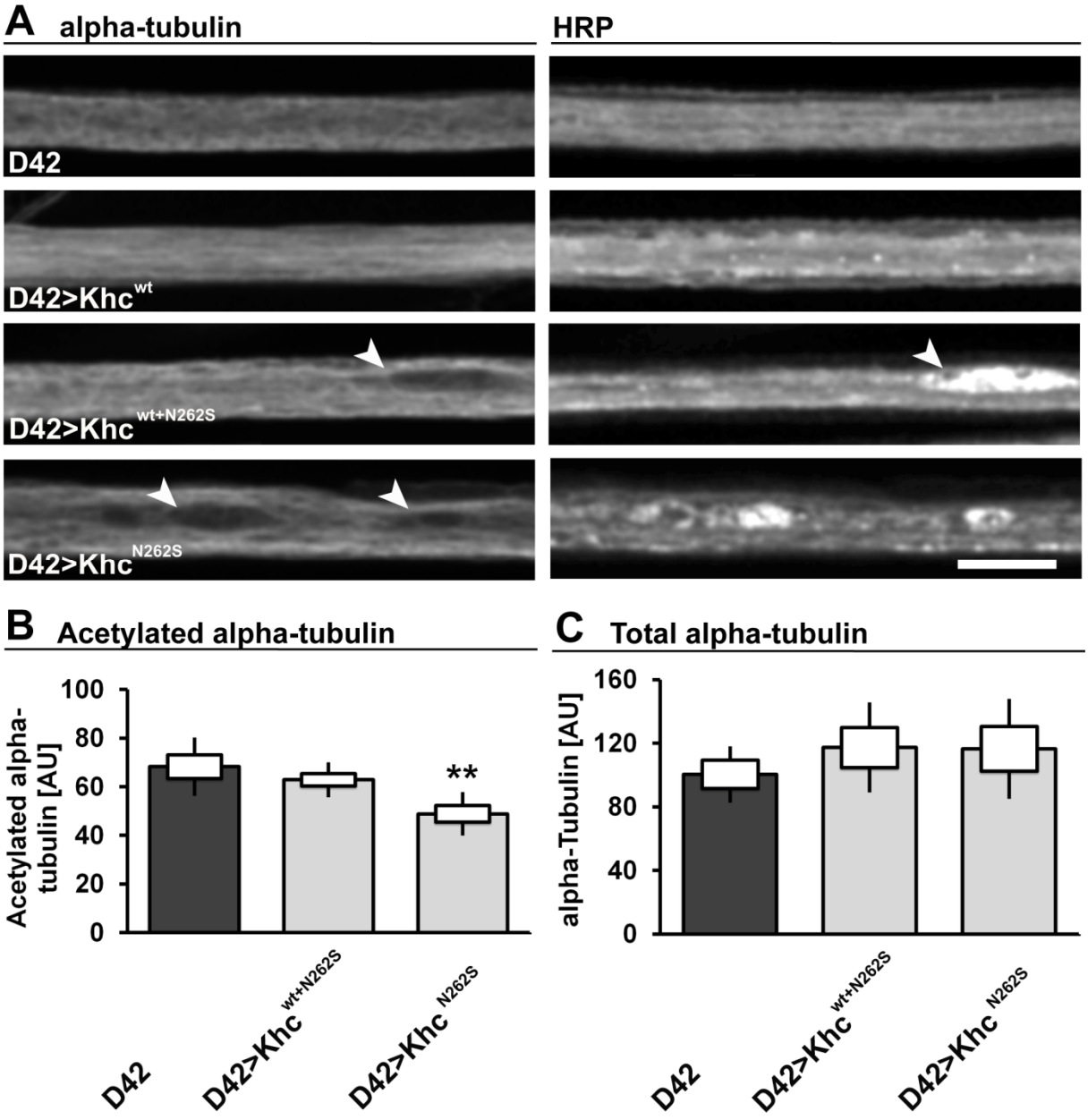

Figure 34: Motor-neuron expression of Khc^{N262S} disturbs axonal microtubules in *Drosophila* larvae.

(A) Total alpha-tubulin and anti-HRP staining in segmental nerves of *Drosophila* larvae Images shown are projections of three planes of the original stack. Scale bar, 10 µm. (B) Quantification of acetylated alpha-tubulin (stable microtubules) levels in segmental nerves. For quantification 6-8 segmental nerves per genotype were analyzed. (C) Quantification of total alpha-tubulin levels in segmental nerves. For quantification five segmental nerves per genotype were analyzed. AU, arbitrary units. Statistical significance was determined by using One-way ANOVA ** $p < 0.01$. The SEM is shown as a box, the SD as a black line.

	Acetylated alpha-tubulin			*Total alpha-tubulin*		
	[AU]	***n***	***p-value***	***[AU]***	***n***	***p-value***
D42	68 ± 12	6	-	100 ± 18	5	-
D42>Khc$^{wt+N262S}$	63 ± 7	8	0.545	117 ± 28	5	0.733
D42>Khc^{N262S}	49 ± 9	7	0.003	116 ± 31	5	0.759

Table 23: Quantification of acetylated and total alpha-tubulin within segmental nerves. Data represent the mean ± SD. Statistical significance was determined using One-way ANOVA. The p-values show probability compared to D42.

Immunohistochemical staining of alpha-tubulin within segmental nerves revealed that the progression of the filamentous microtubules in D42>Khc$^{wt+N262S}$ and D42>Khc^{N262S} animals was disturbed. In the control larvae (D42 and D42>Khc^{wt}) the microtubules progressed almost parallel to each other (Figure 34A), whereas in the D42>Khc$^{wt+N262S}$ and D42>Khc^{N262S} animals the axonal swellings interfered with the progression of the microtubules (Figure 34A, arrowheads). There were “holes” in the alpha-tubulin staining at the sites of axonal swellings (Figure 34A, arrowheads), indicating that the microtubule progression was altered at these sites of the axons.

Quantification of acetylated alpha-tubulin in segmental nerves (stable microtubules) revealed that the levels of acetylated alpha-tubulin were significantly decreased in the D42>Khc^{N262S} larvae ($p < 0.01$ compared to D42), but were unchanged in the D42>Khc$^{wt+N262S}$ larvae compared to the D42 larvae (Figure 34B and Table 23). The total alpha-tubulin levels in segmental nerves were not significantly altered among the three genotypes (Figure 34C and Table 23).

These data show that the organization of the axonal microtubule cytoskeleton is disturbed in the *Drosophila* model of SPG10.

4.2.2.3.2 The NMJ cytoskeleton is disturbed in a *Drosophila* model of SPG10

To visualize the NMJ cytoskeleton in *Drosophila* larvae, staining for the microtubule-associated protein Futsch was performed in D42, D42>Khc^{wt}, D42>Khc^{N262S} and D42>Khc$^{wt+N262S}$ larvae, raised at 29°C. Futsch staining in the NMJ s of muscles 6/7 in abdominal segments A2 and A5 was examined.

Futsch staining was bright at the entry point of the axon into the NMJ and weakened as it extended into the terminal boutons of the NMJs in D42 and D42>Khc^{wt} larvae. However, Futsch extended almost to the tip of all terminal boutons of the NMJs of muscle 6/7 in segment A2 (Figure 35A - B, arrows) and segment A5 (Figure 36A - B, arrows) of the control animals. In contrast, the NMJ cytoskeleton was disturbed in the D42>Khc$^{wt+N262S}$ and D42>Khc^{N262S} larvae. At the NMJs of abdominal segment A2 of D42>Khc$^{wt+N262S}$ and D42>Khc^{N262S} animals, Futsch staining was generally weaker within the branches of the NMJs. Although it extended almost to the tip of some terminal boutons (Figure 35C-D, arrows), some branches of the NMJs showed no Futsch staining (Figure 35C-D, arrowheads). In segment A5 the impairment in the mutant animals was more distinct (Figure 36C-D). Futsch staining was faint (Figure 36C-D, arrows) or completely gone (Figure 36C-D, arrowheads) within the branches of these NMJs.

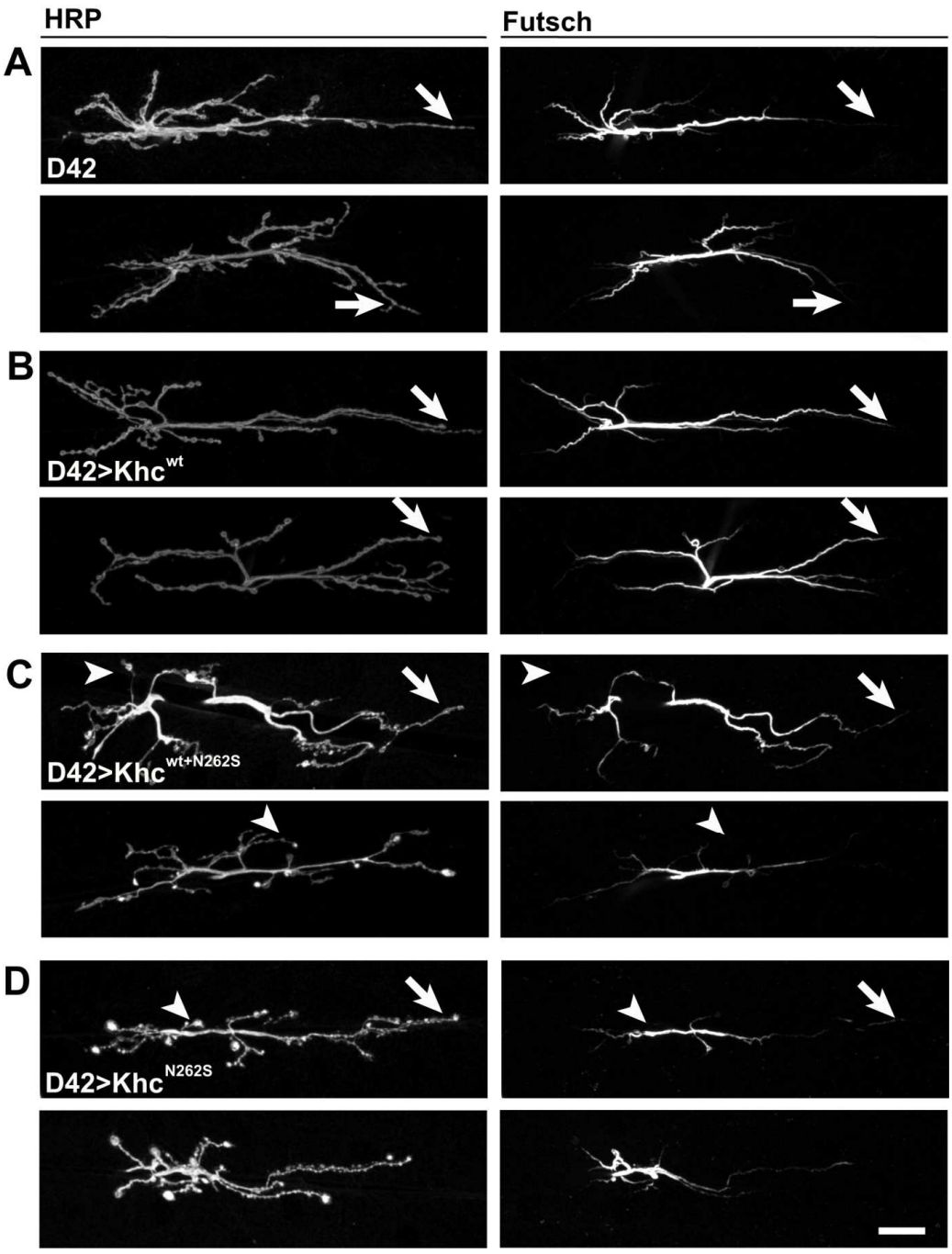

Figure 35: Motor-neuron expression of Khc^{N262S} disturbs cytoskeleton in NMJs of muscle 6/7 in abdominal segment A2 in *Drosophila* larvae.

(A-D) Confocal images of NMJs innervating muscles 6/7 in segment A2 of *Drosophila* larvae. NMJs were stained for Futsch and anti-HRP. In the control larvae (D42 and D42>Khc^{wt}, A-B), Futsch extended to the terminal branches of the NMJ (arrows). In mutant larvae (D42>Khc$^{wt+N262S}$ and D42>Khc^{N262S}, C-D), Futsch was detected in some terminal branches (arrows), but was completely lacking in others (arrowheads). Scale bar, 20 µm.

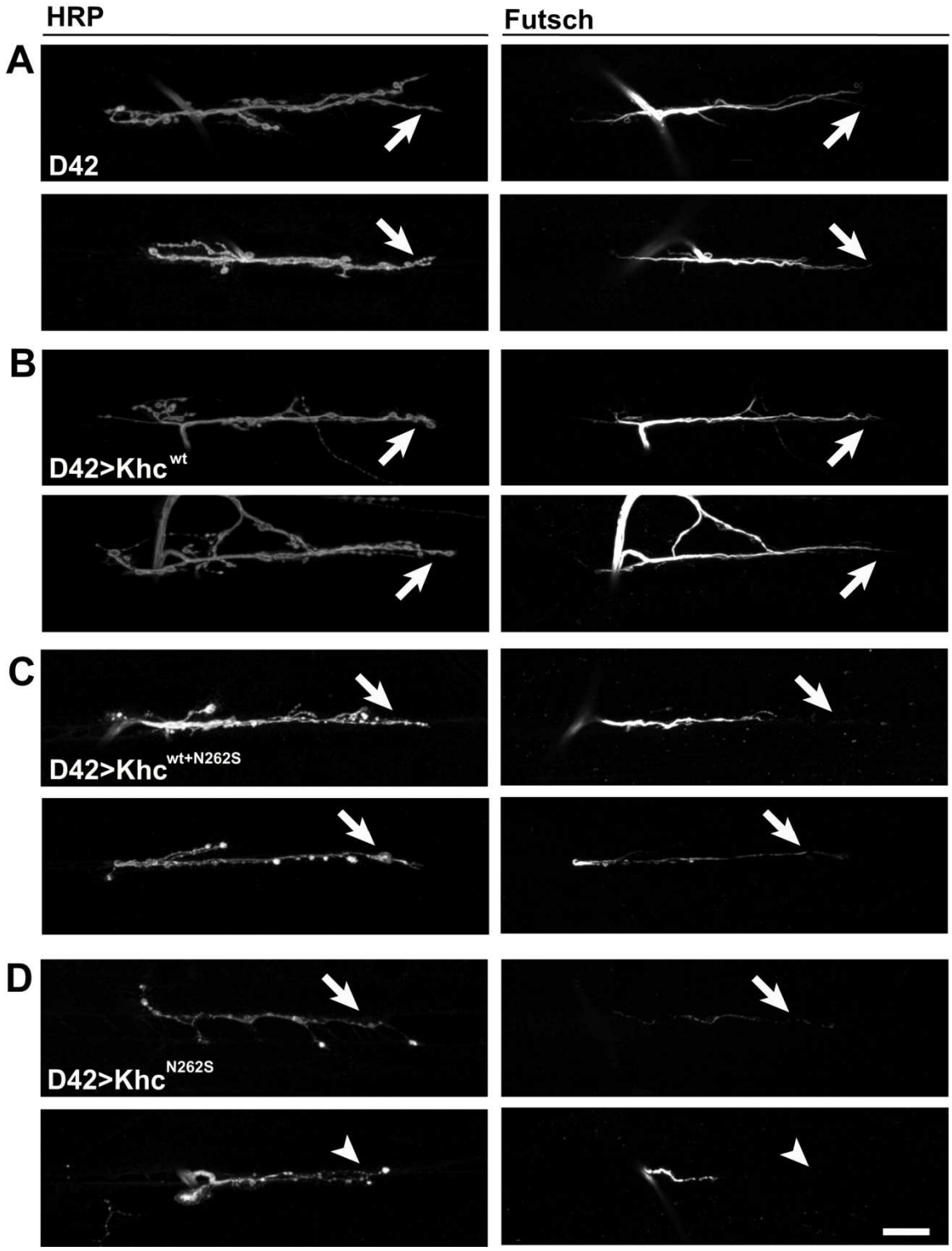

Figure 36: Motor-neuron expression of Khc^{N262S} disturbs cytoskeleton in NMJs of muscle 6/7 in abdominal segment A5 in *Drosophila* larvae.

(A-D) Confocal images of NMJs innervating muscles 6/7 in segment A5 of *Drosophila* larvae. NMJs were stained for Futsch and anti-HRP. In the control larvae (D42 and D42>Khc^{wt}, A-B), Futsch extended to the terminal branches of the NMJ (arrows). In mutant larvae (D42>Khc$^{wt+N262S}$ and D42>Khc^{N262S}, C-D), Futsch was fragmented (arrows) or completely absent in the terminal branches (arrowheads). Scale bar, 20 µm.

In conclusion, the axonal as well as the NMJ cytoskeleton are disturbed in a *Drosophila* SPG10 model. Analysis of the NMJ cytoskeleton revealed that defects were more pronounced at NMJs in the posterior abdominal segment A5. This is consistent with the data showing that the severity of NMJ defects caused by Khc^{N262S} expression depends on the length of the innervating axon (paragraph 4.2.1.8).

4.2.3 Comparative analysis of two HSP-associated mutations in *SPG10*

In a previous study the velocity and microtubule binding affinity of the HSP-associated mutations KIF5A^{K253N} and KIF5A^{N256S} in human KIF5A (*SPG10*) were analyzed *in vitro* (Ebbing et al., 2008). This study showed that both mutations cause a decrease in velocity of homodimeric mutated KIF5A. Furthermore, the mutation K253N reduced the microtubule binding affinity of homodimers, while N256S did not. We were interested whether the differences in biophysical properties of mutated Khc observed *in vitro* might result in different phenotypic characteristics in the *Drosophila* model. For a comparative analysis *Drosophila* Khc^{K259N} (corresponding to the human KIF5A^{K253N}) and *Drosophila* Khc^{N262S} (corresponding to the human KIF5A^{N262S}) were expressed in motor-neurons of *Drosophila*.

4.2.3.1 Motor-neuron expression of Khc^{K259N} and Khc^{N262S} affects locomotion of *Drosophila* larvae

A previous work (Störungen des axonalen Transports bei der hereditären spastischen Spinalparalyse im *Drosophila*-Model (Disturbance of axonal transport in a *Drosophila* model of hereditary spastic paraplegia, Inaugural Dissertation by Vera K. Siegert) showed that the mutation K259N in *Drosophila* Khc displayes a dominant-negative effect *in vivo*. Ectopic expression of Khc^{K259N} in the wild-type background, driven by pan-neuronal elav^{C115}-Gal4, severely impaired larval locomotion of small (1-3mm) as well as big (3-5mm) larvae (Siegert, 2011).

For a comparative analysis of larval locomotion upon motor-neuron specific expression of Khc^{N262S} or Khc^{N259N}, D42, D42>Khc^{wt}, D42>Khc^{N262S} and

D42>Khc^{K259N} larvae were raised at 25℃ and the locomotion of second and third-instar larvae was analyzed.

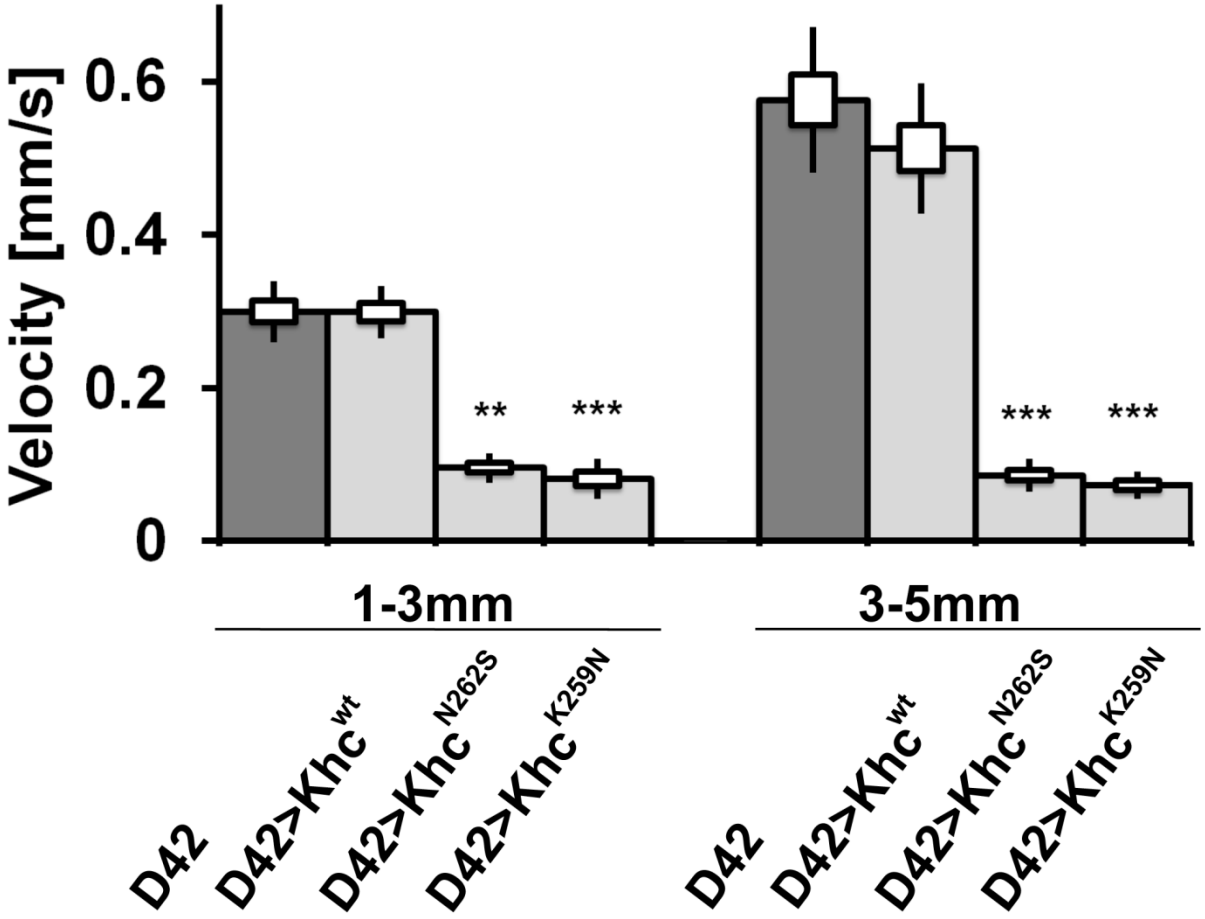

Figure 37: Motor-neuron expression of Khc^{N262S} or Khc^{K259N} strongly impairs locomotion of *Drosophila* larvae.

Boxes indicate SEM; black lines indicate SD. Statistical analysis was performed using a Kruskal-Wallis H-test for multiple comparisons. All genotypes within one size group were compared to D42 (dark gray bare). Eight movies per genotype were analyzed.

	Larval size	***Larval size***
	1-3 mm	***3-5 mm***

	velocity [mm/s]	*p-value*	*velocity [mm/s]*	*p-value*
D42	0.30 ± 0.04	-	0.58 ± 0.09	-
D42>Khc^{wt}	0.30 ± 0.04	n.s	0.51 ± 0.08	n.s
D42>Khc^{N262S}	0.10 ± 0.02	< 0.01	0.09 ± 0.02	< 0.001
D42>Khc^{K259N}	0.08 ± 0.03	< 0.001	0.07 ± 0.02	< 0.001

Table 24: Quantification reveals severe impairment of *Drosophila* larval locomotion upon motor-neuronal expression of Khc^{N262S} or Khc^{K259N}.
Data represent the mean ± SD. Statistical significance was determined using a Kruskal-Wallis H-test for multiple comparisons. A minimum of eight movies per genotype were analyzed. The p-values show probability compared to D42.

The locomotion of small (1-3mm) and large (3-5mm) D42>Khc^{N262S} and D42>Khc^{K259N} larvae was strongly impaired compared to D42 and D42>Khc^{wt} larvae (Figure 37 and Table 24). There was no significant difference in locomotion between the D42>Khc^{K259N} and the D42>Khc^{N262S} animals in either size group. No difference in locomotion was observed between D42 and D42>Khc^{wt} larvae in either size group.

4.2.3.2 Motor-neuron expression of Khc^{K259N} or Khc^{N262S} both cause axonal swellings in *Drosophila* larvae

For the assay D42, D42>Khc^{wt}, D42>Khc^{N262S} and D42>Khc^{K259N} larvae were raised at 29℃ and third-instar larvae were dissected and stained for the kinesin-1 cargo CSP and neuronal membranes (anti-HRP).

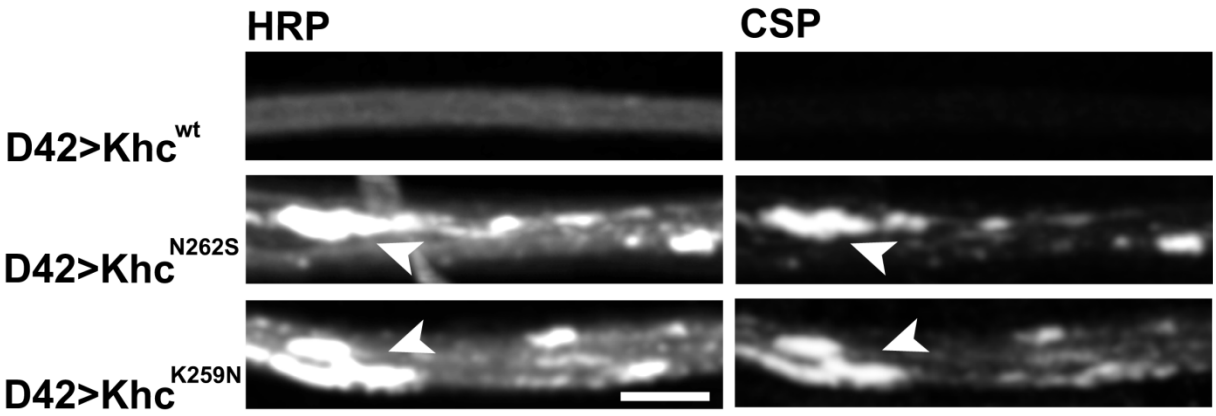

Figure 38: Motor-neuron expression of Khc^{N262S} or Khc^{K259N} cause axonal swellings in *Drosophila* larvae.
Confocal images of anti-HRP and CSP staining in segmental nerves of *Drosophila* larvae. Axonal swellings (arrowheads in A-B) are characterized by a bright anti-HRP staining and the accumulation of CSP. Scale bars, 10 µm.

In vitro analysis of axonal transport revealed that motor-neuron specific expression of Khc^{K259N} also caused the formation of axonal swellings and an accumulation of the kinesin-1 cargo CSP within the swellings (Figure 38, arrowheads), similar to axonal swellings detected in D42>Khc^{N262S} larvae (Figure 38, arrowheads).

4.2.3.3 Motor-neuron expression of Khc^{N262S} and Khc^{K259N} cause a decrease in synapse number at the NMJ that depends on the length of the innervating axon

For comparison of synapse numbers at the NMJ D42, D42>Khc^{wt}, D42>Khc^{N262S} and D42>Khc^{K259N} larvae were raised at 29℃ and third-instar larvae were dissected and stained for the presynaptic marker Brp and the neuronal membrane marker anti-HRP. For quantification of synapses Brp puncta per NMJ were counted. To account for the possible differences in larval size, data were normalized to the area of muscles 6/7 of abdominal segments A2 and A5.

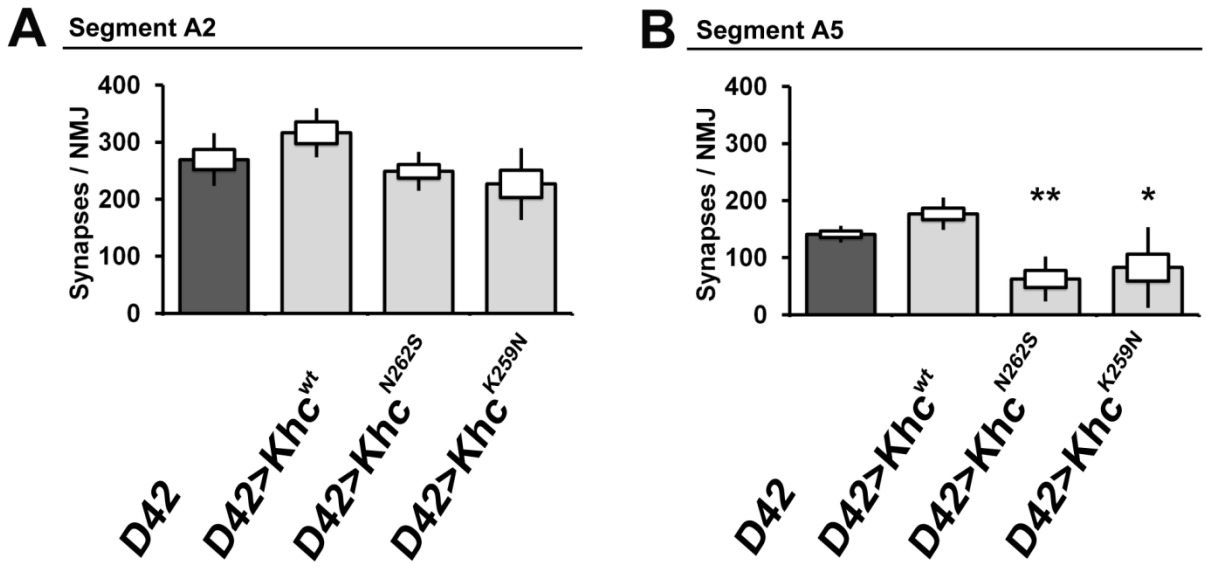

Figure 39: Motor-neuron expression of Khc^{N262S} and Khc^{K259N} reduces synapse numbers at the NMJ of *Drosophila* larvae.

Comparison of synapse numbers in the anterior segment A2 (A) and posterior segment A5 (B). Per genotype, 5-9 NMJs for each segment were analyzed. Statistical significance was determined using One-way ANOVA. * $p < 0.05$; ** $p < 0.01$. Statistical significance was determined by comparison to D42 (dark gray bare). The SEM is shown as a box, the SD as a black line.

	Segment A2			*Segment A5*		
	Synapses [synapses/NMJ]	***n***	***p-value***	***Synapses [synapses/NMJ]***	***n***	***p-value***
D42	269 ± 46	7	-	141 ± 15	7	-
D42>Khc^{wt}	316 ± 43	5	0.311	177 ± 29	8	0.244
D42>Khc^{N262S}	249 ± 34	8	0.865	63 ± 39	7	0.0015
D42>Khc^{K259N}	227 ± 63	7	0.384	83 ± 71	9	0.021

Table 25: Motor-neuron expression of Khc^{N262S} or Khc^{K259N} result in a reduction of synapse numbers at the NMJ of *Drosophila* larvae.

Data represent the mean ± SD. Statistical significance was determined by using One-way ANOVA. The p-values shown are compared to D42.

In the anterior segment A2 there was a trend towards a decrease in synapse number in D42>Khc^{N262S} and D42>Khc^{K259N} animals but this was not statistically significant compared to D42 (Figure 39A and Table 25). In the posterior segment A5, however, the reduction in synapse number was more pronounced (Figure 39A and Table 25) and statistically significant in both mutant genotypes. There was no significant difference in the synapse number of the NMJs of abdominal segments A2 and A5 between D42>Khc^{N262S} and D42>Khc^{K259N} larvae.

4.2.3.4 Motor-neuron expression of Khc^{N262S} and Khc^{K259N} cause a decrease in mitochondrial density at the NMJ of *Drosophila* larvae

To compare mitochondrial density at the NMJs in the D42>Khc^{K259N} and the D42>Khc^{N262S} animals, D42, D42>Khc^{N262S} and D42>Khc^{K259N} larvae that co-expressed mito-GFP were raised at 29℃ and third-in star larvae were analyzed. For quantification the percentage of mitochondrial area per NMJ area was determined.

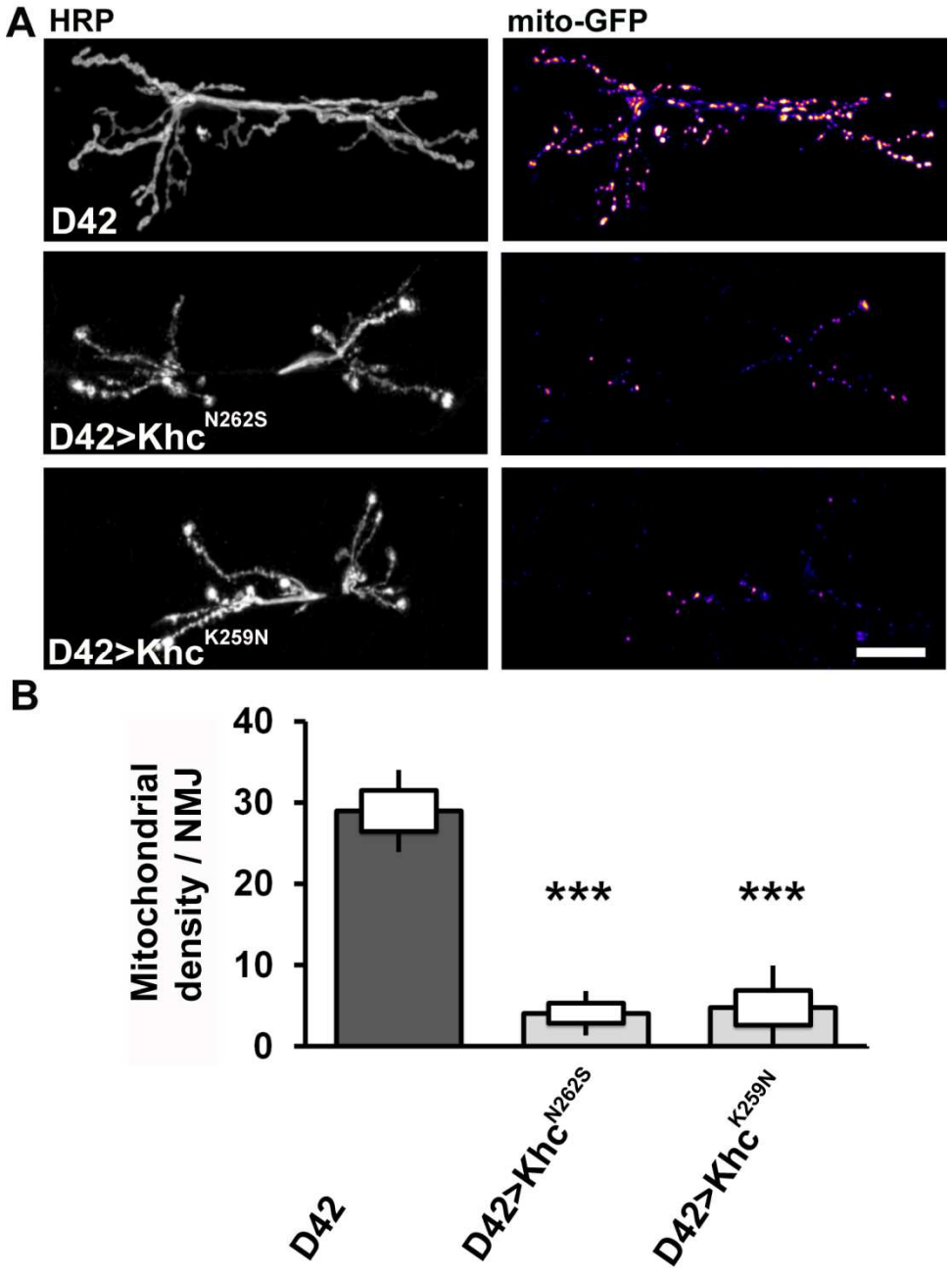

Figure 40: Motor-neuron expression of Khc^{N262S} and Khc^{K259N} reduces mitochondrial density at NMJs of *Drosophila* larvae.

(A) Confocal images of NMJs innervating muscles 6 and 7 of segment A2 of *Drosophila* larvae. Larvae express mito-GFP, a mitochondrial marker, and are stained for anti-HRP. In mutant larvae (D42>Khc^{N262S} and D42>Khc^{K259N}), the mitochondrial density at the NMJ was significantly reduced compared to D42 larvae. Scale bar: 20 µm. (B) Quantification of mitochondrial density per NMJ of muscle 6/7 in abdominal segment A2. For quantification, 5-6 NMJs per genotype were analyzed. Statistical significance was determined by using One-way ANOVA *** $p < 0.001$. The SEM is shown as a box, the SD as a black line.

	Mitochondrial density / NMJ	*n*	*p-value*
D42	28.9 ± 5.1	5	-
D42>Khc^{N262S}	4.1 ± 2.7	5	0.00019
D42>Khc^{K259N}	4.7 ± 5.2	6	0.00019

Table 26: Mitochondrial density per NMJs of muscles 6/7 in segments A2 is reduced when Khc^{N262S} or Khc^{K259N} is expressed in motor-neurons of *Drosophila* larvae.
Data represent the mean ± SD. Statistical significance was determined using One-way ANOVA. The p-values show probability compared to D42.

Quantification of mitochondrial density per NMJs of muscle 6 and 7 in segment A2 revealed a reduction of mitochondria at the NMJs of the D42>Khc^{N262S} and D42>Khc^{K259N} animals compared to D42 larvae (Figure 40 and Table 26). The severity of reduction was similar in D42>Khc^{K259N} and D42>Khc^{N262S} animals.

4.2.3.5 Motor-neuron expression of Khc^{N262S} and Khc^{K259N} cause disorganization of the NMJ cytoskeleton in *Drosophila* larvae

To compare cytoskeletal defects at the NMJ D42, D42>Khc^{N262S} and D42>Khc^{K259N} larvae were raised at 29℃ and third-instar larvae were dissected and stained for neuronal membranes (anti-HRP) and the microtubule associated protein Futsch. For analysis, the NMJs of muscle 6 and 7 in the anterior segment A2 were used. For quantification the percentage of Futsch area per NMJ area was determined.

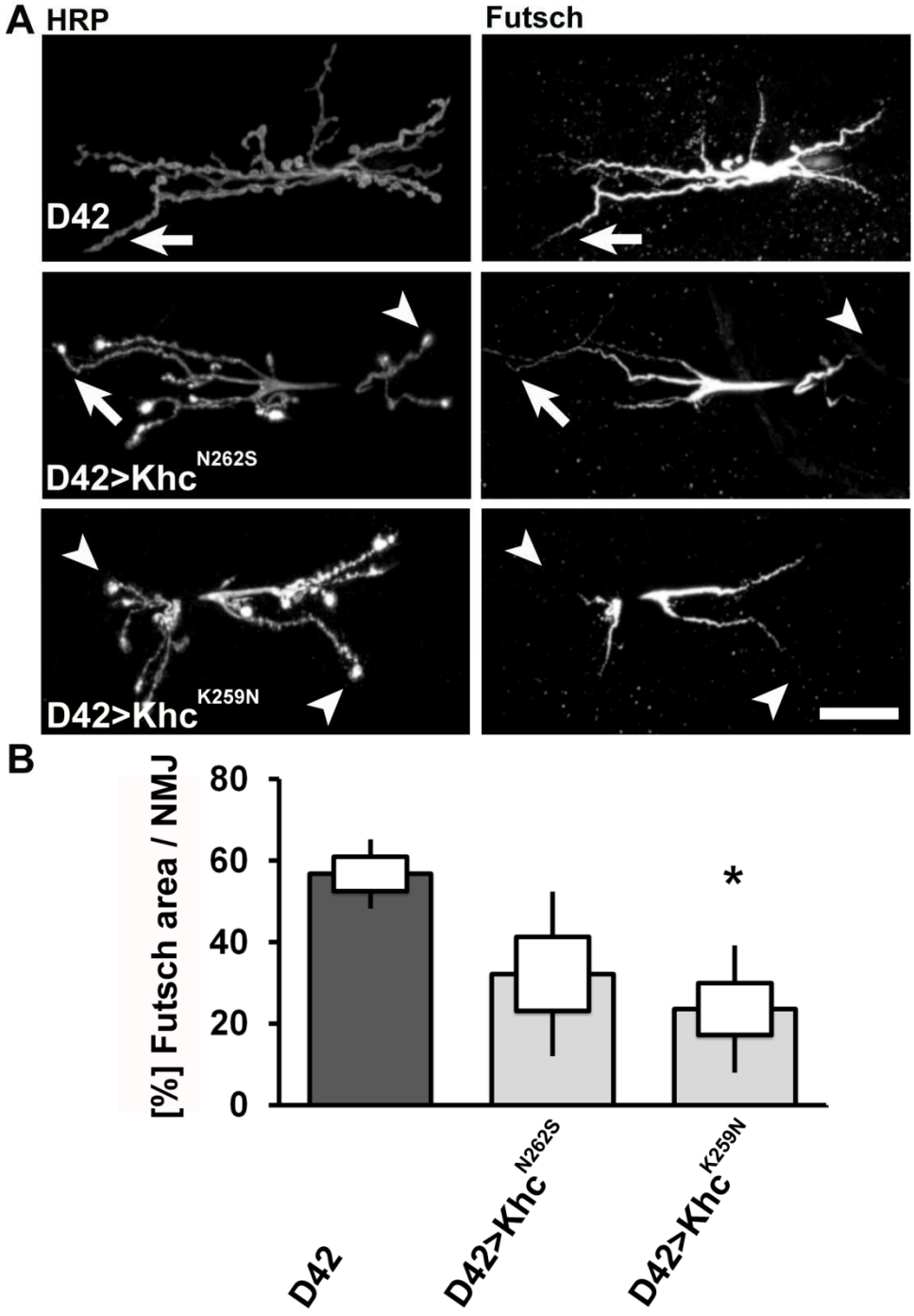

Figure 41: Motor-neuron expression of Khc^{N262S} and Khc^{K259N} alters the cytoskeleton of the NMJ in *Drosophila* larvae.

(A) Confocal images of Futsch and anti-HRP staining of NMJs innervating muscles 6/7 of abdominal segment A2 of *Drosophila* larvae. In the D42 larvae Futsch extended to the terminal branches of the NMJ (arrows). In D42>Khc^{N262S} mutant larvae Futsch was detected in some terminal branches (arrows), but was lacking in others (arrowheads). In D42>Khc^{K259N} mutant larvae Futsch was lacking in almost all terminal branches of the NMJs (arrowheads). Scale bar, 20 µm. (B) Quantification of the percentage of Futsch area per NMJs innervating

muscles 6/7 of abdominal segment A2. For quantification, 5-6 NMJs per genotype were analyzed. Statistical significance was determined using Kruskal-Wallis H-test. * $p < 0.05$. The SEM is shown as a box, the SD as a black line.

	[%] Futsch area / NMJ	*n*	*p-value*
D42	56.7 ± 8.5	5	-
D42>Khc^{N262S}	32.2 ± 20.2	5	0.199
D42>Khc^{K259N}	23.5 ± 15.6	6	0.043

Table 27: The cytoskeleton of the NMJs of muscles 6/7 in segments A2 is altered when Khc^{N262S} or Khc^{K259N} is expressed in motor-neurons of *Drosophila* larvae.
Data represent mean ± SD. Statistical significance was determined using Kruskal-Wallis H-test. The p-values show probability compared to D42.

Immunofluorescent staining of the microtubule associated protein Futsch at the NMJ showed that in D42 larvae Futsch was extending almost to the tip of all terminal boutons of the NMJs of muscle 6/7 in segment A2 (Figure 41A, arrows). In D42>Khc^{N262S} animals Futsch was observable in some terminal boutons (Figure 41A, arrows), but was gone from other terminal boutons of the NMJ (Figure 41A, arrowheads). In D42>Khc^{N259N} animals the alterations in NMJ cytoskeleton seemed more severe, as Futsch was lacking from terminal boutons more frequently (Figure 41A, arrowheads) than in D42>Khc^{N262S} animals.

Quantification of the percentage of Futsch area per NMJ area showed that in the D42 larvae around 60% of the NMJ area was covered with Futsch (Figure 41B and Table 27). In the D42>Khc^{N262S} larvae around 30% of the NMJ area was covered with Futsch. However there was no statistically significant difference compared to D42 larvae, most likely due to the high variability in the D42>Khc^{N262S} animals.

In D42>Khc^{K259N} animals the Futsch area per NMJ was reduced to around 23% (Figure 41B and Table 27) and was significantly different compared to D42 larvae. Although there was a trend towards a reduction in Futsch area per NMJ in D42>Khc^{K259N} compared to D42>Khc^{N262S} larvae, no statistically significant difference was observed between the two genotypes (p=0.946).

V. Discussion

5.1 A role of PP2A in synapse development in *Drosophila melanogaster*

Chapter 5.1 of the discussion is adapted from: "PP2A and GSK-3β Act Antagonistically to Regulate Active Zone Development", N.M. Viquez, P. Füger et al., Journal of Neuroscience, 2009.

Reversible protein phosphorylation is a key regulatory mechanism in many cell biological processes. Recently a B^{I} regulatory subunit of PP2A, named Well-rounded was indentified in *Drosophila* by the group of Prof. DiAntonio (Viquez et al., 2006). In that study it was demonstrated that PP2A acts in the motor-neuron to control synaptic terminal morphology likely via regulation of microtubules (Viquez et al., 2006). Here we investigate a possible role of PP2A on the level of the individual synapse.

The *Drosophila* NMJ is organized in a string of boutons, each bouton containing 10-50 individual synapses. Within each synapse a cluster of postsynaptic GluRs is directly apposed to an AZ and the presynaptic AZ protein Brp. When PP2A is inhibited, individual GluR clusters are found to be unapposed to AZs and Brp. The unapposed GluR clusters are distributed throughout the boutons, however they are more prevalent in the distal boutons of the NMJ, a part were new synapses tend to be added. Quantification of the size of these unapposed GluR clusters in PP2A inhibited larvae revealed that these GluR clusters were substantially smaller than GluR clusters apposed to presynaptic Brp. At the NMJ newly formed postsynaptic

GluR clusters are quite small and precede the presynaptic localization of Brp (Rasse et al., 2005). Taken together this suggests that neuronal inhibition of PP2A impairs presynaptic maturation (i.e. delivery of Brp to a part of the synapses) rather than maintenance of Brp at the synapses. However, to better understand the impact of neuronal PP2A inactivation on Brp delivery or maintenance at individual synapses the dynamics of Brp should be investigated *in vivo*.

In addition to affecting presynaptic maturation neuronal inhibition of PP2A impairs GluR clustering in the postsynaptic muscle at the NMJ. *In vivo* imaging showed that within six hours of larval development the addition of new GluR clusters was 5-fold higher in control larvae compared to dnPP2A larvae. Furthermore the size of GluR clusters was strongly increased in dnPP2A larvae. Thus neuronal inhibition of PP2A impairs presynaptic maturation of synapses and in addition causes defects in postsynaptic development.

The group of Prof. DiAntonio further identified the serine-threonine kinase glycogen synthase kinase-3β (GSK-3β) as an antagonist of PP2A function. Neuronal inactivation of GSK-3β function suppresses the synaptic misapposition phenotype and the disruption of the NMJ cytoskeleton induced by neuronal PP2A inactivation. However GSK-3β inactivation does not rescue the defects in axonal transport and evoked transmitter release observed upon inactivation of PP2A function. Thus GSK-3β / PP2A act as an antagonistic kinase/phosphatase pair to regulate some aspects of synapse development.

Interestingly GSK-3β / PP2A also act antagonistically on the phosphorylation state of the microtubule associated protein tau in models of Alzheimer´s disease. Defects in axonal cytoskeleton and synapse loss are suggested to be early events in the

pathogenesis of Alzheimer´s disease. Thus studying the role of the antagonistic GSK-3β / PP2A pair in regulating synaptic cytoskeleton and integrity during development might provide important insights into their possible role in disease manifestation.

5.2 *Drosophila melanogaster* as a model of the SPG10 subtype of the neurodegenerative disorder Hereditary Spastic Paraplegia

Parts of the following discussion are adapted from:

"Spastic paraplegia mutation N256S in the neuronal microtubule motor KIF5A disrupts axonal transport in a Drosophila HSP model", P. Füger, V. Sreekumar et al., Manuscript accepted for publication

HSPs are a group of clinically and genetically heterogeneous neurological disorders characterized by a progressive spasticity and weakness of the lower extremities, caused by a progressive retrograde axonopathy of the longest corticospinal motor neurons (Salinas et al., 2008). Of the 48 genetic loci related to HSP (SPG 1-48) (Slabicki et al., 2010, Blackstone et al., 2011), 25 genes have been identified (Schule and Schols, 2011). One of the genes identified is *kif5a (SPG10)* that encodes a neuron specific kinesin heavy chain of human kinesin-1.

Here we establish a *Drosophila* model for the HSP subtype SPG10, thereby focusing on the HSP related point mutation N256S in KIF5A, which corresponds to N262S in *Drosophila* Khc.

5.2.1 The *Drosophila* SPG10 model replicates main disease features of HSP

5.2.1.1 *Drosophila* larvae exhibit impaired locomotion upon motor-neuron expression of Khc^{N262S}

Motor-neuron expression of Khc^{N262S} alone or in combination with a copy of Khc^{wt} ($Khc^{wt+N262S}$) in *Drosophila* caused a tail-flipping phenotype of the larvae, due to a more pronounced paralysis in the ventral distal parts of the larvae. Furthermore D42>Khc^{N262S} and D42>$Khc^{wt+N262S}$ larvae exhibit impaired locomotion compared to control groups. In the D42>$Khc^{wt+N262S}$ larvae the locomotion phenotype was less severe than in D42>Khc^{N262S} larvae, presumably due to a higher availability of wild-type Khc in D42>$Khc^{wt+N262S}$ animals. Generally the locomotion defects caused by the motor-neuron expression of mutated Khc were more pronounced in larger larvae, resembling the degenerative character of HSP pathology.

5.2.1.2 *Drosophila* larvae exhibit axonal swellings upon motor-neuron expression of Khc^{N262S}

Axonal swellings filled with kinesin-1 as well as kinesin-3 transport cargo, indicating disturbed axonal transport, were detected in D42>Khc^{N262S} and D42>$Khc^{wt+N262S}$ animals. Again the phenotype, i.e. the prevalence of swellings, was more distinct in the D42>Khc^{N262S} larvae. The occurrence of axonal swellings, that contain cargo of axonal transport such as neurofilaments, mitochondria and multivesicular bodies, has been reported before as a HSP-associated pathological finding from autopsies of human SPG4 patients (Kasher et al., 2009), as well as mouse models of SPG4 (Kasher et al., 2009) and SPG7 (Ferreirinha et al., 2004).

5.2.1.3 Khc^{N262S} expression causes pathological changes at the *Drosophila* NMJ that depend on the length of the innervating axon

HSP is a degenerative disorder affecting primarily the longest motor axons of the corticospinal tract (Salinas et al., 2008, Blackstone et al., 2011). In the *Drosophila* model likewise longer axons were more severely affected. Analysis of the NMJ area and the synapse number revealed that motor-neuron expression of Khc^{N262S} causes defects at the NMJs of *Drosophila* larvae. The severity of these defects depends on the length of the innervating axon. NMJs innervating muscle 6/7 in the posterior segment A5 were more severely impaired than those innervating muscle 6/7 in the anterior segment A2. In *Drosophila*, axons innervating the posterior abdominal segments are considerably longer than those innervating anterior abdominal segments and seem to be more compromised in their function by impaired axonal transport.

The more prominent NMJ defects in distal segments as well as the distal paralysis of *Drosophila* larvae resemble human pathological symptoms that are characterized by a particular affection of the longest motor-neurons. (Blackstone et al., 2011).

5.2.1.4 Presynaptic degeneration can be observed in the *Drosophila* SPG10 model

The retrograde axonopathy described in HSP, is presumably initiated by degeneration of the synapses (Blackstone et al., 2011). To address presynaptic degenerative alterations in the *Drosophila* model the synaptic footprint assay (Eaton et al., 2002) was used. This assay was established to score for retraction events,

occurring during synaptic development at the *Drosophila* NMJ. Retraction and degeneration have been described to occur via different mechanisms (Saxena and Caroni, 2007). Since retraction is a regulated process the presynaptic material is transported back to more proximal sections of the axon before retraction of the axon. In degeneration the presynaptic material is fractionized at the synapse and in the axon, presumably followed by local uptake by phagocytes (Saxena and Caroni, 2007). Thus, if presynaptic degenerative changes occur, we would detect a gradual diminishment of presynaptic components rather than synaptic footprints. In consistence with this assumption we found reduced abundance and altered distribution of synaptic vesicles as well as alterations in neuronal membrane organization in the D42>Khc$^{wt+N262S}$ and D42>Khc^{N262S} larvae. The abundance of presynaptic vesicles was significantly decreased in relation to the SSR marker Dlg, compared to D42 larvae. The ratio of neuronal membrane area to Dlg was decreased in D42>Khc^{N262S} animals but not in the D42>Khc$^{wt+N262S}$ larvae. The decrease in the abundance of presynaptic vesicles was more pronounced, which might indicate that degeneration processes at the synapse start by disassembly of synaptic components such as synaptic vesicles, before neuronal membranes are degraded. Synaptic footprints, NMJ areas positive for the SSR marker Dlg, but devoid of synaptic vesicles and neuronal membrane area, were infrequently detected. They might represent sites were degradation of presynaptic material was complete.

The presynaptic alterations detected in the *Drosophila* SPG10 model, were not accompanied by loss of motor-neuron cell bodies. This is in agreement with the concept that HSP is primarily caused by synaptopathy and axonopathy, whereas motor-neuron cell body loss is neither causative nor an early feature of the pathological process of HSP (Blackstone et al., 2011).

In summary, pathological features, associated with HSP, can be replicated in the *Drosophila* model of SPG10. Generally the HSP-associated phenotypes were more pronounced in D42>Khc^{N262S} than in D42>Khc$^{wt+N262S}$ larvae. This shows that the occurring phenotypes in *Drosophila* are attributable to the expression of Khc^{N262S} and the severity of the phenotypes depends on the ratio of mutated Khc to wild-type Khc. *Drosophila* is a suited model to investigate mechanisms of pathology of the HSP subtype SPG10.

5.2.2. Khc^{N262S} acts as a dominant negative allele in *Drosophila*

SPG10 is inherited in an autosomal dominant way. This is consistent with a dominant negative function of the KIF5A^{N256S} allele (Reid et al., 2002). This hypothesis was backed up by *in vitro* analysis of homodimeric KIF5A^{N256S}, showing that KIF5A^{N256S} exerts a dominant-negative effect *in vitro* (Ebbing et al., 2008).

Drosophila larvae carrying only one copy of endogenous wild-type *khc* (Khc$^{+/-}$) did not exhibit impaired locomotion compared to larvae carrying two copies of endogenous wild-type *khc* (D42 larvae). One wild-type copy of Khc is therefore sufficient to sustain normal larval locomotion. Expression of Khc^{N262S} in animals carrying two copies of endogenous wild-type *khc* severely impaired larval locomotion, comparable to the locomotion deficits of *khc* null animals (Khc$^{-/-}$). Thus in the presence of the Khc^{N262S} allele two copies of endogenous Khc are not sufficient to sustain normal larval locomotion. This demonstrates that *Drosophila* Khc carrying the corresponding point mutation (Khc^{N262S}) acts as a dominant negative allele *in vivo* and thus confirms the proposed dominant-negative function of the KIF5A^{N256S} allele.

5.2.3 Khc^{N262S} does not act as a roadblock in the *Drosophila* SPG10 model

A question arising is whether the axonal swellings in *Drosophila* motor axons, containing axonal transport cargo, represent sites of abnormal Khc accumulations. From *in vitro* studies it was suggested that KIF5A^{N256S} might act as a roadblock (Ebbing et al., 2008). Although there was a trend towards elevated Khc levels in D42>Khc^{N262S} and D42>Khc$^{wt+N262S}$ larvae, no abnormal Khc accumulations were present in axonal swellings of *Drosophila* larvae expressing Khc^{N262S}. Thus it seems most unlikely that abnormal accumulations of kinesin-1 cause the establishment of axonal swellings in the *Drosophila* SPG10 model. In consistence with this finding it was reported from a study of axonal transport of mitochondria in *Drosophila* Khc mutants that axonal swellings do not cause a general blockage of the microtubules (Pilling et al., 2006), as organelles in swellings were found to be quite mobile (Pilling et al., 2006). The authors hypothesize that axonal swellings rather represent sites of local axonal autophagocytosis (Pilling et al., 2006), possibly triggered by cell death signals released by trapped mitochondria that have passed the membrane permeability transition.

If Khc^{N262S} does not act as a roadblock to disturb axonal transport how does its expression affect axonal transport in *Drosophila* motor-axons? A second hypothesis is that expression of Khc^{N262S} diminishes cargo delivery within the axon or to the synapses. The lack of cargo necessary for maintenance of synaptic and/or axonal structure and/or function, might then trigger degeneration of the axons. This hypothesis is strengthened by preliminary results using a truncated Khc protein, which is able to dimerize and move along microtubules (Sung et al., 2008), but lacks the domain to bind to Klc. This truncated Khc protein will not compete for cargo

binding with the full length Khc, thereby leaving more cargo available for fully functional motor complexes. Motor-neuron specific expression of a mutated truncated Khc ($Khc^{truncN262S}$) increased Khc levels in segmental nerves but did not cause axonal swellings and had no impact on larval locomotion. Thus binding cargo and retaining it from its destination by the full length Khc^{N262S} seems necessary for the establishment of axonal swellings and further HSP-pathology like characteristics in the *Drosophila* model. The finding that the severity of the HSP-pathology like phenotypes in the *Drosophila* model depends on the amount of available wild-type Khc is consistent with this hypothesis.

So far there is only indirect evidence that the truncated Khc is stably expressed and dimerizes *in vivo*. This needs to be confirmed in future experiments.

5.2.4 Axonal transport is disturbed in the *Drosophila* SPG10 model

Over the years several reports link defects in axonal transport to degeneration of motor-neurons in a variety of motor-neuron diseases (Ikenaka et al., 2012). In HSP the most direct evidence for an implication of disturbed axonal transport in the pathology comes from *SPG10*. Preliminary results indicate that ectopic expression of Khc^{N262S} might reduce the frequency of cargo transported along the axon. To investigate this axonal transport of mitochondria was analyzed *in vivo*.

Analysis of axonal transport of mitochondria in *Drosophila*, revealed a strong reduction of mitochondrial transport frequency in both anterograde and retrograde direction in D42>$Khc^{wt+N262S}$ and D42>Khc^{N262S} larvae. The transport velocity in either direction was unchanged among the genotypes analyzed. Furthermore, no

differences in the number or the duration of pauses between single runs of mitochondria in either direction were observed.

In line with these observations Wang and colleagues reported that expression of KIF5A^{N256S} in cultured mouse cortical neurons decreases both the anterograde and the retrograde frequency of neurofilament transport while having no effect on transport velocities (Wang and Brown, 2010).

The fact that transport velocities of mitochondria were unchanged in *Drosophila* larvae expressing Khc^{N262S}, seemed surprising first, as *in vitro* analysis of the corresponding point mutation in vertebrate KIF5A revealed a reduction of microtubule gliding velocities more than two fold upon mixture of wild-type and N256S-mutant KIF5A at a stoichiometric ratio of 1:1 compared to wild-type KIF5A only (Ebbing et al., 2008). However, when a modified bead assay was used in the same study, velocities were only slightly reduced by less than 10%. For this assay quantum dots were coated randomly with 3-6 motors derived from a 1:2:1 mixture of wild-type homodimer : heterodimer : N256S homodimer (Ebbing et al., 2008). Using this assay different KIF5A dimer populations could be visualized and a histogram plot of the KIF5A^{N256S} data showed a pronounced fraction of slowly moving quantum dots compared to wild-type KIF5A alone (Ebbing et al., 2008). The differences in quantum dot velocities presumably depend on the number of wild-type homodimer : heterodimer : N256S homodimer attached to the quantum dot. This assay might be more akin to the *in vivo* situation, where one would also expect random attachment of wild-type homodimer : heterodimer : N256S homodimer to the cargo.

When analyzing anterograde transport velocities in *Drosophila* expressing Khc^{N262S} *in vivo* we could not distinguish fractions of mitochondria moving with different velocities. We hypothesize that the majority of mitochondria analyzed were attached

predominantly to wild-type motors, while mitochondria predominantly attached to mixed or mutant motors did not move along microtubules very effectively, if at all. Therefore we conclude that *in vivo* transport of mitochondria in *Drosophila* larvae expressing $Khc^{wt+N262S}$ or Khc^{N262S} is primarily driven by the Khc^{wt}-homodimers. In the D42>$Khc^{wt+N256S}$ larvae, that possess more Khc^{wt}-homodimers than D42>Khc^{N262S} animals an increased mitochondrial transport frequency compared to D42>Khc^{N262S} larvae was observed. These data likewise support the notion that expression of Khc^{N262S} in *Drosophila* causes a diminishment of cargo arriving at the synapses and does not hinder the movement of wild-type kinesin-1 along microtubules.

Different studies have shown that mutations in anterograde motor proteins not only disturb anterograde but also retrograde transport. In cultured mouse neurons transport frequency of neurofilaments was reduced in anterograde as well as retrograde direction upon knockdown of KIF5A function (Uchida et al., 2009) or overexpression of mutated $KIF5A^{N256S}$ (Wang and Brown, 2010). Furthermore the transport velocities of mitochondria were reduced in anterograde and retrograde direction in KIF5A knockout mice (Karle et al., 2012) and Khc mutant *Drosophila* larvae revealed a reduction in mitochondrial flux in both transport directions (Pilling et al., 2006).

In the *Drosophila* SPG10 model we also observed a reduction in both anterograde and retrograde transport frequencies of mitochondria, but not in transport velocities. However the reduction of retrograde transport frequency of mitochondria most likely arises from the low availability of mitochondria at the NMJ. Thus our data do not prove disturbed retrograde transport in the *Drosophila* SPG10 model. However we hypothesize that retrograde transport is also disturbed in this model and different

approaches are possible to further investigate retrograde transport in the *Drosophila* SPG10 model.

5.2.5 Possible mechanisms contributing to SPG10 pathology

What are the pathophysiological mechanisms possibly causing or contributing to neurodegeneration of the longest corticospinal motor-axons in SPG10? Different mechanisms have been implicated to play a role in the pathology of neurodegenerative diseases.

Mitochondrial dysfunction, changes in mitochondrial dynamics and mobility, and perturbation of mitochondrial turnover are involved in the pathology of some neurodegenerative disorders such as Parkinson´s, Alzheimer's and ALS (Reviewed in Schon and Przedborski, 2011). Cytoskeletal changes (Goellner and Aberle, 2012) and changes in the microtubule-associated proteins (MAPs) have been linked to neurodegeneration in human neurodegenerative disorders and in *Drosophila* (Bettencourt da Cruz et al., 2005). Furthermore, alterations in BMP signaling are emerging as a possible mechanism in some neurodegenerative disorders (Bayat et al., 2011).

5.2.5.1 Mitochondrial density is reduced at the NMJ of the *Drosophila* SPG10 model

In vivo imaging of axonal transport of mitochondria revealed a severe reduction of anterograde mitochondrial transport frequency along the axon in D42>Khc$^{wt+N262S}$ and D42>Khc^{N262S} larvae. This resulted in a similar reduction of mitochondrial density

at the NMJs innervating muscles 6/7 in abdominal segment A2. As mitochondria are the main site of ATP production, a strong reduction of mitochondria in presynaptic terminals reduces local ATP supply and thus affects ATP-dependent processes such as neurotransmission. At the *Drosophila* NMJ a reduction of synaptic mitochondria impairs mobilization of the reserve synaptic vesicle pool resulting in a faster decrease in EJP amplitude during prolonged trains of stimulation pulses (Verstreken et al., 2005). Thus defects in synaptic function caused by a reduction of mitochondrial density at the NMJ and local ATP depletion may contribute to synaptic loss/degeneration in the *Drosophila* SPG10 model. Loss/degeneration of synapses may then instigate retrograde axonopathy.

5.2.5.2 BMP signaling is impaired in the *Drosophila* SPG10 model

Alterations in BMP signaling might be a unifying mechanism in causing axonopathy in some classes of HSP (Blackstone et al., 2011). The spastic paraplegia genes Atlastin, Spastin, NIPA1 and Spartin have all been shown to be negative regulators of BMP signaling (Wang et al., 2007, Tsang et al., 2009, Fassier et al., 2010), presumably by regulation of BMP receptor trafficking.

In the *Drosophila* motor-neuron presynaptic BMP receptors at the NMJ are activated by postsynaptically released Gbb (Marques et al., 2003, McCabe et al., 2003) inducing the phosphorylation of Mad, which in turn translocates to the nucleus of motor-neuron cell bodies, where it acts as a transcription factor.

Quantification of pMad levels in the *Drosophila* SPG10 model revealed a strong decrease of pMad in the motor-neuron cell bodies of the VNC. This is due to impaired retrograde translocation of pMad to the VNC as activation of the BMP signaling

pathway at the NMJ was unchanged in these larvae. We hypothesize that retrograde transport of pMad from the NMJ to the motor-neuron cell body is impaired in the *Drosophila* SPG10 model. However, so far direct evidence showing impairment of retrograde transport is lacking. This is going to be the subject of continuative investigation.

A loss of pMad accumulation from motor-neuron cell bodies was also found in *Drosophila* mutants of the type II BMP receptor *wit* (Marques et al., 2002). Notably some phenotypic characteristics observed in the *Drosophila* SPG10 model, such as reduced NMJ size and accumulation of axonal transport cargo in segmental nerves have also been described for mutants of BMP signaling components. Drosophila *Wit* mutants exhibit small NMJs, severe defects in evoked junctional potentials and a lower frequency of spontaneous vesicle release (Marques et al., 2002). In addition, the cargo of fast axonal transport accumulates in segmental nerves of larvae with mutations in the BMP receptor *wit* (Aberle et al., 2002). Also mutations in other components of the BMP signaling cascade, the type I receptors Tkv and Sax, the R-Smad Mad and the Co-Smad Med were reported to cause a reduction in NMJ size (McCabe et al., 2004). Our data suggest that the loss of pMad accumulation in the motor-neuron cell bodies reduces BMP signaling in the *Drosophila* SPG10 model. The alteration of BMP signaling might cause or contribute to the establishment of pathology in the *Drosophila* model.

What are the cellular processes affected by altered BMP signaling? Several studies demonstrated interactions between altered BMP signaling and cytoskeletal integrity. It has been shown that BMP signaling regulates microtubule dynamics (Wang et al., 2007, Fassier et al., 2010). Wang and colleagues demonstrated a connection between down regulation of BMP signaling in *Drosophila* and perturbations of axonal

and neuromuscular cytoskeleton (Wang et al., 2007). Down regulation of BMP signaling caused a loss of Futsch from distal boutons of the NMJs (Wang et al., 2007) and a reduction of total and acetylated (stable microtubules) tubulin levels in the axons, implying a loss and destabilization of microtubules from the axons (Wang et al., 2007). In contrast a study on the role of Atlastin (SPG3A) showed that an up regulation of BMP signaling decreased levels of acetylated tubulin in motor-neurons of zebrafish (Fassier et al., 2010). Recently a study showed that retrograde BMP signaling, regulates neuromuscular growth in *Drosophila* via modulation of the actin cytoskeleton (Ball et al., 2010). Thereby BMP signaling regulates expression of Trio, a guanine nucleotide exchange factor (GEF) of Rac (Ball et al., 2010). Racs are major intracellular regulators of the actin cytoskeleton in many cells, including neurons (Ball et al., 2010).

5.2.5.3 Disorganization of the cytoskeleton is detected in the *Drosophila* SPG10 model

An undisturbed cytoskeleton is crucial for the maintenance of stability and functionality of neurons. As a link between BMP signaling and cytoskeletal integrity has been described in different studies we investigated cytoskeletal changes in segmental nerves and at the NMJs of the *Drosophila* SPG10 model.

We observed a loss of the microtubule associated protein (MAP) Futsch from distal boutons of the NMJs and a reduction of acetylated tubulin in segmental nerves of mutant *Drosophila* larvae.

Futsch is the *Drosophila* homolog of mammalian MAP1A, a member of the MAP1 family, representing microtubule associated proteins. In mammals the MAP1 family

comprises MAP1A and MAP1B, which are predominantly expressed in neurons and are important for formation and maintenance of axons and synapses. In *Drosophila* Futsch represents the only MAP1 family member. Mutations in Futsch have been reported to cause alterations in the microtubule network, causing progressive degeneration of neurons in the fly brain (Bettencourt da Cruz et al., 2005). From the same study it was reported that in primary neuronal cultures prepared from the *futsch* mutants, significant reduction in mitochondrial movement compared with wild-type neurons was observed, most likely reflecting a general reduction in axonal and dendritic transport due to disruptions in the microtubule network (Bettencourt da Cruz et al., 2005). Recently it was shown that TDPH, the *Drosophila* homolog of TDP-43, is necessary in the regulation of cellular Futsch levels (Godena et al., 2011). TDP-43 is an RNA binding protein and large insoluble aggregates of TDP-43 redistributed within the cytoplasm have been associated to neurodegenerative disorders such as ALS and frontotemporal lobar degeneration (FTLD) (Neumann et al., 2006). It was shown that TBPH maintains NMJ growth and microtubule organization through Futsch protein action (Godena et al., 2011). Flies lacking TDPH exhibit ALS like symptoms such as progressive defects in locomotion and reduced life span (Feiguin et al., 2009).

Destabilization of the NMJ cytoskeleton due to reduced Futsch levels may contribute to synaptic dysfunction and synaptic loss in the *Drosophila* model of SPG10. In addition, unstable and distorted microtubule tracks likely interfere with axonal transport processes to and from synapses and thus contribute to the axonal transport defects observed in D42>Khc$^{wt+N262S}$ and D42>Khc^{N262S} animals. These cytoskeletal changes observed might be caused by reduced BMP signaling in the motor-neurons of the *Drosophila* larvae. These data are in consistence with findings of Wang and

colleagues (Wang et al., 2007). However a different study postulated that an up regulation of BMP signaling reduces levels of acetylated tubulin in motor-axons of zebrafish (Fassier et al., 2010). Thus, a fine regulation of BMP signaling seems to be necessary for a proper maintenance of the cytoskeleton.

5.2.6 Comparative analysis of two SPG10-associated mutations in *Drosophila*

In vitro analysis of the HSP related mutations KIF5A^{K253N} and KIF5A^{N256S} revealed differences in the biophysical properties of the mutated proteins (Ebbing et al., 2008). Both mutations caused a decrease in velocity of homodimeric mutated KIF5A. The mutation K253N further reduced the microtubule binding affinity. Both mutations, K253N (Siegert, 2011) and N256S (this study) act in a dominant-negative way *in vivo* when introduced at the corresponding sites into *Drosophila* Khc. Motor-neuron specific expression of Khc^{K259N} caused an slightly earlier lethality of the *Drosophila* larvae compared to expression of Khc^{N262S}. Furthermore larvae were generally weaker upon expression of Khc^{K259N}. Analyses of larval locomotion, synapse number, mitochondrial density at the NMJ and cytoskeleton of the NMJ revealed no significant differences between D42>Khc^{N262S} and D42>Khc^{N253N} larvae. Also no clear trend was discernible in the severity of the occurring phenotypes in D42>Khc^{N262S} and D42>Khc^{N253N} larvae.

In conclusion, two HSP-associated mutations that exhibited different biophysical properties *in vitro* result in the same phenotypic characteristics in a *Drosophila* model. Although no significant differences in the occurring phenotypes became obvious, D42>Khc^{K259N} larvae exhibited earlier lethality than D42>Khc^{N262S} animals,

implying some differences in the severity of pathology between D42>Khc^{K259N} and D42>Khc^{N262S} animals. It is conceivable that a combination of reduced microtubule binding affinity and reduced gliding velocity of Khc^{K259N} might affect cellular processes that depend on efficient axonal transport more severely than a reduction in the gliding velocity only. The biophysical differences of Khc caused by the two mutations might have differential impact on axonal transport *in vivo*. This might cause differences in the establishment and progression of pathology in D42>Khc^{K259N} and D42>Khc^{N262S} *Drosophila* larvae, that are not obvious in the final stage of pathology.

Gaining insight into the progression of the disease dependent on the mutations in Khc in *Drosophila* might be a first step to predict disease progression in SPG10 patients.

5.2.7 Conclusion

We established a *Drosophila* model of the HSP subtype SPG10, which recapitulates key disease features such as impairments in locomotion, axonal swellings, degeneration of synapses and a more severe affliction of longer axons. The occurring phenotypes in *Drosophila* are attributable to the expression of Khc^{N262S} and the severity of the occurring phenotypes depends on the amount of available wild-type Khc. Thus pathology in the *Drosophila* SPG10 model seems to be caused by a reduction of axonal cargo transport frequency due to impaired anterograde transport. This might affect proper localization of a specific cargo necessary for maintenance of synaptic and/or axonal structure and/or function. Therefore it seems crucial to investigate depletion of which cargo or multiple cargos might initiate and progress the disease.

As possible mechanisms contributing to pathology in the *Drosophila* SPG10 model reduced mitochondrial density at the NMJ, a reduction in BMP signaling and alterations in axonal as well as neuromuscular cytoskeleton were identified. All of these findings have been linked to neurodegenerative disorders before. Several studies demonstrated interactions between altered BMP signaling, cytoskeletal integrity and mitochondrial movement. Destabilization of microtubules was shown to contribute to a reduction in mitochondrial movement (Bettencourt da Cruz et al., 2005). In turn reduction of ATP supply due to a reduction of availability of mitochondria might further enhance axonal transport deficits. Thus, there might be an interaction between a reduction in BMP signaling, alterations in axonal as well as neuromuscular cytoskeleton and reduced mitochondrial density at the NMJ, in the *Drosophila* SPG10 model, affecting each other reciprocal.

The *Drosophila* SPG10 model provides a good means to follow the establishment and progression of pathology *in vivo* and thereby decipher cause and consequence of SPG10 pathology in the *Drosophila* model.

VI. References

Aberle H, Haghighi AP, Fetter RD, McCabe BD, Magalhaes TR, Goodman CS (2002) wishful thinking encodes a BMP type II receptor that regulates synaptic growth in Drosophila. Neuron 33:545-558.

Adams MD, Celniker SE, Holt RA, Evans CA, Gocayne JD, Amanatides PG, Scherer SE, Li PW, Hoskins RA, Galle RF, George RA, Lewis SE, Richards S, Ashburner M, Henderson SN, Sutton GG, Wortman JR, Yandell MD, Zhang Q, Chen LX, Brandon RC, Rogers YH, Blazej RG, Champe M, Pfeiffer BD, Wan KH, Doyle C, Baxter EG, Helt G, Nelson CR, Gabor GL, Abril JF, Agbayani A, An HJ, Andrews-Pfannkoch C, Baldwin D, Ballew RM, Basu A, Baxendale J, Bayraktaroglu L, Beasley EM, Beeson KY, Benos PV, Berman BP, Bhandari D, Bolshakov S, Borkova D, Botchan MR, Bouck J, Brokstein P, Brottier P, Burtis KC, Busam DA, Butler H, Cadieu E, Center A, Chandra I, Cherry JM, Cawley S, Dahlke C, Davenport LB, Davies P, de Pablos B, Delcher A, Deng Z, Mays AD, Dew I, Dietz SM, Dodson K, Doup LE, Downes M, Dugan-Rocha S, Dunkov BC, Dunn P, Durbin KJ, Evangelista CC, Ferraz C, Ferriera S, Fleischmann W, Fosler C, Gabrielian AE, Garg NS, Gelbart WM, Glasser K, Glodek A, Gong F, Gorrell JH, Gu Z, Guan P, Harris M, Harris NL, Harvey D, Heiman TJ, Hernandez JR, Houck J, Hostin D, Houston KA, Howland TJ, Wei MH, Ibegwam C, Jalali M, Kalush F, Karpen GH, Ke Z, Kennison JA, Ketchum KA, Kimmel BE, Kodira CD, Kraft C, Kravitz S, Kulp D, Lai Z, Lasko P, Lei Y, Levitsky AA, Li J, Li Z, Liang Y, Lin X, Liu X, Mattei B, McIntosh TC, McLeod MP, McPherson D, Merkulov G, Milshina NV, Mobarry C, Morris J, Moshrefi A, Mount SM, Moy M, Murphy B, Murphy L, Muzny DM, Nelson DL, Nelson DR, Nelson KA, Nixon K, Nusskern DR, Pacleb JM, Palazzolo M, Pittman GS, Pan S, Pollard J, Puri V, Reese MG, Reinert K, Remington K, Saunders RD, Scheeler F, Shen H, Shue BC, Siden-Kiamos I, Simpson M, Skupski MP, Smith T, Spier E, Spradling AC, Stapleton M, Strong R, Sun E, Svirskas R, Tector C, Turner R, Venter E, Wang AH, Wang X, Wang ZY, Wassarman DA, Weinstock GM, Weissenbach J, Williams SM, WoodageT, Worley KC, Wu D, Yang S, Yao QA, Ye J, Yeh RF, Zaveri JS, Zhan M, Zhang G, Zhao Q, Zheng L, Zheng XH, Zhong FN, Zhong W, Zhou X, Zhu S, Zhu X, Smith HO, Gibbs RA, Myers EW, Rubin GM, Venter JC (2000) The genome sequence of Drosophila melanogaster. Science 287:2185-2195.

Albin SD, Davis GW (2004) Coordinating structural and functional synapse development: postsynaptic p21-activated kinase independently specifies glutamate receptor abundance and postsynaptic morphology. J Neurosci 24:6871-6879.

Atwood HL, Govind CK, Wu CF (1993) Differential ultrastructure of synaptic terminals on ventral longitudinal abdominal muscles in Drosophila larvae. J Neurobiol 24:1008-1024.

Ball RW, Warren-Paquin M, Tsurudome K, Liao EH, Elazzouzi F, Cavanagh C, An BS, Wang TT, White JH, Haghighi AP (2010) Retrograde BMP signaling controls synaptic growth at the NMJ by regulating trio expression in motor neurons. Neuron 66:536-549.

Barkus RV, Klyachko O, Horiuchi D, Dickson BJ, Saxton WM (2007) Identification of an Axonal Kinesin-3 Motor for Fast Anterograde Vesicle Transport that Facilitates Retrograde Transport of Neuropeptides. Mol Biol Cell E07-03-0261.

Barnes GN, Slevin JT, Vanaman TC (1995) Rat brain protein phosphatase 2A: an enzyme that may regulate autophosphorylated protein kinases. J Neurochem 64:340-353.

Bayat V, Jaiswal M, Bellen HJ (2011) The BMP signaling pathway at the Drosophila neuromuscular junction and its links to neurodegenerative diseases. Curr Opin Neurobiol 21:182-188.

Bellen HJ, Tong C, Tsuda H (2010) 100 years of Drosophila research and its impact on vertebrate neuroscience: a history lesson for the future. Nat Rev Neurosci 11:514-522.

Belmeguenai A, Hansel C (2005) A role for protein phosphatases 1, 2A, and 2B in cerebellar long-term potentiation. J Neurosci 25:10768-10772.

Bettencourt da Cruz A, Schwarzel M, Schulze S, Niyyati M, Heisenberg M, Kretzschmar D (2005) Disruption of the MAP1B-related protein FUTSCH leads to changes in the neuronal cytoskeleton, axonal transport defects, and progressive neurodegeneration in Drosophila. Mol Biol Cell 16:2433-2442.

Blackstone C, O'Kane CJ, Reid E (2011) Hereditary spastic paraplegias: membrane traffic and the motor pathway. Nat Rev Neurosci 12:31-42.

Blair MA, Ma S, Hedera P (2006) Mutation in KIF5A can also cause adult-onset hereditary spastic paraplegia. Neurogenetics 7:47-50.

Bloom FE, Aghajanian GK (1968) Fine structural and cytochemical analysis of the staining of synaptic junctions with phosphotungstic acid. J Ultrastruct Res 22:361-375.

Bloom GS, Wagner MC, Pfister KK, Brady ST (1988) Native structure and physical properties of bovine brain kinesin and identification of the ATP-binding subunit polypeptide. Biochemistry 27:3409-3416.

Bragdon B, Moseychuk O, Saldanha S, King D, Julian J, Nohe A (2011) Bone morphogenetic proteins: a critical review. Cell Signal 23:609-620.

Brand AH, Perrimon N (1993) Targeted gene expression as a means of altering cell fates and generating dominant phenotypes. Development 118:401-415.

Budnik V, Koh YH, Guan B, Hartmann B, Hough C, Woods D, Gorczyca M (1996) Regulation of synapse structure and function by the Drosophila tumor suppressor gene dlg. Neuron 17:627-640.

Buszczak M, Paterno S, Lighthouse D, Bachman J, Planck J, Owen S, Skora AD, Nystul TG, Ohlstein B, Allen A, Wilhelm JE, Murphy TD, Levis RW, Matunis E, Srivali N, Hoskins RA, Spradling AC (2007) The carnegie protein trap library: a versatile tool for Drosophila developmental studies. Genetics 175:1505-1531.

Carmine-Simmen K, Proctor T, Tschape J, Poeck B, Triphan T, Strauss R, Kretzschmar D (2009) Neurotoxic effects induced by the Drosophila amyloid-beta peptide suggest a conserved toxic function. Neurobiol Dis 33:274-281.

Castiglioni MC (1951) [Distribution of pigments in the eye of alleles of white and their compounds in Drosophila melanogaster]. Sci Genet 4:57-60.

Chen Y, Yang M, Deng J, Chen X, Ye Y, Zhu L, Liu J, Ye H, Shen Y, Li Y, Rao EJ, Fushimi K, Zhou X, Bigio EH, Mesulam M, Xu Q, Wu JY (2011) Expression of human FUS protein in Drosophila leads to progressive neurodegeneration. Protein Cell 2:477-486.

Collins CA, DiAntonio A (2007) Synaptic development: insights from Drosophila. Curr Opin Neurobiol 17:35-42.

Crimella C, Baschirotto C, Arnoldi A, Tonelli A, Tenderini E, Airoldi G, Martinuzzi A, Trabacca A, Losito L, Scarlato M, Benedetti S, Scarpini E, Spinicci G, Bresolin N, Bassi M (2011) Mutations in the motor and stalk domains of KIF5A in spastic paraplegia type 10 and in axonal Charcot-Marie-Tooth type 2. Clin Genet.

Derivery E, Sousa C, Gautier JJ, Lombard B, Loew D, Gautreau A (2009) The Arp2/3 activator WASH controls the fission of endosomes through a large multiprotein complex. Dev Cell 17:712-723.

Doe CQ, Smouse D, Goodman CS (1988) Control of neuronal fate by the Drosophila segmentation gene even-skipped. Nature 333:376-378.

Draeger N (2009) Impact of different kinesins on synaptic plasticity in Drosophila. Tuebingen.

Du F, Ozdowski EF, Kotowski IK, Marchuk DA, Sherwood NT (2010) Functional conservation of human Spastin in a Drosophila model of autosomal dominant-hereditary spastic paraplegia. Hum Mol Genet 19:1883-1896.

Duncan JE, Goldstein LS (2006) The genetics of axonal transport and axonal transport disorders. PLoS Genet 2:e124.

Eaton BA, Fetter RD, Davis GW (2002) Dynactin is necessary for synapse stabilization. Neuron 34:729-741.

Ebbing B, Mann K, Starosta A, Jaud J, Schols L, Schule R, Woehlke G (2008) Effect of spastic paraplegia mutations in KIF5A kinesin on transport activity. Hum Mol Genet 17:1245-1252.

Erichsen AK, Koht J, Stray-Pedersen A, Abdelnoor M, Tallaksen CM (2009) Prevalence of hereditary ataxia and spastic paraplegia in southeast Norway: a population-based study. Brain 132:1577-1588.

Fassier C, Hutt JA, Scholpp S, Lumsden A, Giros B, Nothias F, Schneider-Maunoury S, Houart C, Hazan J (2010) Zebrafish atlastin controls motility and spinal motor axon architecture via inhibition of the BMP pathway. Nat Neurosci 13:1380-1387.

Feiguin F, Godena VK, Romano G, D'Ambrogio A, Klima R, Baralle FE (2009) Depletion of TDP-43 affects Drosophila motoneurons terminal synapsis and locomotive behavior. FEBS Lett 583:1586-1592.

Fernandes C, Rao Y (2011) Genome-wide screen for modifiers of Parkinson's disease genes in Drosophila. Mol Brain 4:17.

Ferreirinha F, Quattrini A, Pirozzi M, Valsecchi V, Dina G, Broccoli V, Auricchio A, Piemonte F, Tozzi G, Gaeta L, Casari G, Ballabio A, Rugarli EI (2004) Axonal degeneration in paraplegin-deficient mice is associated with abnormal mitochondria and impairment of axonal transport. J Clin Invest 113:231-242.

Fichera M, Lo Giudice M, Falco M, Sturnio M, Amata S, Calabrese O, Bigoni S, Calzolari E, Neri M (2004) Evidence of kinesin heavy chain (KIF5A) involvement in pure hereditary spastic paraplegia. Neurology 63:1108-1110.

Fuger P, Behrends LB, Mertel S, Sigrist SJ, Rasse TM (2007) Live imaging of synapse development and measuring protein dynamics using two-color fluorescence recovery after photo-bleaching at Drosophila synapses. Nat Protoc 2:3285-3298.

Godena VK, Romano G, Romano M, Appocher C, Klima R, Buratti E, Baralle FE, Feiguin F (2011) TDP-43 regulates Drosophila neuromuscular junctions growth by modulating Futsch/MAP1B levels and synaptic microtubules organization. PLoS One 6:e17808.

Goellner B, Aberle H (2012) The synaptic cytoskeleton in development and disease. Dev Neurobiol 72:111-125.

Goguel V, Belair AL, Ayaz D, Lampin-Saint-Amaux A, Scaplehorn N, Hassan BA, Preat T (2011) Drosophila amyloid precursor protein-like is required for long-term memory. J Neurosci 31:1032-1037.

Goizet C, Boukhris A, Mundwiller E, Tallaksen C, Forlani S, Toutain A, Carriere N, Paquis V, Depienne C, Durr A, Stevanin G, Brice A (2009) Complicated forms of autosomal dominant hereditary spastic paraplegia are frequent in SPG10. Hum Mutat 30:E376-385.

Gomez TS, Billadeau DD (2009) A FAM21-containing WASH complex regulates retromer-dependent sorting. Dev Cell 17:699-711.

Greeve I, Kretzschmar D, Tschape JA, Beyn A, Brellinger C, Schweizer M, Nitsch RM, Reifegerste R (2004) Age-dependent neurodegeneration and Alzheimer-amyloid plaque formation in transgenic Drosophila. J Neurosci 24:3899-3906.

Guan B, Hartmann B, Kho YH, Gorczyca M, Budnik V (1996) The Drosophila tumor suppressor gene, dlg, is involved in structural plasticity at a glutamatergic synapse. Curr Biol 6:695-706.

Gustafson K, Boulianne GL (1996) Distinct expression patterns detected within individual tissues by the GAL4 enhancer trap technique. Genome 39:174-182.

Hannus M, Feiguin F, Heisenberg CP, Eaton S (2002) Planar cell polarization requires Widerborst, a B' regulatory subunit of protein phosphatase 2A. Development 129:3493-3503.

Heckmann M, Dudel J (1997) Desensitization and resensitization kinetics of glutamate receptor channels from Drosophila larval muscle. Biophys J 72:2160-2169.

Holzbaur EL (2004) Motor neurons rely on motor proteins. Trends Cell Biol 14:233-240.

Horiuchi D, Barkus RV, Pilling AD, Gassman A, Saxton WM (2005) APLIP1, a kinesin binding JIP-1/JNK scaffold protein, influences the axonal transport of both vesicles and mitochondria in Drosophila. Curr Biol 15:2137-2141.

Hummel T, Krukkert K, Roos J, Davis G, Klambt C (2000) Drosophila Futsch/22C10 is a MAP1B-like protein required for dendritic and axonal development. Neuron 26:357-370.

Hurd DD, Saxton WM (1996a) Kinesin Mutations Cause Motor Neuron Disease Phenotypes by Disrupting Fast Axonal Transport in Drosophila. Genetics 144:1075-1085.

Hurd DD, Saxton WM (1996b) Kinesin mutations cause motor neuron disease phenotypes by disrupting fast axonal transport in Drosophila. Genetics 144:1075-1085.

Ikenaka K, Katsuno M, Kawai K, Ishigaki S, Tanaka F, Sobue G (2012) Disruption of axonal transport in motor neuron diseases. Int J Mol Sci 13:1225-1238.

Ingold AL, Cohn SA, Scholey JM (1988) Inhibition of kinesin-driven microtubule motility by monoclonal antibodies to kinesin heavy chains. J Cell Biol 107:2657-2667.

Janssens V, Goris J (2001) Protein phosphatase 2A: a highly regulated family of serine/threonine phosphatases implicated in cell growth and signalling. Biochem J 353:417-439.

Jouvenceau A, Billard JM, Haditsch U, Mansuy IM, Dutar P (2003) Different phosphatase-dependent mechanisms mediate long-term depression and depotentiation of long-term potentiation in mouse hippocampal CA1 area. Eur J Neurosci 18:1279-1285.

Junco A, Bhullar B, Tarnasky HA, van der Hoorn FA (2001) Kinesin light-chain KLC3 expression in testis is restricted to spermatids. Biol Reprod 64:1320-1330.

Kanai Y, Okada Y, Tanaka Y, Harada A, Terada S, Hirokawa N (2000) KIF5C, a novel neuronal kinesin enriched in motor neurons. J Neurosci 20:6374-6384.

Karle KN, Mockel D, Reid E, Schols L (2012) Axonal transport deficit in a KIF5A (-/-) mouse model. Neurogenetics.

Kasher PR, De Vos KJ, Wharton SB, Manser C, Bennett EJ, Bingley M, Wood JD, Milner R, McDermott CJ, Miller CC, Shaw PJ, Grierson AJ (2009) Direct evidence for axonal transport defects in a novel mouse model of mutant spastin-induced hereditary spastic paraplegia (HSP) and human HSP patients. J Neurochem 110:34-44.

Katsuno M, Adachi H, Minamiyama M, Waza M, Doi H, Kondo N, Mizoguchi H, Nitta A, Yamada K, Banno H, Suzuki K, Tanaka F, Sobue G (2010) Disrupted transforming growth factor-beta signaling in spinal and bulbar muscular atrophy. J Neurosci 30:5702-5712.

Katsuno M, Adachi H, Minamiyama M, Waza M, Tokui K, Banno H, Suzuki K, Onoda Y, Tanaka F, Doyu M, Sobue G (2006) Reversible disruption of dynactin 1-mediated retrograde axonal transport in polyglutamine-induced motor neuron degeneration. J Neurosci 26:12106-12117.

Kaufmann N, DeProto J, Ranjan R, Wan H, Van Vactor D (2002) Drosophila liprin-alpha and the receptor phosphatase Dlar control synapse morphogenesis. Neuron 34:27-38.

Kittel RJ, Wichmann C, Rasse TM, Fouquet W, Schmidt M, Schmid A, Wagh DA, Pawlu C, Kellner RR, Willig KI, Hell SW, Buchner E, Heckmann M, Sigrist SJ (2006) Bruchpilot promotes active zone assembly, Ca2+ channel clustering, and vesicle release. Science 312:1051-1054.

Klagges BR, Heimbeck G, Godenschwege TA, Hofbauer A, Pflugfelder GO, Reifegerste R, Reisch D, Schaupp M, Buchner S, Buchner E (1996) Invertebrate synapsins: a single gene codes for several isoforms in Drosophila. J Neurosci 16:3154-3165.

Klymkowsky MW, Maynell LA, Polson AG (1987) Polar asymmetry in the organization of the cortical cytokeratin system of Xenopus laevis oocytes and embryos. Development 100:543-557.

Knopp M (2008) Systematische Identizierung von Genen, die zur Stabilisierung von Synapsen beitragen. Tuebingen.

Kozielski F, Sack S, Marx A, Thormahlen M, Schonbrunn E, Biou V, Thompson A, Mandelkow EM, Mandelkow E (1997) The crystal structure of dimeric kinesin and implications for microtubule-dependent motility. Cell 91:985-994.

Lahey T, Gorczyca M, Jia XX, Budnik V (1994) The Drosophila tumor suppressor gene dlg is required for normal synaptic bouton structure. Neuron 13:823-835.

Landgraf M, Bossing T, Technau GM, Bate M (1997) The origin, location, and projections of the embryonic abdominal motorneurons of Drosophila. J Neurosci 17:9642-9655.

Lee M, Paik SK, Lee MJ, Kim YJ, Kim S, Nahm M, Oh SJ, Kim HM, Yim J, Lee CJ, Bae YC, Lee S (2009) Drosophila Atlastin regulates the stability of muscle microtubules and is required for synapse development. Dev Biol 330:250-262.

Lin DM, Goodman CS (1994) Ectopic and increased expression of Fasciclin II alters motoneuron growth cone guidance. Neuron 13:507-523.

Liu W, Acin-Perez R, Geghman KD, Manfredi G, Lu B, Li C (2011a) Pink1 regulates the oxidative phosphorylation machinery via mitochondrial fission. Proc Natl Acad Sci U S A 108:12920-12924.

Liu Z, Hamamichi S, Lee BD, Yang D, Ray A, Caldwell GA, Caldwell KA, Dawson TM, Smith WW, Dawson VL (2011b) Inhibitors of LRRK2 kinase attenuate

neurodegeneration and Parkinson-like phenotypes in Caenorhabditis elegans and Drosophila Parkinson's disease models. Hum Mol Genet 20:3933-3942.

Lo Giudice M, Neri M, Falco M, Sturnio M, Calzolari E, Di Benedetto D, Fichera M (2006) A missense mutation in the coiled-coil domain of the KIF5A gene and late-onset hereditary spastic paraplegia. Arch Neurol 63:284-287.

Lorenzo DN, Li MG, Mische SE, Armbrust KR, Ranum LP, Hays TS (2010) Spectrin mutations that cause spinocerebellar ataxia type 5 impair axonal transport and induce neurodegeneration in Drosophila. J Cell Biol 189:143-158.

Marques G (2005) Morphogens and synaptogenesis in Drosophila. J Neurobiol 64:417-434.

Marques G, Bao H, Haerry TE, Shimell MJ, Duchek P, Zhang B, O'Connor MB (2002) The Drosophila BMP type II receptor Wishful Thinking regulates neuromuscular synapse morphology and function. Neuron 33:529-543.

Marques G, Haerry TE, Crotty ML, Xue M, Zhang B, O'Connor MB (2003) Retrograde Gbb signaling through the Bmp type 2 receptor wishful thinking regulates systemic FMRFa expression in Drosophila. Development 130:5457-5470.

Marrus SB, Portman SL, Allen MJ, Moffat KG, DiAntonio A (2004) Differential localization of glutamate receptor subunits at the Drosophila neuromuscular junction. J Neurosci 24:1406-1415.

McCabe BD, Hom S, Aberle H, Fetter RD, Marques G, Haerry TE, Wan H, O'Connor MB, Goodman CS, Haghighi AP (2004) Highwire regulates presynaptic BMP signaling essential for synaptic growth. Neuron 41:891-905.

McCabe BD, Marques G, Haghighi AP, Fetter RD, Crotty ML, Haerry TE, Goodman CS, O'Connor MB (2003) The BMP homolog Gbb provides a retrograde signal that regulates synaptic growth at the Drosophila neuromuscular junction. Neuron 39:241-254.

McGuire SE, Mao Z, Davis RL (2004) Spatiotemporal gene expression targeting with the TARGET and gene-switch systems in Drosophila. Sci STKE 2004:pl6.

McMonagle P, Webb S, Hutchinson M (2002) The prevalence of "pure" autosomal dominant hereditary spastic paraparesis in the island of Ireland. J Neurol Neurosurg Psychiatry 72:43-46.

Muqit MM, Feany MB (2002) Modelling neurodegenerative diseases in Drosophila: a fruitful approach? Nat Rev Neurosci 3:237-243.

Musumeci O, Bassi MT, Mazzeo A, Grandis M, Crimella C, Martinuzzi A, Toscano A (2011) A novel mutation in KIF5A gene causing hereditary spastic paraplegia with axonal neuropathy. Neurol Sci 32:665-668.

Nakamura M, Ito H, Wate R, Nakano S, Hirano A, Kusaka H (2008) Phosphorylated Smad2/3 immunoreactivity in sporadic and familial amyotrophic lateral sclerosis and its mouse model. Acta Neuropathol 115:327-334.

Neumann M, Sampathu DM, Kwong LK, Truax AC, Micsenyi MC, Chou TT, Bruce J, Schuck T, Grossman M, Clark CM, McCluskey LF, Miller BL, Masliah E, Mackenzie IR, Feldman H, Feiden W, Kretzschmar HA, Trojanowski JQ, Lee VM (2006) Ubiquitinated TDP-43 in frontotemporal lobar degeneration and amyotrophic lateral sclerosis. Science 314:130-133.

Niclas J, Navone F, Hom-Booher N, Vale RD (1994) Cloning and localization of a conventional kinesin motor expressed exclusively in neurons. Neuron 12:1059-1072.

Pack-Chung E, Kurshan PT, Dickman DK, Schwarz TL (2007) A Drosophila kinesin required for synaptic bouton formation and synaptic vesicle transport. Nature Neurosci 10:980-989.

Padgett RW, Wozney JM, Gelbart WM (1993) Human BMP sequences can confer normal dorsal-ventral patterning in the Drosophila embryo. Proc Natl Acad Sci U S A 90:2905-2909.

Park SH, Zhu PP, Parker RL, Blackstone C (2010) Hereditary spastic paraplegia proteins REEP1, spastin, and atlastin-1 coordinate microtubule interactions with the tubular ER network. J Clin Invest 120:1097-1110.

Paschinger K, Rendic D, Wilson IB (2009) Revealing the anti-HRP epitope in Drosophila and Caenorhabditis. Glycoconj J 26:385-395.

Persson U, Izumi H, Souchelnytskyi S, Itoh S, Grimsby S, Engstrom U, Heldin CH, Funa K, ten Dijke P (1998) The L45 loop in type I receptors for TGF-beta family members is a critical determinant in specifying Smad isoform activation. FEBS Lett 434:83-87.

Phillips GR, Huang JK, Wang Y, Tanaka H, Shapiro L, Zhang W, Shan WS, Arndt K, Frank M, Gordon RE, Gawinowicz MA, Zhao Y, Colman DR (2001) The presynaptic particle web: ultrastructure, composition, dissolution, and reconstitution. Neuron 32:63-77.

Pielage J, Cheng L, Fetter RD, Carlton PM, Sedat JW, Davis GW (2008) A presynaptic giant ankyrin stabilizes the NMJ through regulation of presynaptic microtubules and transsynaptic cell adhesion. Neuron 58:195-209.

Pilling AD, Horiuchi D, Lively CM, Saxton WM (2006) Kinesin-1 and Dynein are the primary motors for fast transport of mitochondria in Drosophila motor axons. Mol Biol Cell 17:2057-2068.

Price NE, Wadzinski B, Mumby MC (1999) An anchoring factor targets protein phosphatase 2A to brain microtubules. Brain Res Mol Brain Res 73:68-77.

Prokop A, Meinertzhagen IA (2006) Development and structure of synaptic contacts in Drosophila. Semin Cell Dev Biol 17:20-30.

Qin G, Schwarz T, Kittel RJ, Schmid A, Rasse TM, Kappei D, Ponimaskin E, Heckmann M, Sigrist SJ (2005) Four different subunits are essential for expressing the synaptic glutamate receptor at neuromuscular junctions of Drosophila. J Neurosci 25:3209-3218.

Raftery LA, Sutherland DJ (1999) TGF-beta family signal transduction in Drosophila development: from Mad to Smads. Dev Biol 210:251-268.

Rasse TM (2004) In vivo imaging of long-term changes in the Drosophila neuromuscular junction. Goettingen.

Rasse TM, Fouquet W, Schmid A, Kittel RJ, Mertel S, Sigrist CB, Schmidt M, Guzman A, Merino C, Qin G, Quentin C, Madeo FF, Heckmann M, Sigrist SJ (2005) Glutamate receptor dynamics organizing synapse formation in vivo. Nat Neurosci 8:898-905.

Ratnaparkhi A, Lawless GM, Schweizer FE, Golshani P, Jackson GR (2008) A Drosophila model of ALS: human ALS-associated mutation in VAP33A suggests a dominant negative mechanism. PLoS One 3:e2334.

Reid E, Kloos M, Ashley-Koch A, Hughes L, Bevan S, Svenson IK, Graham FL, Gaskell PC, Dearlove A, Pericak-Vance MA, Rubinsztein DC, Marchuk DA (2002) A kinesin heavy chain (KIF5A) mutation in hereditary spastic paraplegia (SPG10). Am J Hum Genet 71:1189-1194.

Reiter LT, Potocki L, Chien S, Gribskov M, Bier E (2001) A systematic analysis of human disease-associated gene sequences in Drosophila melanogaster. Genome Res 11:1114-1125.

Rubin GM, Spradling AC (1982) Genetic transformation of Drosophila with transposable element vectors. Science 218:348-353.

Salinas S, Proukakis C, Crosby A, Warner TT (2008) Hereditary spastic paraplegia: clinical features and pathogenetic mechanisms. Lancet Neurol 7:1127-1138.

Sampath TK, Rashka KE, Doctor JS, Tucker RF, Hoffmann FM (1993) Drosophila transforming growth factor beta superfamily proteins induce endochondral bone formation in mammals. Proc Natl Acad Sci U S A 90:6004-6008.

Sang, Jackson (2005) Drosophila models of neurodegenerative disease.

Sanyal S (2009) Genomic mapping and expression patterns of C380, OK6 and D42 enhancer trap lines in the larval nervous system of Drosophila. Gene Expr Patterns 9:371-380.

Saxena S, Caroni P (2007) Mechanisms of axon degeneration: from development to disease. Prog Neurobiol 83:174-191.

Saxton WM, Hicks J, Goldstein LS, Raff EC (1991) Kinesin heavy chain is essential for viability and neuromuscular functions in Drosophila, but mutants show no defects in mitosis. Cell 64:1093-1102.

Schon EA, Przedborski S (2011) Mitochondria: the next (neurode)generation. Neuron 70:1033-1053.

Schule R, Kremer BP, Kassubek J, Auer-Grumbach M, Kostic V, Klopstock T, Klimpe S, Otto S, Boesch S, van de Warrenburg BP, Schols L (2008) SPG10 is a rare cause of spastic paraplegia in European families. J Neurol Neurosurg Psychiatry 79:584-587.

Schule R, Schols L (2011) Genetics of hereditary spastic paraplegias. Semin Neurol 31:484-493.

Schuster CM, Davis GW, Fetter RD, Goodman CS (1996) Genetic dissection of structural and functional components of synaptic plasticity. I. Fasciclin II controls synaptic stabilization and growth. Neuron 17:641-654.

Seitz A, Surrey T (2006) Processive movement of single kinesins on crowded microtubules visualized using quantum dots. EMBO J 25:267-277.

Sheng ZH, Cai Q (2012) Mitochondrial transport in neurons: impact on synaptic homeostasis and neurodegeneration. Nat Rev Neurosci 13:77-93.

Sherwood NT, Sun Q, Xue M, Zhang B, Zinn K (2004) Drosophila spastin regulates synaptic microtubule networks and is required for normal motor function. PLoS Biol 2:e429.

Siegert VK (2011) Störungen des axonalen Transports bei der hereditären spastischen Spinalparalyse im Drosophila-Modell. Tuebingen.

Silva MC, Coutinho P, Pinheiro CD, Neves JM, Serrano P (1997) Hereditary ataxias and spastic paraplegias: methodological aspects of a prevalence study in Portugal. J Clin Epidemiol 50:1377-1384.

Slabicki M, Theis M, Krastev DB, Samsonov S, Mundwiller E, Junqueira M, Paszkowski-Rogacz M, Teyra J, Heninger AK, Poser I, Prieur F, Truchetto J, Confavreux C, Marelli C, Durr A, Camdessanche JP, Brice A, Shevchenko A, Pisabarro MT, Stevanin G, Buchholz F (2010) A genome-scale DNA repair RNAi screen identifies SPG48 as a novel gene associated with hereditary spastic paraplegia. PLoS Biol 8:e1000408.

Sontag E, Hladik C, Montgomery L, Luangpirom A, Mudrak I, Ogris E, White CL, 3rd (2004a) Downregulation of protein phosphatase 2A carboxyl methylation and methyltransferase may contribute to Alzheimer disease pathogenesis. J Neuropathol Exp Neurol 63:1080-1091.

Sontag E, Luangpirom A, Hladik C, Mudrak I, Ogris E, Speciale S, White CL, 3rd (2004b) Altered expression levels of the protein phosphatase 2A ABalphaC enzyme are associated with Alzheimer disease pathology. J Neuropathol Exp Neurol 63:287-301.

Sontag E, Nunbhakdi-Craig V, Bloom GS, Mumby MC (1995) A novel pool of protein phosphatase 2A is associated with microtubules and is regulated during the cell cycle. J Cell Biol 128:1131-1144.

Spradling AC, Stern D, Beaton A, Rhem EJ, Laverty T, Mozden N, Misra S, Rubin GM (1999) The Berkeley Drosophila Genome Project gene disruption project: Single P-element insertions mutating 25% of vital Drosophila genes. Genetics 153:135-177.

Sung HH, Telley IA, Papadaki P, Ephrussi A, Surrey T, Rorth P (2008) Drosophila ensconsin promotes productive recruitment of Kinesin-1 to microtubules. Dev Cell 15:866-876.

Tarrade A, Fassier C, Courageot S, Charvin D, Vitte J, Peris L, Thorel A, Mouisel E, Fonknechten N, Roblot N, Seilhean D, Dierich A, Hauw JJ, Melki J (2006) A mutation of spastin is responsible for swellings and impairment of transport in a region of axon characterized by changes in microtubule composition. Hum Mol Genet 15:3544-3558.

Tessa A, Silvestri G, de Leva MF, Modoni A, Denora PS, Masciullo M, Dotti MT, Casali C, Melone MA, Federico A, Filla A, Santorelli FM (2008) A novel KIF5A/SPG10 mutation in spastic paraplegia associated with axonal neuropathy. J Neurol 255:1090-1092.

Thazhath R, Liu C, Gaertig J (2002) Polyglycylation domain of beta-tubulin maintains axonemal architecture and affects cytokinesis in Tetrahymena. Nat Cell Biol 4:256-259.

Tsang HT, Edwards TL, Wang X, Connell JW, Davies RJ, Durrington HJ, O'Kane CJ, Luzio JP, Reid E (2009) The hereditary spastic paraplegia proteins NIPA1, spastin and spartin are inhibitors of mammalian BMP signalling. Hum Mol Genet 18:3805-3821.

Uchida A, Alami NH, Brown A (2009) Tight functional coupling of kinesin-1A and dynein motors in the bidirectional transport of neurofilaments. Mol Biol Cell 20:4997-5006.

Vale RD, Fletterick RJ (1997) The design plan of kinesin motors. Annu Rev Cell Dev Biol 13:745-777.

Venkatachalam K, Long AA, Elsaesser R, Nikolaeva D, Broadie K, Montell C (2008) Motor deficit in a Drosophila model of mucolipidosis type IV due to defective clearance of apoptotic cells. Cell 135:838-851.

Verstreken P, Ly CV, Venken KJ, Koh TW, Zhou Y, Bellen HJ (2005) Synaptic mitochondria are critical for mobilization of reserve pool vesicles at Drosophila neuromuscular junctions. Neuron 47:365-378.

Viquez NM, Li CR, Wairkar YP, DiAntonio A (2006) The B' protein phosphatase 2A regulatory subunit well-rounded regulates synaptic growth and cytoskeletal stability at the Drosophila neuromuscular junction. J Neurosci 26:9293-9303.

Vogelsberg-Ragaglia V, Schuck T, Trojanowski JQ, Lee VM (2001) PP2A mRNA expression is quantitatively decreased in Alzheimer's disease hippocampus. Exp Neurol 168:402-412.

Wagh DA, Rasse TM, Asan E, Hofbauer A, Schwenkert I, Durrbeck H, Buchner S, Dabauvalle MC, Schmidt M, Qin G, Wichmann C, Kittel R, Sigrist SJ, Buchner E (2006) Bruchpilot, a protein with homology to ELKS/CAST, is required for structural integrity and function of synaptic active zones in Drosophila. Neuron 49:833-844.

Wang JW, Brent JR, Tomlinson A, Shneider NA, McCabe BD (2011) The ALS-associated proteins FUS and TDP-43 function together to affect Drosophila locomotion and life span. J Clin Invest 121:4118-4126.

Wang L, Brown A (2010) A hereditary spastic paraplegia mutation in kinesin-1A/KIF5A disrupts neurofilament transport. Mol Neurodegener 5:52.

Wang X, Shaw WR, Tsang HT, Reid E, O'Kane CJ (2007) Drosophila spichthyin inhibits BMP signaling and regulates synaptic growth and axonal microtubules. Nat Neurosci 10:177-185.

Woo NH, Nguyen PV (2002) "Silent" metaplasticity of the late phase of long-term potentiation requires protein phosphatases. Learn Mem 9:202-213.

Yang JT, Laymon RA, Goldstein LS (1989) A three-domain structure of kinesin heavy chain revealed by DNA sequence and microtubule binding analyses. Cell 56:879-889.

Yang JT, Saxton WM, Goldstein LS (1988) Isolation and characterization of the gene encoding the heavy chain of Drosophila kinesin. Proc Natl Acad Sci U S A 85:1864-1868.

Zeidler MP, Tan C, Bellaiche Y, Cherry S, Hader S, Gayko U, Perrimon N (2004) Temperature-sensitive control of protein activity by conditionally splicing inteins. Nat Biotechnol 22:871-876.

Zhai RG, Bellen HJ (2004) The architecture of the active zone in the presynaptic nerve terminal. Physiology (Bethesda) 19:262-270.

Zhang Y, Fuger P, Hannan SB, Kern JV, Lasky B, Rasse TM (2010) In vivo imaging of intact Drosophila larvae at sub-cellular resolution. J Vis Exp.

Zinsmaier KE, Eberle KK, Buchner E, Walter N, Benzer S (1994) Paralysis and early death in cysteine string protein mutants of Drosophila. Science 263:977-980.